PULSE SHAPING MECHANISMS FOR HIGH PERFORMANCE MODE-LOCKED FIBER LASERS

A Dissertation

Presented to the Faculty of the Graduate School

of Cornell University

in Partial Fulfillment of the Requirements for the Degree of

Doctor of Philosophy

by

William Henry Renninger

August 2012

PULSE SHAPING MECHANISMS FOR HIGH PERFORMANCE MODE-LOCKED FIBER LASERS

William Henry Renninger, Ph.D.

Cornell University 2012

Fiber lasers offer several clear advantages over solid-state systems: compact design, thermal management, minimal alignment, spatial beam quality and low cost. Consequently, fiber systems have become a valued option for applications requiring continuous-wave or long-pulse operation. However, for pulsed operation the benefits of fiber come at the cost of tighter confinement of the light, leading to the accumulation of nonlinear optical effects which can rapidly degrade the pulse. For this reason, the performance of mode-locked fiber lasers has until recently lagged behind that of their solid-state counterparts. Nonetheless, recent developments in managing nonlinearity have led to mode-locked fiber systems with performance that directly competes with solid-state systems.

The aim of this thesis is to investigate the ultrashort pulse propagation physics which helps to render the nonlinear limitations of fiber systems obsolete. From the development of dissipative soliton mode-locking, which allows for an order of magnitude increase in pulse energies, to mode-locking based on self-similar pulse evolution which allows for the shortest pulses from a fiber laser to date, this thesis covers recent significant developments in laser mode-locking in systems featuring normal group-velocity dispersion. In addition, preceding pulse evolutions which were investigated experimentally, such as lasers based on self-similar propagation in a passive fiber and so-called "wave-breaking free" lasers are analyzed numerically and integrated theoretically with recent developments. Finally, several notable

future directions in fiber laser research are identified and a new technique for the possible generation of ever-higher performance mode-locked fiber lasers is explored.

BIOGRAPHICAL SKETCH

William Henry Renninger was born in Red Bank, New Jersey in 1983. After a couple years of moving around New Jersey, his family settled in rural Hunterdon County, New Jersey. Here he received a high quality public education for twelve years before completing high school. There was never any doubt that he wanted to be a physicist from the moment he knew he no longer wanted to be a bad-guy-slaying action hero from Saturday morning cartoons. As a consequence his choice over colleges was easily simplified.

Will enrolled at Rensselaer Polytechnic Institute (RPI) in Troy, NY for his freshman year of college in 2002. Upon completion of his initial year, while appreciating the quality of eduction at RPI, he felt unsatisfied with the environment, attitude and atmosphere surrounding this school. It was then, in 2003, that he began his journey at Cornell University as a transfer student in the School of Electrical and Computer Engineering. Finally, after a few short months, he found his home as a student in the School of Applied and Engineering Physics. Here he found the students, faculty and environment all to be exceptional and he enjoyed every class and experience. During his undergraduate years, he held two summer internships at Agere Systems in Allentown, PA. As a senior, after being intrigued by his nonlinear optics course, Will worked for Professor Frank Wise as an undergraduate researcher. At this point, knowing he wanted to pursue a doctoral degree, and having already found his perfect environment, staying on to work as a Ph.D. candidate under Professor Wise was an easy choice.

Will continued on to research with Professor Wise on nonlinear optics and ultrafast pulse propagation phenomena. Having had a wonderful experience in this group, he will proudly stay in the Wise group for another year as a post-graduate researcher.

To my family, Mom, Dad, Rob, Ed, Richard, and Maria for their undying support.

ACKNOWLEDGEMENTS

It is often said that "the quality of one's Ph.D. experience is entirely determined by the quality of one's Ph.D. advisor." I've come to understand how true this statement really is. I can never be thankful enough to Professor Frank Wise for his depth of knowledge, sharply skilled analysis, and perhaps more importantly, his ability to work with any student at any level. His patience, flexibility, true passion for teaching and adept management style has allowed for simply an amazing learning experience as a student in his group. As it is often hard to know a good advisor before working with him or her, I consider myself truly lucky to have landed in Professor Wise's group.

I am also thankful for Professor Gaeta, who as my undergraduate advisor helped steer me in the right direction, as well as to the many other faculty at Cornell, whose many inspiring lectures keep the wonder of learning alive every day. I'll never forget when Professor Gaeta told us in his intro quantum mechanics class that "if you walk into a wall enough times you will eventually go through it!"

As a Ph.D. student I am more than grateful for the students, particularly Andy Chong and Joel Buckley, who took time from their busy day to teach me even the tiniest details about everything in the lab. This group has always been very supportive and collaborative and so thank you Lyuba Kuznetsova, Shian Zhou, Khanh Kieu, Heng Li, Hui Liu and Erin Stranford. Also, an extra big thank you to the guys who I would consistently ask questions to about topics of any nature and who always made the time to have a discussion, Adam Bartnik and Simon Lefrancois. Last but not least, I would like to thank our many stimulating collaborators, particularly Nathan Kutz and Brandon Bale for their enthusiastic support.

TABLE OF CONTENTS

LIST OF TABLES

LIST OF FIGURES

BIBLIOGRAPHY

[1] W. H. Renninger, A. Chong, and F. W. Wise, Physical Review A **77**, 23814 (2008).

[2] A. Chong, W. H. Renninger, and F. W. Wise, J. Opt. Soc. Am. B **25**, 140 (2008).

[3] W. H. Renninger, A. Chong, and F. W. Wise, J. Opt. Soc. Am. B **27**, 1978 (2010).

[4] A. Chong, W. H. Renninger, and F. W. Wise, Opt. Lett. **32**, 2408 (2007).

[5] A. Chong, W. H. Renninger, and F. W. Wise, Opt. Lett. **33**, 2638 (2008).

[6] K. Kieu, W. H. Renninger, A. Chong, and F. W. Wise, Opt. Lett. **34**, 593 (2009).

[7] S. Lefrançois, K. Kieu, Y. Deng, J. D. Kafka, and F. W. Wise, Opt. Lett. **35**, 1569 (2010).

[8] S. Lefrancois, T. S. Sosnowski, C.-H. Liu, A. Galvanauskas, and F. W. Wise, Opt. Express **19**, 3464 (2011).

[9] A. Chong, W. H. Renninger, and F. W. Wise, Opt. Lett. **33**, 1071 (2008).

[10] W. H. Renninger, A. Chong, and F. W. Wise, Opt. Lett. **33**, 3025 (2008).

[11] M. E. Fermann, V. I. Kruglov, B. C. Thomsen, J. M. Dudley, and J. D. Harvey, Phys. Rev. Lett. **84**, 6010 (2000).

CHAPTER 1

INTRODUCTION

Ultrafast science is a steadily growing field which has major impact over both industrial applications as well as basic scientific research. Continued progress in this field relies on the development of ultrashort pulse sources. Solid-state lasers have traditionally fulfilled this role as a wide variety and arrangements for gain media exist. Recent developments have come in Nd:glass [1], Yb:glass [2], and Yb: tungstate [3]. But a particularly notable example for femtosecond pulse generation is the mode-locked Ti:sapphire laser.

The Ti:sapphire laser, which owes its use to the discovery of Kerr-lens mode-locking [4], has a combination of both spectroscopic and material properties which allow for some very high-performance and useful lasers and amplifiers. In the last two decades, these systems have been largely responsible for new developments in ultrafast science and are still in great use today.

Unfortunately, Ti:sapphire-based systems come with some caveats. In general, use of one of these systems requires trained personnel to keep it maintained and running at its highest performance. This is due to environmental stress which can cause free-space components to shift slightly, decreasing laser performance dramatically. In addition, the cost of Ti:sapphire-based systems is still very high, which creates an ultrafast science barrier of entry for many research groups. It is clear that applications and research could benefit from a source of ultrafast light which is cost-efficient and highly robust.

A new generation of ultrafast sources has been available in recent decades with the rapid development of fiber laser technology. Fiber lasers can avoid the sensi-

tivity to alignment which plagues solid-state sources because the light is confined in the core of the waveguide. In particular, in systems where the fiber is fully connected around the oscillator, all-fiber systems, there is no need for trained personnel to make adjustments because there are no moving parts to adjust. Fiber systems are also very cost-effective as compared to solid-state systems partly because they benefit strongly from economies of scale owing to their use in the telecommunications industry. Additional benefits include good heat dissipation because the fibers have a large surface to volume ratio. This allows for kilowatt devices.

These features have made fiber sources a staple for the generation of continuous-wave and long pulse sources. However, the advantages of fiber-based systems also comes with a caveat: the tight confinement in the core of the optical wave-guide leads to higher brightness in the fiber, which leads to the accumulation of various nonlinear optical effects, which in turn can rapidly degrade the pulse. Nonetheless, substantial research has gone into the development of ultrashort pulsed sources [5–8]. Recent results include picosecond pulses with ∼100-W average powers [9, 10]. This particular work was a landmark because it became clear that fiber-based systems generating short pulses should compete directly with solid-state laser performance.

Further progress in the development of high performance fiber sources relies on various methods of managing or balancing the negative effects resulting from the accumulation of nonlinear phase in the fiber. This involves the study of nonlinear pulse evolution, which is a rich subject in its own right. While there are only a handful of physical mechanisms acting on the pulse, their interplay can lead to varied and even counter-intuitive results. Despite the substantial research effort in this field, qualitatively new phenomena are still being discovered.

Recent research into these nonlinear managing techniques for mode-locking fiber lasers has allowed for order-of magnitude increases in the pulse performance, bringing even femtosecond sources to the level of solid-state sources with the additional benefits that come with fiber. Furthermore, it appears as if higher performance levels will be possible. The primary goal of this thesis is to summarize these developments. In the next section basic pulse-propagation in an optical fiber is reviewed (section 1.1). In section 1.2, the foundations for mode-locking are introduced, including the development of a master mode-locking equation. Various extensions and reductions of this model are then introduced in order to examine early mode-locking mechanisms, including soliton (section 1.2.1) and stretched-pulse (section 1.2.2) mode-locking. Then three new mode-locking concepts will be introduced before deeper investigations in the body of the thesis. Finally, in section 1.3, major fiber laser components and key implementations are discussed.

1.1 Pulse propagation in a fiber

The propagation of optical fields in fibers is governed by Maxwell's equations. The combination of these equations results in

$$\nabla^2 E - \frac{1}{c^2}\frac{\partial^2 E}{\partial t^2} = \mu_0 \frac{\partial^2 P_L}{\partial t^2} + \mu_0 \frac{\partial^2 P_{NL}}{\partial t^2}, \tag{1.1}$$

where we include only the third-order nonlinear effects governed by $\chi^{(3)}$, the induced polarization consists of the sum of P_L and P_{NL}, and P_{NL} is treated as a small perturbation to P_L. Given that $P_{NL} \approx \varepsilon_0 \frac{3}{4}\chi^{(3)}_{xxxx}|E|^2 E$ and following a detailed derivation [11–13], one can define the slowly varying amplitude, $A(z,t)$, as $E(r,t) = \frac{1}{2}\hat{x}(F(x,y)A(z,t)exp[i(\beta_0 z - \omega_0 t)] + complexcongjugate)$ and write

the resultant temporal equation for the pulse duration in a single-mode fiber as:

$$\begin{aligned}\frac{\partial A}{\partial z} + \frac{\alpha}{2}A + \frac{i\beta_2}{2}\frac{\partial^2 A}{\partial t^2} - \frac{\beta_3}{6}\frac{\partial^3 A}{\partial t^3} \\ = i\gamma\left(1 + \frac{i}{\omega_0}\frac{\partial}{\partial t}\right)\left(A(z,t)\int_{-\infty}^{\infty} R(t')|A(z,t-t')|^2 dt'\right),\end{aligned} \tag{1.2}$$

where t is the time in the frame of the pulse, α is the linear loss, β_2 refers to the group-velocity dispersion, β_3 refers to the third order dispersion (TOD), $\gamma = \frac{n_2\omega_0}{cA_{eff}}$ is the nonlinear parameter, and $R(t)$ is the nonlinear response function. The nonlinear terms on the right hand side are responsible for self-phase modulation, the self-frequency shift induced by intra-pulse Raman scattering, self-steepening and shock formation. For relatively long pulses ($>$ 100fs) the third-order dispersion and higher order nonlinearities can be neglected (i.e. the nonlinear response can be considered instantaneous and ω_0 times the pulse duration is much greater than 1). This is the case for most of the results presented in this thesis. In addition, because optical attenuation in fiber is on the order of 0.1 dB/km, $\alpha \approx 0$. The final simplified equation to be used for modeling pulse propagation in a fiber is therefore given by the nonlinear Schrödinger equation (NLSE):

$$\frac{\partial A}{\partial z} = -\frac{i\beta_2}{2}\frac{\partial^2 A}{\partial t^2} + i\gamma|A|^2 A. \tag{1.3}$$

1.2 Mode-locking of lasers

Mode-locking refers to the locking of the phases of the longitudinal cavity modes of an optical resonator. This can be achieved in two general ways: active and passive mode-locking. Active mode-locking involves the periodic modulation of the res-

onator losses to create a pulsed output with the same period. This can be achieved, for example, with an acousto- or electro-optic modulator. Output pulse durations from active mode-locked lasers are limited by the speed of the modulator and tend to produce longer pulses than passive mode-locking. Passive mode-locking, as the name suggests, uses the intensity of the pulse itself to modulate the loss of the cavity through interaction with a saturable absorber. Available in many forms, a saturable absorber is an optical element which, in general, transmits higher intensity light (low loss in the presence of the pulse) and blocks low intensity light (high loss in the absence of the pulse). An excellent review of basic mode-locking techniques authored by a major contributor to the field can be found in Ref. [14]. Passive mode-locking is the subject of this thesis owing to its superior performance and its use of simple optical elements.

In passively mode-locked fiber lasers, in addition to the saturable absorber, the bandwidth-limited gain of the lasing medium, loss around the cavity, additional spectral filtering, group-velocity dispersion and self-phase modulation all play a role in the shaping of a pulse around the cavity. More importantly, for stable mode-locking, all of these effects must exactly balance one another after one round trip of the oscillator. In other words, for a stable (steady-state) pulse to exist in the oscillator, its complex amplitude must end a round trip with the same profile as it began it with. In the language on nonlinear dynamics, a mode-locked pulse is an attracting nonlinear limit cycle solution to the equation which governs the cavity. It is this language that underlies the approaches used in this thesis to develop new mode-locking mechanisms. In other words, various cavity models are studied with particular attention paid to bright pulse solutions which may have useful properties in a fiber laser.

Before discussing individual models for mode-locking, it is useful to examine the most basic equation which results from combining all of the relevant physical mechanisms discussed in the previous paragraph. To do this, assume the gain per pass is small, so it can be considered a Gaussian spectral filter and a linear gain, lump the loss and gain into a single parameter, $g(z)$, lump all of the spectral filtering into a term corresponding to a Gaussian spectral filter multiplied by $1/\Omega(z)$, and assume the saturable absorber can be expanded in a Taylor series about zero intensity and keep only the first order term multiplied by $\alpha(z)$:

$$\frac{\partial A(t,z)}{\partial z} = g(z)A(t,z) + \left(\frac{1}{\Omega(z)} - \frac{i\beta_2(z)}{2}\right)\frac{\partial^2 A(t,z)}{\partial t^2} + (\alpha(z) + i\gamma(z))|A(t,z)|^2 A(t,z). \tag{1.4}$$

This equation is known as the Ginzburg-Landau equation with varying coefficients. While this model assumes that the spectral filtering is strictly of a Gaussian profile and that the saturable absorber can be modeled only with the lowest order nonlinear term, its use is justified because it describes all of the relevant fundamental mechanisms to their lowest order. This is a useful equation because any $A(t,z)$ that satisfies $A(t,L_c) = A(t,0)e^{i\phi}$ (L_c is the cavity length and ϕ is an arbitrary phase) and is stable against perturbations is a mode-locked solution. In fact, to first order, to date, all known mode-locked lasers can be modeled with this equation. Unfortunately, however, this partial differential equation with varying coefficients is analytically intractable and can only be solved with time consuming numerical simulations. As a consequence, to obtain useful and general information about a mode-locked laser, simplifications must be made to this equation. In this vein, to obtain a broad understanding of mode-locked solutions the best simplification to make is that, aside from a linear phase, the electric field does not vary

as a function of z. Put in another way, this model assumes small changes of the pulse after one period of the equation. This equation can be written as

$$0 = (g - i\phi)A(t) + \left(\frac{1}{\Omega} - \frac{i\beta_2}{2}\right)\frac{\partial^2 A(t)}{\partial t^2} + (\alpha + i\gamma)|A(t)|^2 A(t). \tag{1.5}$$

This equation is known commonly as the "master-equation" and was developed by a group at MIT in the early 1990s [15]. This equation has a general exact solution, which is given by:

$$A(t,z) = \sqrt{A}Sech(\frac{t}{\tau})e^{i\beta \ln Sech(\frac{t}{\tau}) + i\theta z}. \tag{1.6}$$

While the solution is unstable, its utility is great because it allows for the explicit representation of qualitative features of the pulse as a function of the most important system parameters. Its use is justified because there are several known mechanisms to stabilize the solution, such as gain saturation and higher order saturable absorber terms. The most important system parameter, which can be seen from immediate inspection of this solution is the group-velocity dispersion (GVD). With anomalous GVD the pulses are close to the transform limit (small temporal phase, β) and at normal dispersion the pulses are highly chirped (large temporal phase, β). Also in terms of performance, from this analysis, one can see that the shortest pulses (or more accurately the largest bandwidths) are found near zero net GVD. As a final observation, this analysis shows us that larger energy solutions exist when the absolute value of the GVD is larger. In the next few sections of the introduction, specific reductions and expansions of this master-equation will be analyzed with the goal of boiling down each regime to its simplest underlying features.

1.2.1 Soliton mode-locking

When the net GVD of the laser cavity is anomalous, the master-equation is superfluous because a reduced version of this equation has stable bight-pulse solutions. The reduced equation is the same as the basic equation for a fiber and is written again here:

$$\frac{\partial A(t,z)}{\partial z} = -\frac{i\beta_2}{2}\frac{\partial^2 A(t,z)}{\partial t^2} + i\gamma|A(t,z)|^2 A(t,z). \tag{1.7}$$

This is the well-studied NLSE. The equation is integrable and can be solved exactly with the inverse scattering technique. Its solutions are given by a reduced version of Eq. 1.6:

$$A(t,z) = \sqrt{A}Sech(\frac{t}{\tau})e^{i\theta z}. \tag{1.8}$$

In this case the relation of the pulse parameters to the system parameters can be expressed simply in a single expression with what is called an area theorem (so-named because of its relation to the pulse's energy or 'area'):

$$E\tau = \frac{2|\beta_2|}{\gamma}, \tag{1.9}$$

where E is the energy of the pulse and is given by the integration of the intensity profile over all time. From this simple expression one can see why this reduction from the master-equation is justified: like the anomalous GVD solutions to the master-equation, these solutions have no chirp (no temporal phase), and for constant system parameters, larger energies exist at larger GVD and shorter

pulses exist at smaller GVD. From these observations, one can conclude that the spectral filter, gain and saturable absorber contribute little to the mode-locking of pulses at anomalous GVD and pulse solutions can be accurately modeled using the simpler NLSE.

Indeed this has been the case and simple short-pulse fiber source can be designed at net-anomalous GVD [16–19]. While this mode-locking mechanism is simple and robust, its performance is limited by the onset of multiple-pulsing at pulse energies around 100pJ. The limitation arises from the tendency of solitons to fission in the presence of perturbations, or from peak power clamping in an effective saturable absorber [20].

1.2.2 Stretched-pulse mode-locking

An effective way to increase the allowed energy is to construct lasers with segments of normal and anomalous GVD [21, 22]. The variation of dispersion with position in the laser cavity is referred to as a dispersion map. The breathing evolution of the so-called dispersion-managed soliton, reduces nonlinear phase accumulation, and allows the stable pulse energy to increase by an order of magnitude.

The underlying pulse shaping mechanism is still dominated by the NLSE, or in other words by a direct balance between an effective anomalous GVD and a self-focusing nonlinearity. However, the pulse evolution in one round trip is such that the pulse can have more energy with the accumulation of the same amount of nonlinear phase. This pulse evolution can be modeled successfully with both the NLSE with varying coefficients [23] and the full master-equation with varying coefficients [24]. Qualitatively the soliton area theorem is still useful for such pulses

(Eq. 1.9).

1.2.3 Dissipative soliton mode-locking

When the GVD is normal, no solutions to the NLSE exist and one must extend the model at least to the master-equation, where this model predicts high energy, chirped pulses. However, as will be investigated in detail in chapter 2, the master-equation often fails to model pulse parameters even qualitatively in the normal dispersion regime and so the master-equation must be extended to a more complete model which includes a higher order nonlinear parameter (the cubic-quintic Ginzburg Landau equation (CQGLE)). This lack of stable solutions from the master-equation underlies the need for a more complete model. Mode-locked pulse solutions in the normal dispersion regime allow for another order of magnitude increase in performance.

1.2.4 Passive similariton mode-locking

Although no soliton solutions exist to the NLSE at normal GVD, another type of solution, a self-similar solution exists. Self-similarity refers to a pulse which is form invariant upon propagation. For the NLSE the form-invariant solution is parabolic [25]:

$$A^2(t,0) = A_0^2\left(1 - (\frac{t}{\tau})^2\right). \tag{1.10}$$

The self-similar propagation of a parabolic pulse in normal dispersion fiber can

be understood intuitively. A parabolic pulse with a parabolic phase profile in the time domain has a parabolic spectrum with a parabolic phase profile in the spectral domain. Group velocity dispersion has the effect of adding a parabolic phase in the spectral domain and self-phase modulation has the effect of adding a parabolic phase in the temporal domain (because the temporal intensity is also parabolic). Therefore, neither effects can change the shape of the pulse or spectrum; the pulse remains parabolic.

While Eq. 1.10 is a solution to the NLSE, it is not a nonlinear attractor. This means that an arbitrary pulse shape will not necessarily evolve into this parabolic pulse shape. This self-similar pulse (or "similariton") only stays parabolic if it starts parabolic. Therefore, this solution alone can not be used to stabilize and form a mode-locked laser. However, as we investigate in detail in chapter 3, it can be an integral part of the evolution in a mode-locked fiber laser with normal GVD fiber [26], which as will be demonstrated, can have its mode-locked stability attributed primarily to dissipative soliton mechanisms.

1.2.5 Amplifier similariton mode-locking

The last of the known major bright pulse solutions to NLSE based equations is also a self-similarly evolving parabola [27]. This solution exists for the case of the NLSE with the addition of linear gain:

$$\frac{\partial A(t,z)}{\partial z} = \frac{g}{2}A(t,z) - \frac{i\beta_2}{2}\frac{\partial^2 A(t,z)}{\partial t^2} + i\gamma|A(t,z)|^2 A(t,z). \tag{1.11}$$

This is the simplest model for a gain fiber in a fiber laser which is why its

self-similar solutions are called amplifier similaritons. The self similar solution can be written exactly:

$$A(z,t) = A_0(z)\sqrt{1-(t/t_0(z))^2}e^{i(a(z)-bt^2)}, \tag{1.12}$$

for $t \leq t_0(z)$. The most important feature of amplifier similaritons is that they are a strong nonlinear attractor. This means that given a close enough initial condition, any pulse form, when seeded into an amplifier must evolve (or be 'attracted') to the self-similar parabolic solution. It follows that the amplifier similariton concept might be useful for mode-locking a laser. That is, if the pulse is always the same parabola at the end of the gain fiber, then the pulse evolves self-consistently around the laser and a mode-locked pulse results. In this case we can no longer assume small changes of the pulse per pass, and the sum of all physical mechanisms in the oscillator is not directly important, but rather only the specific details of the gain fiber which stabilizes the solution. As a consequence, 'averaged-cavity' models like the NLSE, the master-equation, or the CQGLE will not be relevant and a new system of understanding based on local nonlinear attraction in a specific part of the cavity must be developed. Initial developments in this field are presented in chapter 4. Because the sum of all effects is not important, this laser can be built at any net value of GVD, which allows for a large range of tunability for applications. This dispersion-mapped amplifier similariton regime is discussed in section 4.2. Finally, the local attraction mechanism of amplifier similariton mode-locking allows for exotic pulse evolution in the rest of the cavity which can be exploited for its useful features. This phenomena used for ultra-short pulse durations is discussed in section 4.3.

1.3 Fiber laser components and useful implementations

To design high performance mode-locked fiber lasers, it is important to understand the major mode-locking mechanisms. Of course, to implement this knowledge one must also carefully consider the individual components to be used in the system. Along with the physical mechanisms in a fiber (section 1.1), the saturable absorber and the spectral filter are both crucial to high performance fiber laser mode-locking.

1.3.1 Saturable absorbers

As discussed in section 1.2, the saturable absorber (SA) is arguably the most important component for a mode-locked oscillator. The SA works by selectively passing higher intensity light and blocking lower intensity light. This property serves both to build up to a pulse from noise and also to help with the pulse shaping of a mode-locked pulse. To date, there are two long-standing types of saturable absorbers: Semiconductor saturable absorber mirrors (SESAM) and some variation of nonlinear polarization evolution (NPE).

The SESAM consists of a Bragg-mirror on a semiconductor wafer with a saturable absorber semiconductor material [28–30]. If the absorber is sufficiently fast, its reflection can be modeled by:

$$R = 1 - T_0 / \left(1 + \frac{|A(t)|^2}{P_{sat}}\right), \tag{1.13}$$

where T_0 is the unsaturated loss and P_{sat} is the saturation energy. SESAMs allow for stable and consistent mode-locking but are susceptible to damage at high

powers or with extended use.

NPE, the absorber of choice for the research in this thesis, is an ultra-fast passive absorber which relies on the nonlinearity in the fiber for operation. It is highly tunable and exhibits the highest performance for mode-locking but comes at the cost of a difficult theoretical analysis and a strong sensitivity to environmental perturbations.

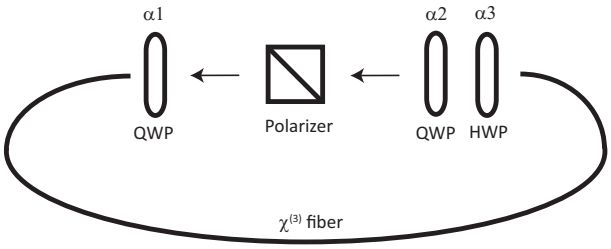

Figure 1.1: Basic schematic for the complete operation of NPE. HWP: half-waveplate and QWP: quarter-waveplate.

With a linear polarization basis, the coupled-mode equations for an arbitrary beat length, L_B, neglecting group-velocity dispersion, loss, and higher order terms is [11]

$$\begin{aligned}\frac{\partial u}{\partial z} &= i\gamma(|u|^2 + \frac{2}{3}|v|^2)u + \frac{i\gamma}{3}u^* v^2 e^{\frac{-4\pi i z}{L_B}} \\ \frac{\partial v}{\partial z} &= i\gamma(|v|^2 + \frac{2}{3}|u|^2)v + \frac{i\gamma}{3}v^* u^2 e^{\frac{4\pi i z}{L_B}}.\end{aligned} \tag{1.14}$$

Adapting a Jones matrix formalism, the waveplates can be represented as

$$HWP[\phi] = \begin{pmatrix} \cos(2\phi) & \sin(2\phi) \\ \sin(2\phi) & -\cos(2\phi) \end{pmatrix}$$

and (1.15)

$$QWP[\phi] = \frac{1-i}{2}\begin{pmatrix} i+\cos(2\phi) & \sin(2\phi) \\ \sin(2\phi) & i-\cos(2\phi) \end{pmatrix}.$$

Eq. 1.14 has a simple solution if $L_B = 0$ or $L_B = \infty$. Because the beat length in typical fibers is ~ 20 m, and typical cavity lengths are about an order of magnitude shorter, $L_B = \infty$ is more appropriate. In this case, Eq. 1.14 becomes

$$\begin{aligned} \frac{\partial u}{\partial z} &= i\gamma(|u|^2 + \frac{2}{3}|v|^2)u + \frac{i\gamma}{3}u^* v^2 \\ \frac{\partial v}{\partial z} &= i\gamma(|v|^2 + \frac{2}{3}|u|^2)v + \frac{i\gamma}{3}v^* u^2, \end{aligned} \tag{1.16}$$

with a solution that gives the Kerr matrix [31]

$$Kerr = e^{i\gamma(|u(0)|^2+|v(0)|^2)L_{eff}} \begin{pmatrix} \cos(\frac{2}{3}\gamma \mathrm{Im}[u(0)v^*(0)]) & \sin(\frac{2}{3}\gamma \mathrm{Im}[u(0)v^*(0)]) \\ -\sin(\frac{2}{3}\gamma \mathrm{Im}[u(0)v^*(0)]) & \cos(\frac{2}{3}\gamma \mathrm{Im}[u(0)v^*(0)]) \end{pmatrix}. \tag{1.17}$$

Without loss of generality, the polarizer can be aligned to the x-axis giving:

$$P = \begin{pmatrix} 1 & 0 \\ 0 & 0 \end{pmatrix}. \tag{1.18}$$

Assuming the light is initially polarized along the x-axis, the light is then operated on by the elements of the oscillator in the order in which they appear in Figure 1.1:

$$\begin{pmatrix} u_{n+1}(t) \\ 0 \end{pmatrix} = P \cdot QWP[\alpha_2] \cdot HWP[\alpha_3] \cdot Kerr \cdot QWP[\alpha_1] \cdot \begin{pmatrix} u_n(t) \\ 0 \end{pmatrix}. \tag{1.19}$$

From here it is straightforward to calculate the effective transmission curve of the NPE:

$$T(I) = \frac{I_{n+1}}{I_n}(I_n) = \frac{|u_{n+1}|^2}{|u_n|^2}(|u_n|^2). \tag{1.20}$$

After some cumbersome transformations and with $\alpha_3^* = 2\alpha_3 - \alpha_1 - \alpha_2$, $T(\alpha_1, \alpha_2, \alpha_3^*, I)_{L_B=\infty}$ can be represented in its fundamental form as

$$T(\alpha_1, \alpha_2, \alpha_3^*, I)_{L_B=\infty} = A + B\cos(\mathrm{I}\omega) + C\sin(\mathrm{I}\omega), \tag{1.21}$$

where

$$\begin{aligned} A &= \frac{1}{8}(4\sin(2\alpha_1)\sin(2\alpha_2) + 4) \\ B &= \frac{1}{2}\cos(2\alpha_1)\cos(2\alpha_2)\cos(2\alpha_3^*) \\ C &= -\frac{1}{2}\cos(2\alpha_1)\cos(2\alpha_2)\sin(2\alpha_3^*) \\ \omega &= \frac{2}{3}\sin(2\alpha_1). \end{aligned} \tag{1.22}$$

Clearly, the resultant transmission function is both a function of the waveplates and the input intensity. If the waveplates are biased correctly, the transmission curve can be biased such that higher intensity has a higher transmission, thus allowing for a pulse to form from noise. In addition, it is also possible to fine-tune the mode-locked pulse state by additionally tuning the wave-plates to achieve maximum performance.

1.3.2 Spectral filters

The use of an additional spectral filter is required for both dissipative soliton and amplifier similariton mode-locking. In this thesis, we make use of two specific types

of spectral filters: a birefringence based filter and a dispersive element/waveguide filter.

Birefringent filter

The birefringent filter is based on the wavelength dependant phase shift that orthogonal polarization states of light accumulate upon propagation through a birefringent material. If light which has a wavelength dependant polarization rotation propagates through a polarizer, it will have a wavelength dependant loss.

The Jones matrix, $M(\lambda, \theta, d)$ for propagation through a birefringent material with arbitrary angle θ of the optical axis from the angle of the input polarization, with ne and no the orthogonal refractive indices, λ the wavelength, and d the thickness of the plate is:

$$M(\lambda,\theta,d) = \begin{pmatrix} e^{\frac{2id\mathrm{ne}\pi}{\lambda}}\cos^2(\theta) + e^{\frac{2id\mathrm{no}\pi}{\lambda}}\sin^2(\theta) & \left(e^{\frac{2id\mathrm{ne}\pi}{\lambda}} - e^{\frac{2id\mathrm{no}\pi}{\lambda}}\right)\cos(\theta)\sin(\theta) \\ \left(e^{\frac{2id\mathrm{ne}\pi}{\lambda}} - e^{\frac{2id\mathrm{no}\pi}{\lambda}}\right)\cos(\theta)\sin(\theta) & e^{\frac{2id\mathrm{no}\pi}{\lambda}}\cos^2(\theta) + e^{\frac{2id\mathrm{ne}\pi}{\lambda}}\sin^2(\theta) \end{pmatrix}. \tag{1.23}$$

After propagation through a polarizer, the transmission as a function of wavelength becomes:

$$T = \left| e^{\frac{2id\mathrm{ne}\pi}{\lambda}}\cos^2(\theta) + e^{\frac{2id\mathrm{no}\pi}{\lambda}}\sin^2(\theta) \right|^2. \tag{1.24}$$

This expresses a sinusoidal spectral filter which has a modulation depth which varies from 100% as the optical axis is tuned from 45°. The Gaussian variation of the modulation depth is depicted in Figure 1.2 for the case of 1-μm wavelength with a crystal quartz birefringent material.

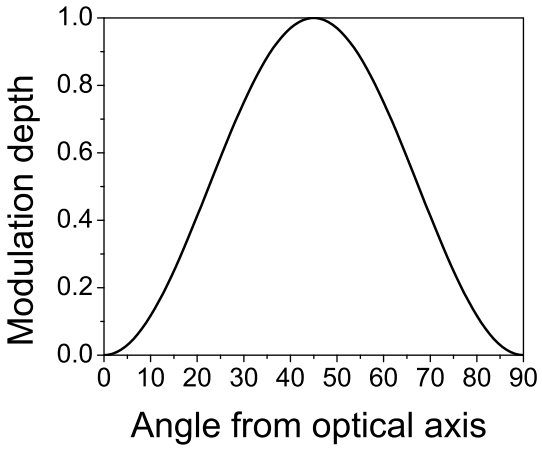

Figure 1.2: Variation of the modulation depth of a birefringent filter as a function of the angle from the optical axis.

In order to determine the bandwidth of the filter, Eq. 1.24 can be simplified if the optical axis is at 45°:

$$T = \cos^2\left(\frac{\pi d(\mathrm{ne} - \mathrm{no})}{\lambda}\right). \tag{1.25}$$

The full-width at half maximum (FWHM) bandwidth of this filter can be calculated numerically and is shown in Figure 1.3 for the case of 1-μm wavelength with crystal quartz birefringent material.

It is also important to be able to tune the center wavelength of the filter. To derive the center wavelength dependence we must take into account the tilt angle of the plate with respect to normal incidence [32]. While the results are too detailed to show here, the conclusion is that for angles near Brewster's angle it is possible to achieve wavelength tunability of one free spectral range of the filter with minimal loss of modulation depth with the optical axis tuned to 45° from the polarizer. This is a simple operational procedure that allows for a high modulation depth, wavelength tunable, smooth sinusoidal spectral filter.

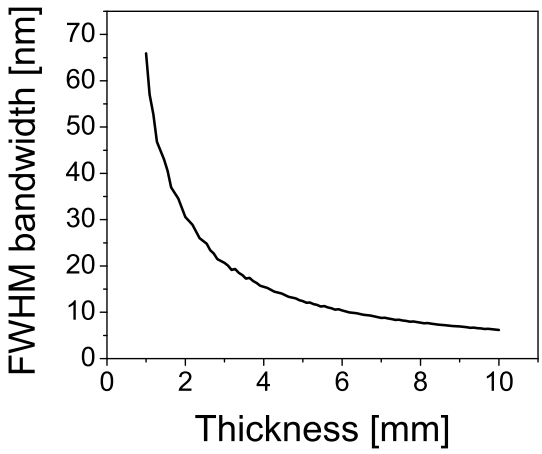

Figure 1.3: Spectral filter bandwidth as a function of plate thickness for 1-μm wavelength with a crystal quartz birefringent material. FWHM: Full-width at half-maximum.

Dispersive element/waveguide filter

While birefringent filters are very nice for their low loss, for narrow filtering, the multiple pass-bands present with sinusoidal filtering can pass unneeded light which can be deleterious for mode-locking. In addition, the exact spectral profile of the filter can be important. For example, for dissipative solitons, the simplest spectral filter model which accounts for all of the key experimental features is a Gaussian, and in fact numerical simulations consistently show better performance with a Gaussian filter. In addition, the smoothness of the filter is important empirically; this underlies the poor performance of off-Gaussian interference filters, for example [33]. These reasons motivate the development of a single-peaked smooth Gaussian filter.

One technique to create a Gaussian filter involves the combination of a dispersive element and a lens and fiber combination (a collimator) as shown in Figure 1.4. The overlap of the wavelength dependant spatial beam with the Gaussian

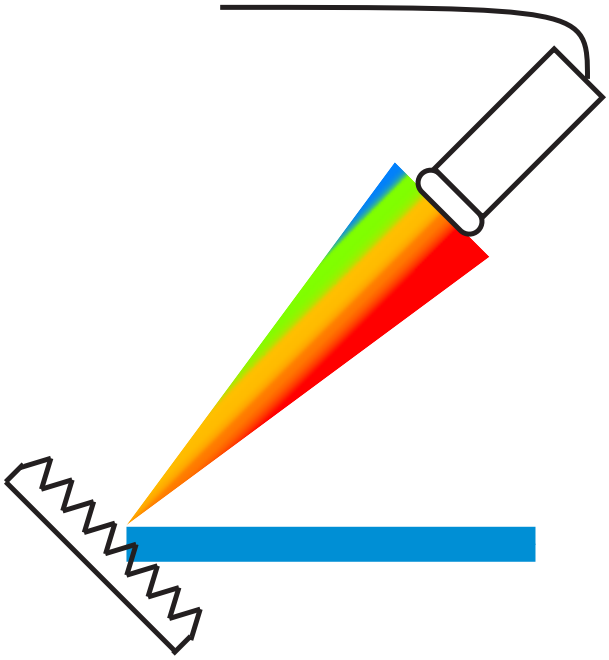

Figure 1.4: Schematic of a dispersive element waveguide filter.

mode of the single-mode fiber results in a spectral filter with a profile of the same form. The bandwidth of the spectral filter is related to the wavelength dependant spreading angle of the dispersive element and the center wavelength can be tuned by offsetting the angle into the collimator. The experimental filter profile is well fit by a Gaussian (Figure 1.5(a)). The bandwidth for several common dispersive elements operating at 1-μm wavelength is shown in Figure 1.5.

The benefits of a smooth Guassian filter with one peak and narrow bandwidths comes at the cost of the loss that comes from the reflection from a grating. However, this loss is typically $\sim 30\%$, which is tolerable for high gain fiber laser systems.

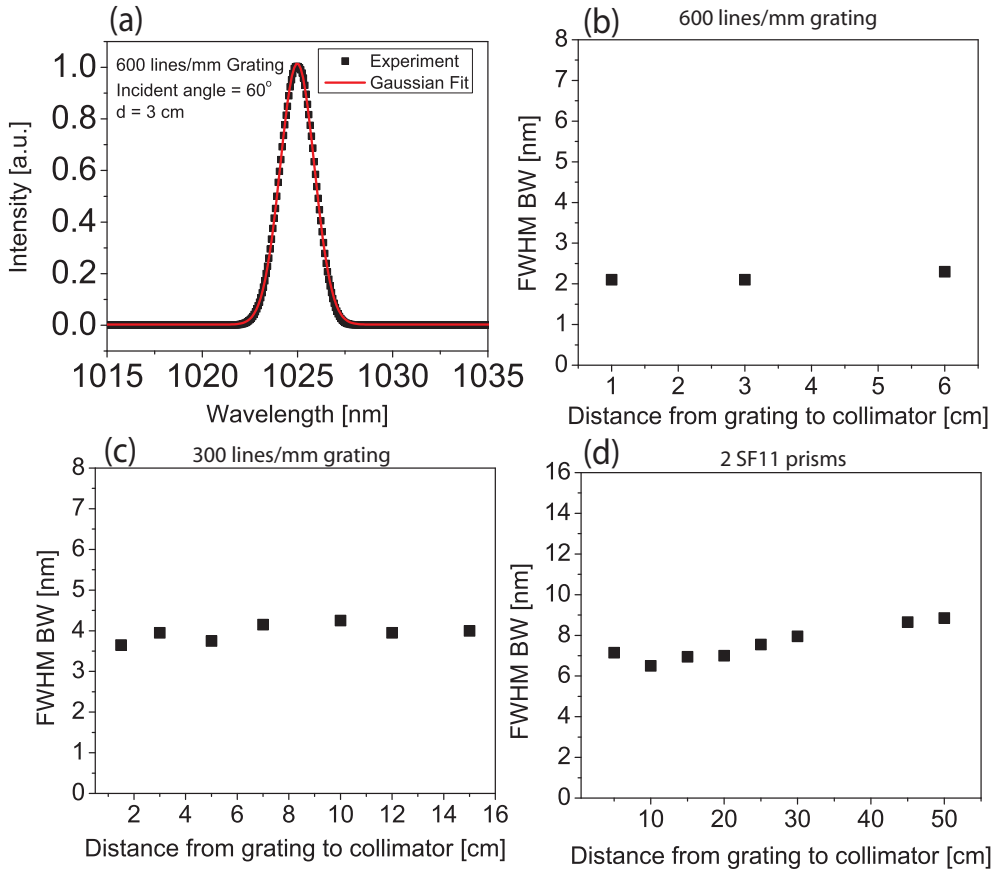

Figure 1.5: (a) Example filter profile; filter bandwidth vs. separation distance for (b) a 600 lines/mm grating, (c) a 300 lines/mm grating and (d) 2 SF11 prisms operating at 1030-nm wavelength.

1.4 Organization of thesis

In chapter 2, the now firmly established dissipative soliton mode-locking regime is analyzed beginning with a comprehensive theoretical framework and moving on to a broad survey of experimental results. The limits to the experimental results are investigated including the development of separate recipes for shorter pulses and higher energies. Then practical extensions are briefly covered, including fiber core-size enhancement techniques as well as methods for creating ultra-robust environmental versions. Finally, the last section details a particular extension of dissipative soliton mode-locking which allows for significant simplification of

chirped-pulse amplification systems.

In chapter 3, the core mechanism for dissipative soliton mode-locking is examined and used to explain two lesser understood mode-locked regimes: passive self-similar mode-locking and stretched dissipative soliton mode-locking. A comprehensive numerical analysis allows for some understanding of the passive similariton in the context of averaged cavity models and stretched dissipative soliton mode-locking is examined theoretically for the first time. The importance of dissipative mechanisms are emphasized and amplifier similariton mode-locking is briefly introduced allowing for a direct comparison of all known mode-locking mechanisms based at normal group-velocity dispersion.

In chapter 4, amplifier similariton mode-locking is investigated for the first time and analyzed as a local nonlinear attraction to the gain section of the oscillator. Experimental results are presented with the goal of both illustrating the concept and for high performance mode-locking. As shown in this chapter, amplifier similariton mode-locking allows for the shortest pulses from a normal dispersion fiber laser. In section 4.2, Amplifier similariton mode-locking is extended by the use of a grating pair for dispersion management. Because mode-locking with this local nonlinear attractor is insensitive to the total cavity GVD, the mode-locked pulses are identical over a wide range of GVD values, from normal through zero to anomalous. This property allows significant tunability for specific performance targets. For example, this technique allows for the highest performance net anomalous dispersion mode-locking as well as the highest performance transform-limited output operation. In section 4.3, amplifier similariton mode-locking is exploited to add a section of fiber into the cavity which allows for significant bandwidth growth. This novel technique allows for the generation of the shortest pulses to date from

a fiber laser and is the clearest illustration of the benefits of amplifier similariton mode-locking.

Finally, in chapter 5, several notable future directions in fiber laser research are identified briefly. In addition, a new mode-locking mechanism which involves the use of dispersion-decreasing fiber is investigated for the possibility of the generation of ever-higher performance mode-locked fiber lasers.

BIBLIOGRAPHY

[1] J. A. der Au, D. Kopf, F. Morier-Genoud, M. Moser, and U. Keller, Opt. Lett. **22**, 307 (1997).

[2] C. Hönninger, F. Morier-Genoud, M. Moser, U. Keller, L. R. Brovelli, and C. Harder, Opt. Lett. **23**, 126 (1998).

[3] F. Druon, F. Balembois, and P. Georges, ANNALES DE CHIMIE-SCIENCE DES MATERIAUX **28**, 47 (2003).

[4] D. E. Spence, P. N. Kean, and W. Sibbett, Opt. Lett. **16**, 42 (1991).

[5] I. N. Duling and M. L. Dennis, in *Compact Sources of Ultrashort Pulses*, edited by I. N. Duling (Cambridge University Press, Cambridge, 1995).

[6] M. Fermann, A. Galvanauskas, G. Sucha, and D. Harter, Applied Physics B: Lasers and Optics **65**, 259 (1997).

[7] D. Jones, H. Haus, L. Nelson, and E. Ippen, IEICE Transactions on Electronics **E81C**, 180 (1998).

[8] A. Galvanauskas, IEEE Journal of Selected Topics in Quantum Electronics **7**, 504 (2001).

[9] J. Limpert, A. Liem, M. Reich, T. Schreiber, S. Nolte, H. Zellmer, A. Tunnermann, J. Broeng, A. Petersson, and C. Jakobsen, Opt. Express **12**, 1313 (2004).

[10] P. Dupriez, A. Piper, A. Malinowski, J. Sahu, M. Ibsen, B. Thomsen, Y. Jeong, L. Hickey, M. Zervas, J. Nilsson, and D. Richardson, IEEE Photonics Technology Letters **18**, 1013 (2006).

[11] G. P. Agrawal, *Nonlinear Fiber Optics*, 3rd ed. (Academic Press, New York, 2001).

[12] R. D. Boyd, *Nonlinear Optics, 2nd Ed.* (Academic Press, New York, 2003).

[13] P. V. Mamyshev and S. V. Chernikov, Opt. Lett. **15**, 1076 (1990).

[14] H. A. Haus, Selected Topics in Quantum Electronics, IEEE Journal of **6**, 1173 (2000).

[15] H. A. Haus, J. G. Fujimoto, and E. P. Ippen, J. Opt. Soc. Am. B **8**, 2068 (1991).

[16] L. Mollenauer and R. H. Stolen, Opt. Lett. **9**, 13 (1984).

[17] K. Suzuki, M. Nakazawa, and H. A. Haus, Jpn. J. Appl. Phys. **28**, 256 (1989).

[18] D. J. Richardson, R. I. Laming, D. N. Payne, M. W. Phillips, and V. J. Matsas, Electronics Letters **27**, 730 (1991).

[19] I. N. Duling, Electron. Lett. **27**, 544 (1991).

[20] H. Haus, E. Ippen, and K. Tamura, IEEE Journal of Quantum Electronics **30**, 200 (1994).

[21] K. Tamura, E. P. Ippen, H. A. Haus, and L. E. Nelson, Opt. Lett. **18**, 1080 (1993).

[22] M. H. Ober, M. Hofer, and M. E. Fermann, Opt. Lett. **18**, 367 (1993).

[23] B. Malomed, *Soliton Management in Periodic Systems* (Springer Science+Business Media, New York, 2006).

[24] S. Namiki and H. A. Haus, IEEE J. Quantum Electron. **33**, 649 (1997).

[25] D. Anderson, M. Desaix, M. Karlsson, M. Lisak, and M. L. Quiroga-Teixeiro, J. Opt. Soc. Am. B **10**, 1185 (1993).

[26] F. O. Ilday, J. R. Buckley, W. G. Clark, and F. W. Wise, Phys. Rev. Lett. **92**, 213902 (2004).

[27] M. E. Fermann, V. I. Kruglov, B. C. Thomsen, J. M. Dudley, and J. D. Harvey, Phys. Rev. Lett. **84**, 6010 (2000).

[28] U. Keller, K. J. Weingarten, F. X. Kartner, D. Kopf, B. Braun, I. D. Jung, R. Fluck, C. Honninger, N. Matuschek, and J. der Au, Selected Topics in Quantum Electronics, IEEE Journal of **2**, 435 (1996).

[29] O. Okhotnikov, A. Grudinin, and M. Pessa, New Journal of Physics **6**, 177 (2004).

[30] C. J. Saraceno, C. Schriber, M. Mangold, M. Hoffmann, O. H. Heckl, C. R. Baer, M. Golling, T. Su anddmeyer, and U. Keller, Selected Topics in Quantum Electronics, IEEE Journal of **18**, 29 (2012).

[31] A. Komarov, H. Leblond, and F. b. c. Sanchez, Phys. Rev. A **71**, 53809 (2005).

[32] J. Mentel, E. Schmidt, and T. Mavrudis, Appl. Opt. **31**, 5022 (1992).

[33] C. Y. Chong, Ph.D. thesis, 2008.

CHAPTER 2

DISSIPATIVE SOLITON FIBER LASERS[1]

2.1 Introduction

Advances in pulse-propagation physics in the past few years [2–4] have enabled order-of-magnitude increases in the pulse energy and peak power from femtosecond fiber lasers. As a result, it is now realistic to design oscillators based on ordinary single-mode fiber (SMF) that can compete with the performance of solid-state lasers.

In general, a femtosecond laser has segments or components with both normal and anomalous GVD. The net or average GVD can be normal or anomalous. When the net GVD is anomalous, the pulse-shaping is soliton-like as the nonlinearity balances the GVD in an average sense. This is the case in standard Ti:sapphire lasers, e.g., although the breathing is weak because the cavity contains much less than one dispersion length of material for all but the shortest pulses. Since the demonstration in 1984 that prism pairs can provide adjustable anomalous GVD with low loss [5], virtually all femtosecond lasers have included anomalous-dispersion segments or components.

The stable pulse energy increases as the dispersion of the laser cavity varies from large and anomalous to zero, and then to large and normal. This trend could be extended by removing the anomalous-dispersion segment from the laser. However, solitons are obviously then impossible. Thus, it is not clear how to generate stable, high-quality pulses. As mentioned above, it has become conventional wisdom

[1]The majority of this chapter is published in pages 97-130 of Ref. [1].

that a femtosecond-pulse laser requires intracavity dispersion control or anomalous dispersion.

Since 2006, our group has demonstrated theoretically and experimentally that a new kind of soliton can in fact form in a fiber laser with only normal-dispersion components[2]. The dominant pulse-shaping mechanism is filtering of a highly-chirped pulse in the cavity. The chirped pulses can be stable with very high energies, and can be compressed to the transform limit outside the laser. Numerical and analytical theories show that the pulses balance amplitude and phase modulations, i.e., dissipation is central to their existence. These so-called dissipative solitons represent a new class of laser pulses with remarkable scientific properties, potential for extremely high energy and peak power, and substantial practical benefits.

2.2 Theory: analytic approach

In this section, we determine a suitable analytic model for a general understanding of normal-dispersion pulse-shaping and mode-locking [4].

2.2.1 Theory

In general, the physical mechanisms that affect the pulse in a fiber laser are not uniformly distributed around the oscillator. However, to make initial analytic progress, we look to model the "average" behavior of a real cavity with a pulse propagation equation with constant coefficients [4, 6] (see Ref. [7] for a theoretical extension to variable coefficients). Femtosecond pulse propagation in a dis-

[2]Such a laser is sometimes referred to as an all-normal-dispersion (ANDi) laser.

persive, electronic Kerr medium can be modeled with the nonlinear Schrodinger equation. Fiber lasers also feature linear gain, some spectral filtering, and an intensity-dependent amplitude modulation, to promote the pulse from noise.

A well-know equation that models this behavior is the cubic-Ginzburg Landau equation (CGLE),which is referred to as the master-equation when used to model laser cavities [6]. The chirped hyperbolic-secant solution of the CGLE has found wide use in the modeling of mode-locked lasers. However, the known solutions of the CGLE fail to account for even qualitative aspects of fiber lasers with large normal GVD, such as the observed spectral shapes, the pulse chirp, stability and a multiplicity of solutions with identical energy. Therefore, we examine the next well-studied equation which can be used to model pulse propagation in the oscillator, the cubic-quintic Ginzburg-Landau equation (CQGLE):

$$\frac{\partial U(z,t)}{\partial z} = gU(z,t)+(\frac{1}{\Omega}-i\frac{D}{2})\frac{\partial^2 U(z,t)}{\partial t^2}+(\alpha+i\gamma)|U(z,t)|^2U(z,t)+\delta|U(z,t)|^4U(z,t), \tag{2.1}$$

where U is the electric field envelope, t is the time from the center of the pulse, z is the propagation coordinate, g is the linear gain, Ω is related to the filter bandwidth, D is the GVD, γ is electronic Kerr nonlinear coefficient, and α and δ are the cubic and quintic saturable absorber terms. Several groups have employed the CQGLE to model fiber lasers with nonlinear polarization evolution [8–11], primarily through numerical solutions. In particular, Akhmediev and co-workers have done much in this area. They recently investigated stable solutions to the CQGLE and determined that along certain lines of parameter space, the pulse energy increases without bound [12, 13]. Komarov et al. showed theoretically that careful filtering can control harmonic mode-locking under some conditions [14].

While the general solution to Eq. 2.1 is not known, a well-known particular solution [15, 16] exists,

$$U(t,z) = \sqrt{\frac{A}{\cosh\left(\frac{t}{\tau}\right) + B}} e^{-i\frac{\beta}{2}\ln\left(\cosh\left(\frac{t}{\tau}\right)+B\right)+i\theta z}. \tag{2.2}$$

A, B, τ, β, and θ are real constants. Because it is only a particular solution, Eq. 2.2 satisfies Eq. 2.1 with an additional constraint on one of the system parameters, α, whereas a larger range of α values give rise to stable solutions in the general solution. Two sets of solutions exist to the six algebraic equations which result from inserting Eq. 2.2 into Eq. 2.1 and separately satisfying the real and imaginary parts. However, one set requires $g > 0$, which we ignore as they will be unstable against the growth of the continuous-wave background.

The energy of the pulse is calculated as the integral over time of the intensity profile and it is reasonable to assume that we have direct experimental control of the pulse energy via the pump. Since varying B changes the pulse energy, we treat B as a system parameter (controlled by the pump) and solve instead for g, which is assumed to be set by the requirements for lasing. The resulting expressions are:

$$
\begin{aligned}
\alpha &= \frac{\gamma\left(3\Delta+4\right)}{D\Omega} \\
A &= -\frac{2\left(B^2-1\right)\gamma\left(\Delta+2\right)}{BD\delta\Omega} \\
\tau^2 &= -\frac{B^2\delta\left(D^2\left(\Delta-8\right)\Omega^2+12\left(\Delta-4\right)\right)}{24\left(B^2-1\right)\gamma^2\Omega\left(D^2\Omega^2+4\right)} \\
\beta &= \frac{\Delta-4}{D\Omega} \\
g &= -\frac{6\left(B^2-1\right)\gamma^2\left(D^2\Omega^2+4\right)\left(-\frac{8(\Delta-4)}{D^2\Omega^2}-\Delta+6\right)}{B^2\delta\left(D^2\left(\Delta-8\right)\Omega^2+12\left(\Delta-4\right)\right)} \\
\theta &= -\frac{2(B^2-1)\gamma^2\left(\Delta+2\right)}{B^2D\delta\Omega} \\
\Delta &= \sqrt{3D^2\Omega^2+16}.
\end{aligned}
\tag{2.3}
$$

First we note that, if the other system parameters are constant, both pulse duration and energy increase as a function of net GVD (Figure 2.1(a)). In addition, the minimum pulse duration occurs at zero GVD. These are important results because they align with the dominant results of the master-equation theory, which is known to be an accurate qualitative predictor for laser cavities [6]. Thus, these trends have also been verified experimentally. Now, with the introduction of the quintic nonlinear absorption coefficient, δ, we find new behavior. The pulse parameter B is particularly important for examining this new behavior as it differentiates the pulse from the master-equation solution. For $\delta > 0$, increasing the energy produces steep-sided spectra with a dip in the middle (Figure 2.2(a)). For $\delta < 0$, increasing the energy produces narrower spectra and longer, flatter pulses in the time domain (Figure 2.2(b)). These have previously been identified as "flat-top solutions" [17]. As the energy approaches a maximum at B=-1 (Figure 2.1(b)) (at which point the solution diverges), the spectra exhibit deep fringes (Figure 2.2(a)).

In agreement with experiments, pulses in the normal GVD regime are highly-chirped. The bottom row of Figure 2.2 shows the autocorrelations that result from

impressing a quadratic spectral phase on the pulses to minimize the duration, as is done in the laboratory. With increasing B, the linear component of the pulse chirp increases (Figure 2.1(d)). The pulse with B=35 is long enough to measure directly, and we show the theoretical intensity profile instead of the autocorrelation.

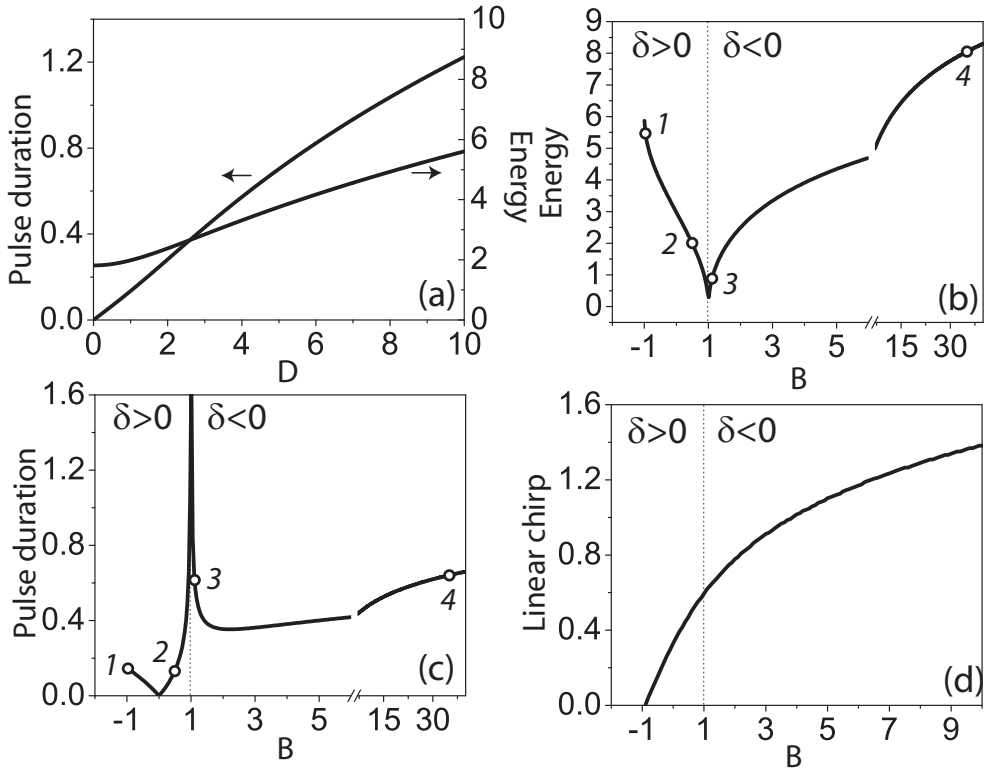

Figure 2.1: (a) Pulse duration and energy plotted vs. GVD parameter D. (b) Energy, (c) pulse duration, and (d) chirp (normalized to that of the pulse with B=-0.9) plotted vs. B. Dotted lines separate the two classes of solutions. Italicized numbers correspond to solutions shown in Figure 2.2. Notice the break in the x-axes in (b) and (c). Figure taken from Ref. [4].

For experimental observation, a model must produce sufficiently stable solutions. A thorough numerical study of the existence and stability of pulse solutions to the CQGLE has been performed for $\delta < 0$ [16]. While numerical solutions are stable for a large region of parameter space, Eq. 2.2 is stable for only one point (corresponding to a pulse as in Figure 2.2(b)). The analytic solution is unstable against collapse for $\delta > 0$, and as a result it has been left unexplored. Remarkably,

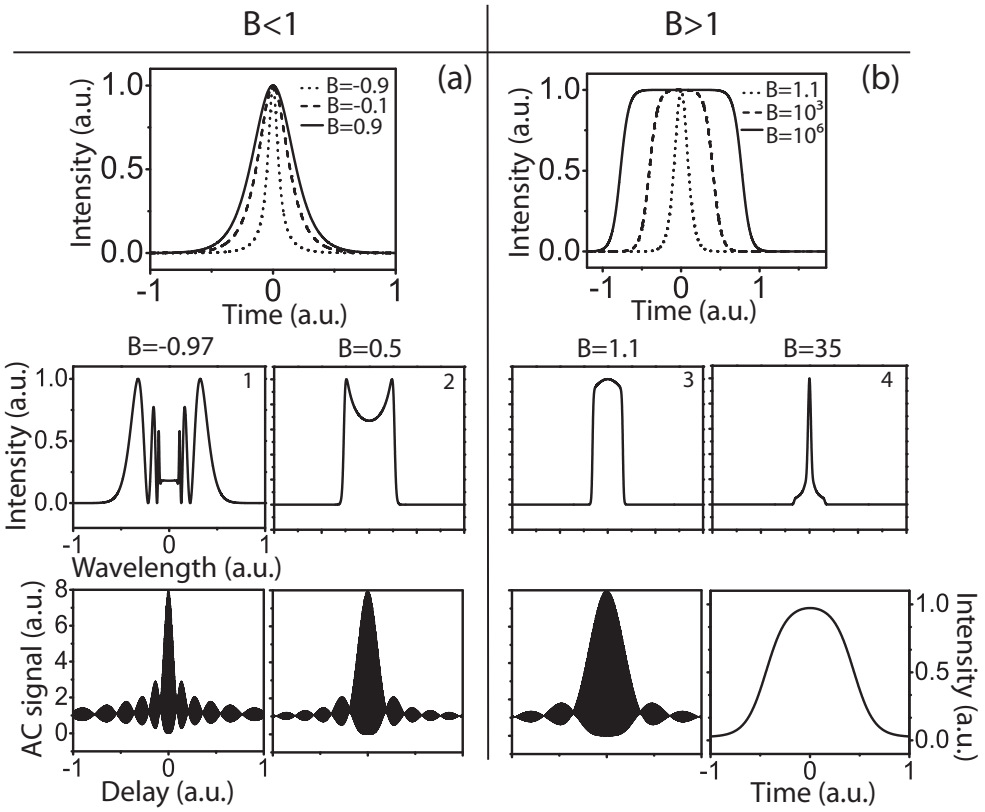

Figure 2.2: Pulse solutions categorized by the value of B. Top row: temporal profiles. Middle row: representative spectral shapes for the indicated values of B. Bottom row: corresponding autocorrelations of the respective dechirped analytical solutions. The intensity profile is shown for B=35. Figure taken from Ref. [4].

solutions represented by both $\delta > 0$ and $\delta < 0$ are stable in the normal dispersion laser. Plausible mechanisms for this stability include (1) gain saturation, which is known to stabilize pulses and is lacking from the model and (2) the possibility that the experimental saturable absorption may well be modeled by terms above the quintic, which could be negative and function as stabilizing coefficients.

2.2.2 Experimental results

We will first use a specific example to introduce the main features of normal-dispersion lasers. A simple and robust manifestation of a dissipative soliton laser

(shown schematically in Figure 2.3) is similar to previous Yb-doped lasers (e.g. see Ref. [18]) but without the grating pair that provides anomalous GVD. The fiber section consists of 3 m of SMF preceding 60 cm of highly-doped Yb gain fiber, which is followed by another 1 m of SMF. The total cavity dispersion is ~ 0.1 ps^2. Nonlinear polarization evolution (NPE) is employed as the saturable absorber, and is implemented with quarter-wave plates, a half-wave plate, and a polarizing beam-splitter. A birefringent filter centered at 1030 nm, with 12-nm bandwidth, is placed after the beam splitter. The output of the laser is taken directly from this beam-splitter for maximum efficiency.

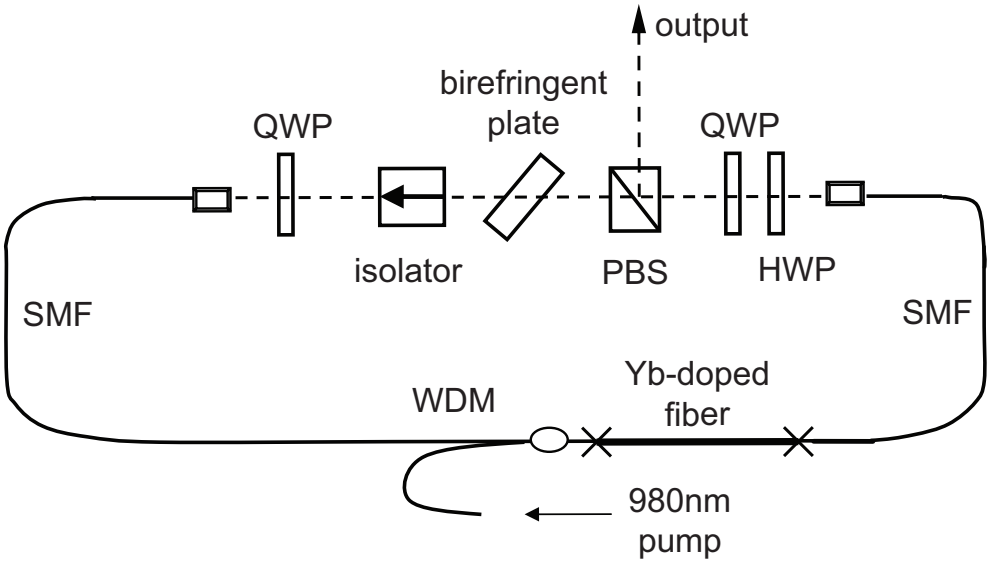

Figure 2.3: Schematic of the experimental setup; PBS: polarization beam splitter; HWP: half-wave plate; QWP: quarter-wave plate; WDM: wavelength division multiplexer.

Self-starting mode-locked operation is achieved by adjustment of the wave plates. Stable single-pulsing is verified with a fast detector with 30-ps resolution, and by monitoring the interferometric autocorrelation out to delays of ~100 ps. Also, the spectrum is carefully monitored for any modulation that would be consistent with multiple pulses in the cavity.

Typical results for the output of the laser are shown in Figure 2.4. The spectrum (Figure 2.4(a)) is consistent with significant SPM within the cavity. The laser generates ∼1-ps chirped pulses, which are dechirped to 195 fs (Figure 2.4(b)) with a pair of diffraction gratings outside the laser. The dechirped pulse duration is within 15% of the Fourier-transform limit. The interferometric autocorrelation shows noticeable side-lobes, which arise from the steep sides and structure of the spectrum. Nevertheless, these amount to only ∼ 10% of the pulse energy. The output pulse energy is 2.5 nJ, and after dechirping with lossy gratings the pulse energy is 1 nJ. The laser is stable and self-starting.

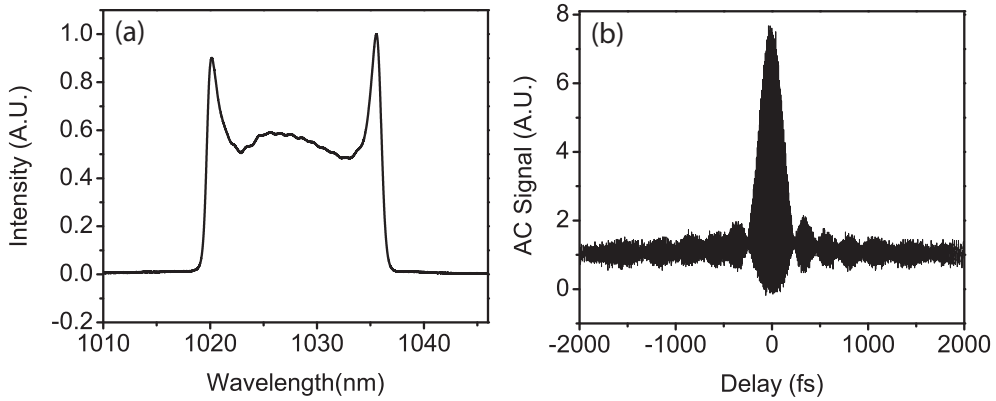

Figure 2.4: (a) Output spectrum and (b) autocorrelation of the dechirped pulse.

The behavior of the laser depends critically on the spectral filter: without it, stable pulse trains are not generated. In some cavities, mode-locking is possible without a filter, but the pulse duration tends to be long (>500 fs) [19, 20]. Important pulse parameters such as bandwidth, pulse duration, chirp, spectral shape and energy can vary over a large range with the variation of the wave plates, pump power, fiber lengths, and filter characteristic. We experimentally access different operating states of the laser via adjustments to the wave plates, the pump power, and the cavity length. These adjustments effectively vary the cubic and quintic saturable absorber terms, the pulse energy, and the GVD, respectively.

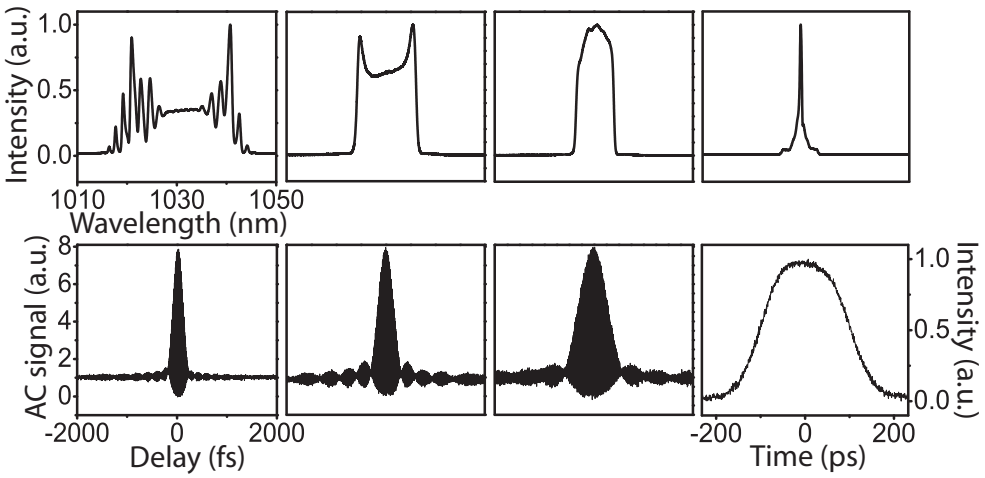

Figure 2.5: Top row: representative experimental spectra corresponding to the theoretical pulses of Figure 2.2. Bottom row: autocorrelation data for the corresponding dechirped pulses. The rightmost pulse is the respective output intensity profile. Figure taken from Ref. [4].

A representative survey of mode-locked outputs is shown in Figure 2.5. The experimental spectra have the same features of the predicted spectra (Figure 2.2), which is remarkable considering the complicated profiles, none of which had been observed previously from mode-locked lasers. However, the spectra in Figure 2.2 are plotted with $\beta = 10$, a factor of 7 from the theoretical value, which is typical of the quantitative agreement with the CQGLE. The range in which the solution lies is determined by the saturable absorber, which is controlled by the wave plates. The dechirped autocorrelations (bottom row of Figure 2.5) agree with the calculated versions (bottom row of Figure 2.2). The experimental chirp values increase monotonically (from 0.084 ps^2 to >10 ps^2) from left to right, as predicted (Figure 2.1(d)). Finally, the measured energies of the pulses shown in Figure 2.5 also follow the theoretical trend of Figure 2.1(b) with 4, 3, 2, and 8 nJ from left to right.

Accurate modeling of the normal-dispersion fiber laser by the analytic solution of the CQGLE confirms the dominant role of dissipative processes in the pulse shaping. From this point of view, it is appropriate to refer to lasers with this pulse

evolution (weakly-breathing and highly-chirped pulses) as dissipative-soliton fiber lasers. "Dissipative" refers to the fact that the system is not conservative, and not to dissipation or decay of the pulse itself. Energy flows through a dissipative soliton. In addition, thanks to the agreement with the analytical solutions of the CQGLE, the dissipative soliton laser constitutes a practical, robust and dynamic test-bed for studying stable solutions to the GLE and to its variants. Dissipative solitons theoretically exist in a diverse range of settings [21, 22], but experimental observations that highlight the distinctions from other solitons are still rare, particularly in optical physics [23–25]. Normal-dispersion fiber lasers provide a convenient and powerful setting for the study of this class of solitary wave.

2.3 Theory: simulations

While the analytic analysis of section 2.2. is useful for large-scale understanding and design, numerical simulations are used to refine and further understand the dissipative soliton laser [26]. In particular, with simulations we can investigate the evolution of the pulses within one round trip of the oscillator (section 2.3.1) and add quantitative information to the variation of important parameters (section 2.3.2). Relevant results are confirmed experimentally (section 2.3.3).

2.3.1 Temporal evolution

To investigate the temporal evolution of the pulses inside the cavity, we simulate the cavity of the example in section 2.2.2. The pulse propagation within a general fiber is modeled by a reduced version of Eq. 2.1:

$$\frac{\partial U(z,t)}{\partial z} = g(E_{pulse})U(z,t) - i\frac{D}{2}\frac{\partial^2 U(z,t)}{\partial t^2} + i\gamma|U(z,t)|^2 U(z,t). \tag{2.4}$$

$D = 230$ fs^2/cm and $\gamma = 0.0047$ (Wm)$^{-1}$ and in the Yb-doped gain fiber there is an additional saturating gain, $g(E_{pulse}) = g_0/(1 + E_{pulse}/E_{sat})$, where g_0 corresponds to 30 dB of small-signal gain, $E_{pulse} = \int_{-T_{R/2}}^{T_{R/2}} |U(z,t)|^2 dt$, where T_R is the cavity round trip time and E_{sat} is the gain saturation energy (varied from 0.25 nJ to 6 nJ). A Lorentzian gain shape with 100-nm bandwidth is assumed. The fiber is followed by a saturable absorber modeled by a monotonically-increasing transfer function, $T = 1 - l_0/(1 + P_0/P_{sat})$ where $l_0 = 0.7$ is the unsaturated loss, P_0 is the instantaneous pulse power and P_{sat} is the saturation power. Mode-locking is rarely affected by a change in P_{sat} and as a consequence, the effects of the saturable absorber are not a focus of this work. To this end, P_{sat} is adjusted (from 0.1 to 2.4 kW) so that the relative transmission of the peak to the wings of the pulse is the same regardless of the energy. A Gaussian spectral filter is placed after the saturable absorber, and the filter bandwidth is varied from 8 nm to 25 nm. A $\sim 70\%$ output coupler is located between the saturable absorber and the spectral filter. The governing equations are solved with a standard symmetric split-step propagation algorithm and are run until the energy converges to a constant value.

The typical spectral and temporal evolution of a dissipative soliton are depicted in Figure 2.6. All of the spectra exhibit the steep edges predicted by the analytical treatment from section 2.2. After traversing the spectral filter, the spectrum acquires a Gaussian-shaped top that follows the filter transmission curve. Small spectral broadening is observed in the first SMF and the gain fiber. Nonlinear phase is accumulated after the pulse has been amplified in the gain fiber, and this produces sharp peaks at the edges of the spectrum. The spectral filter, and to a

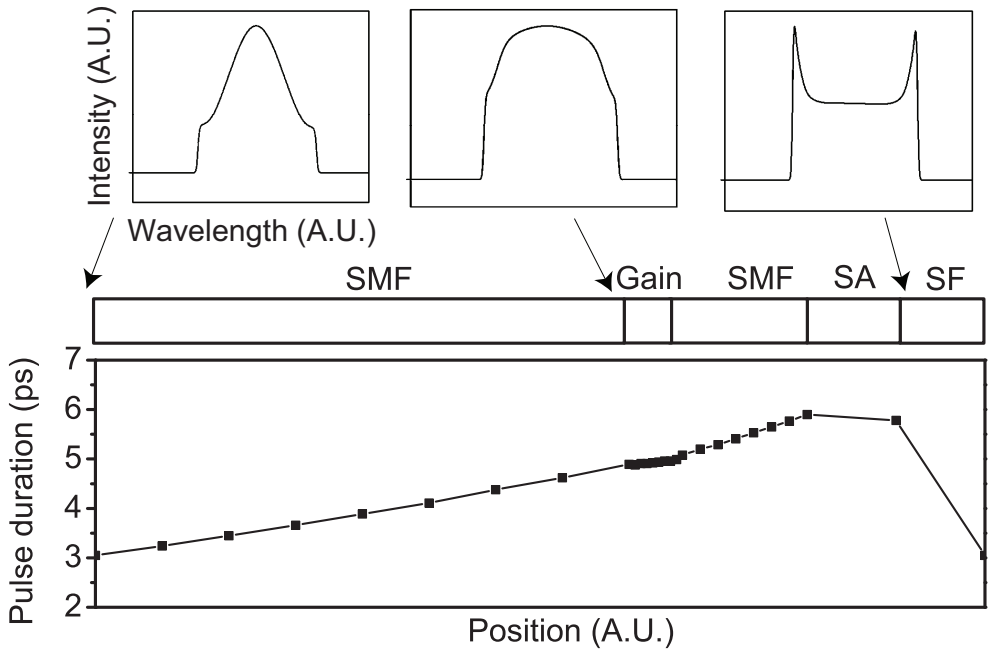

Figure 2.6: Temporal and spectral evolution of a typical numerically simulated dissipative soliton fiber laser; SA: saturable absorber, SF: spectral filter.

lesser degree the saturable absorber, cut off the peaks and return the spectrum to its original shape.

The pulse duration increases monotonically in the fiber sections and after a slight and predictable decrease from the saturable absorber, the spectral filter restores the pulse to its original duration. The analytic theory, numerical simulations, and experiments, all show that the pulse is highly chirped in all sections of the cavity. As a consequence, the spectral filter, rather than increasing the pulse duration as in the case of a transform-limited pulse, decreases the pulse duration. The filter dominates the pulse-shaping and underlies the self-consistency of the solutions in the dissipative soliton laser. For further investigation into pulse-shaping and evolution in normal dispersion fiber lasers, see chapter 3.

2.3.2 Variation of laser parameters

The three most relevant system parameters for the control of the intra-cavity pulse evolution and characteristics are the nonlinear phase (Φ_{NL}), the spectral filter bandwidth, and the GVD. In this section, we describe the effects of each parameter. Interestingly, the qualitative behavior and performance of the laser vary similarly regardless of which parameter is varied.

A reference condition is based on the cavity simulated to show the pulse evolution with the following details: 60 cm of gain follows 3 m of SMF and precedes 1 m of SMF, the Gaussian shaped spectral filter has an 8-nm full-width at half-maximum (FWHM) bandwidth, and the pulse energy is reduced by an additional 10% after the output coupler to account for other losses.

Nonlinear phase shift

The simplest parameter to tune in the laser is the pump power, which controls the pulse energy, which in turn has a direct effect on the Φ_{NL} accumulated by the pulse. The performance of the dissipative soliton fiber laser changes extensively as Φ_{NL} varies. It is worth noting that Φ_{NL} can also be varied by changing the output coupling or the fiber lengths, and will have the same effects, but that control of the pump allows for a convenient way to keep the other parameters constant. With a gradual increase in the pump power, the output spectra display a clear variation (Figure 2.7).

As Φ_{NL} increases, the spectrum broadens and develops sharp peaks around its edges (Figure 2.7(b)). With larger Φ_{NL}, the spectrum broadens further and eventually develops structure or fringes (Figure 2.7(d)). The output spectral bandwidth

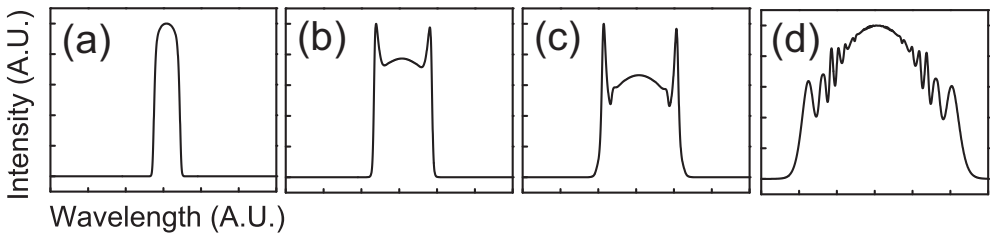

Figure 2.7: Output spectrum with Φ_{NL}: (a) $\sim 1\pi$, (b) $\sim 4\pi$, (c) $\sim 7\pi$, (d) $\sim 16\pi$. Figure taken from Ref. [26].

with $\Phi_{NL} = 16\pi$ is about 6 times larger than that with $\Phi_{NL} = \pi$. Even with Φ_{NL} as large as 10π or more, the output pulse can be dechirped to very close to the transform limit. For example, the pulse with $\Phi_{NL} = 16\pi$ (7π) can be dechirped with a linear dispersive delay to only $\sim 20\%$ (10%) beyond the transform limit.

The dependence of the laser output parameters on Φ_{NL} is summarized in Figure 2.8. The pulse energy increases with Φ_{NL}, as expected (Figure 2.8(a)). The breathing ratio (ratio of maximum and minimum pulse durations in the cavity) increases from $\sim$1 to $\sim$4 as Φ_{NL} increases (Figure 2.8(b)). The spectral amplitude modulation is larger when the output spectral bandwidth is much larger than the filter bandwidth (e.g. $\sim$5 times larger in Figure 2.7(d)) . Since the pulse is highly chirped, strong spectral amplitude modulation translates to strong modulation in the time domain, and thereby a large breathing ratio.

The dechirped pulse duration is inversely proportional to the spectral bandwidth (Figure 2.8(c) is a graphical representation of the bandwidth increase seen in Figure 2.7). Finally, the pulse chirp (the magnitude of anomalous GVD required to dechirp the output pulse to its maximum peak power) decreases as Φ_{NL} increases (Figure 2.8(d)). This indicates that the accumulation of nonlinear phase tends to cancel some of the phase accumulated by the normal GVD of the fiber.

A final point is that stable pulses are found for remarkably-large nonlinear

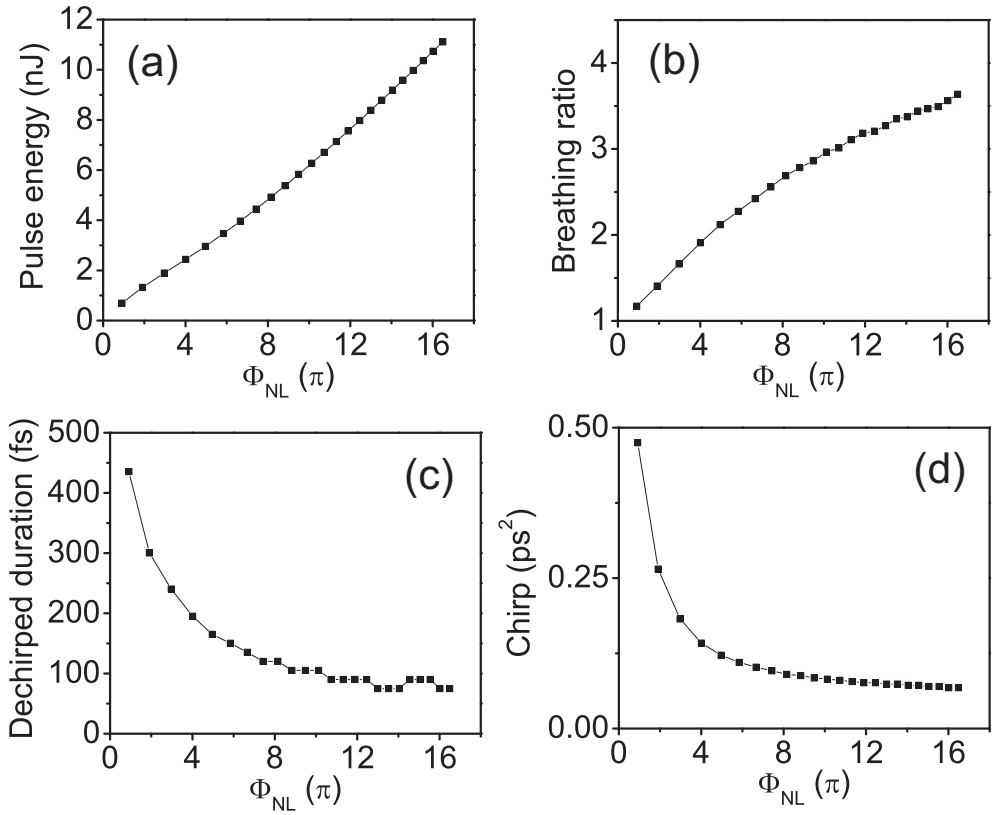

Figure 2.8: Laser performance vs. Φ_{NL}: (a) pulse energy, (b) breathing ratio, (c) dechirped pulse duration, (d) chirp. Figure taken from Ref. [26].

phase shifts. Values of Φ_{NL} up to 20π are observed in the simulations (Figure 2.8), and these will translate directly into high pulse energies, to be discussed below.

Spectral filter bandwidth

Reduction of the filter bandwidth from a reference condition corresponding to the spectrum in Figure 2.7(d), keeping the other parameters constant, produces the same qualitative trend as increasing Φ_{NL} (compare Figure 2.7 and 2.9).

In fact, the variation of the other parameters as the filter bandwidth decreases is also qualitatively similar to the case of increasing Φ_{NL} (Figure 2.10). Notice that the variation of energy is omitted as the energy is held constant to keep Φ_{NL}

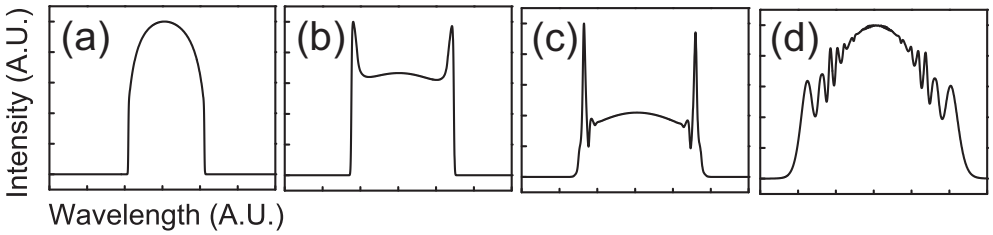

Figure 2.9: Output spectrum with spectral filter bandwidth: (a) 25 nm, (b) 15 nm, (c) 12 nm, (d) 8 nm. Figure taken from Ref. [26].

constant.

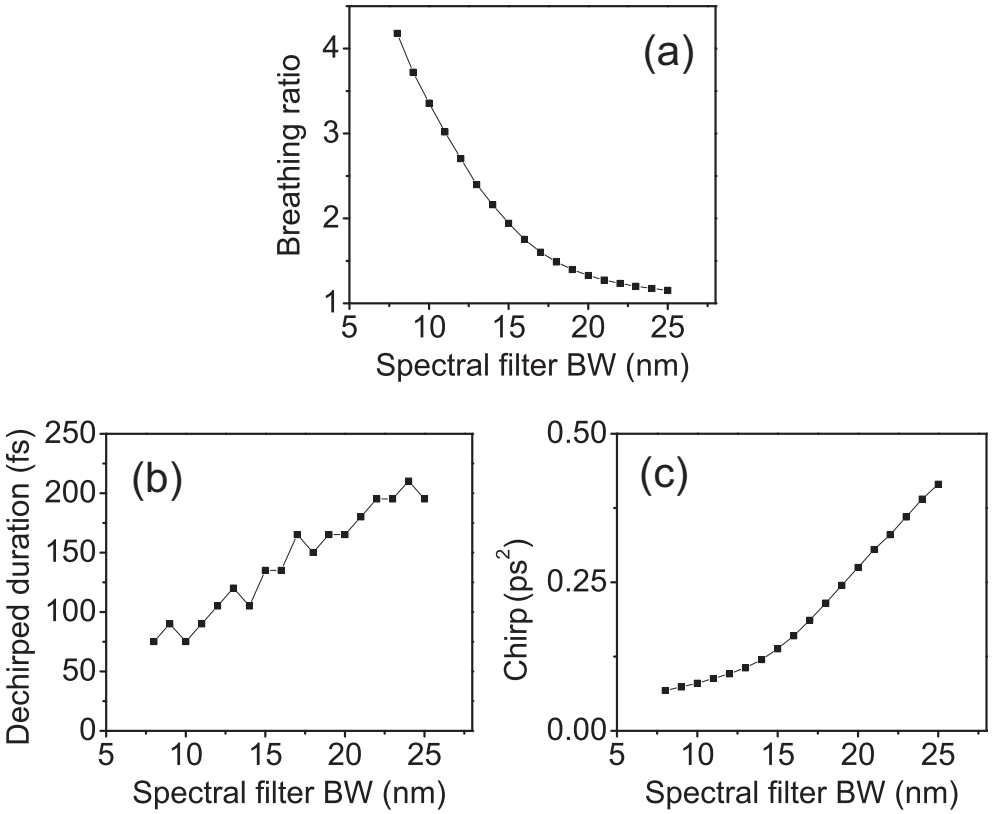

Figure 2.10: Laser performance vs. spectral filter bandwidth: (a) breathing ratio, (b) dechirped pulse duration, (c) chirp. Figure taken from Ref. [26].

Group-velocity dispersion

GVD is varied by increasing the length of the first segment of SMF, starting from the reference condition corresponding to the spectrum in Figure 2.7(d). The GVD

was varied from ~ 0.1 ps^2 to $\sim$0.5 ps^2 , while other parameters are held constant. Again the resulting trend when GVD decreases is similar to those obtained by increasing Φ_{NL} or decreasing the filter bandwidth (Figure 2.11).

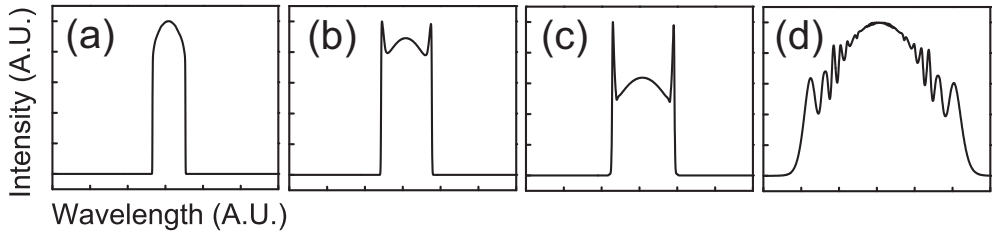

Figure 2.11: Output spectrum with GVD: (a) 0.52 ps^2, (b) 0.31 ps^2, (c) 0.24 ps^2, (d) 0.10 ps^2. Figure taken from Ref. [26].

The variation of the other parameters is also qualitatively similar to the case of increasing Φ_{NL} or decreasing the filter bandwidth (Figure 2.12). The energy is again omitted because it is a controlled variable.

Summary of the effects of laser parameters

In summary, the output spectral shape evolves gradually from a smooth narrow spectrum (Figure 2.13A) to a fringed and broadened spectrum (Figure 2.13B) with decreasing spectral filter bandwidth, decreasing GVD, or increasing Φ_{NL}. More generally, all simulated spectral fall somewhere between spectra A and B in Figure 2.13. This conclusion is consistent with the results of the analytical investigation. The variation of spectral shapes can be described by a variation in the value of the parameter B, which in turn produces variation in other pulse parameters such as the energy and chirp. In fact, the energy increases and the chirp decreases when B goes toward -1, just as in the results shown in the simulations.

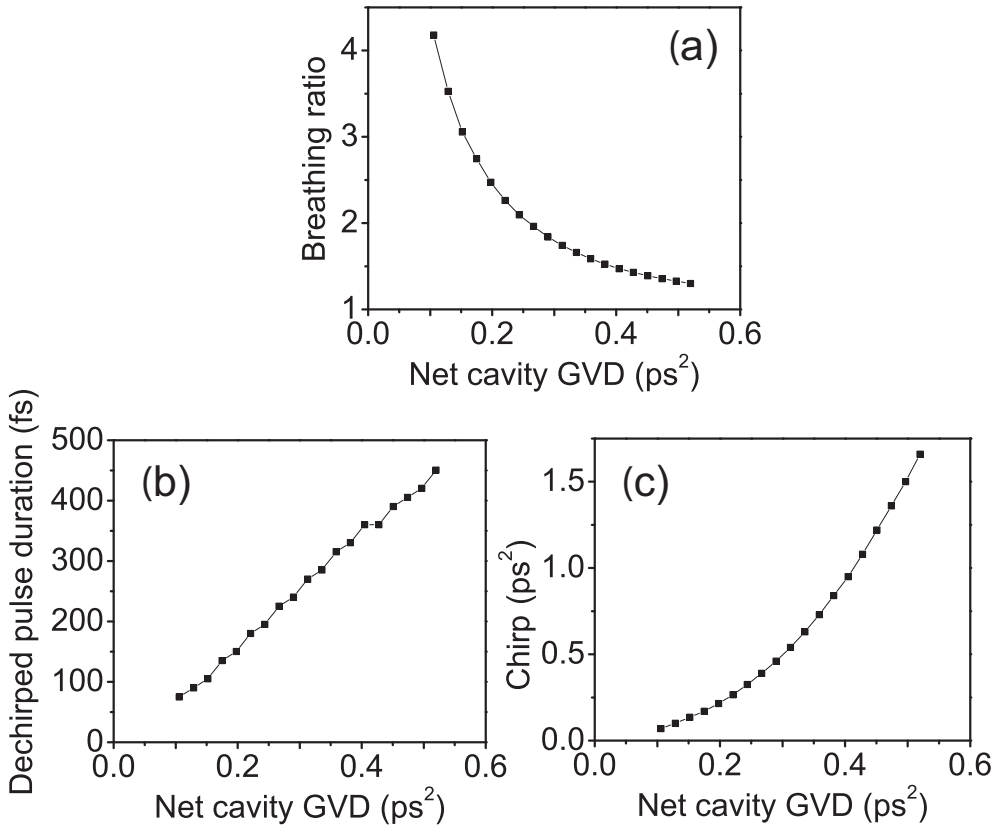

Figure 2.12: Laser performance vs. GVD: (a) breathing ratio, (b) dechirped pulse duration, (c) chirp. Figure taken from Ref. [26].

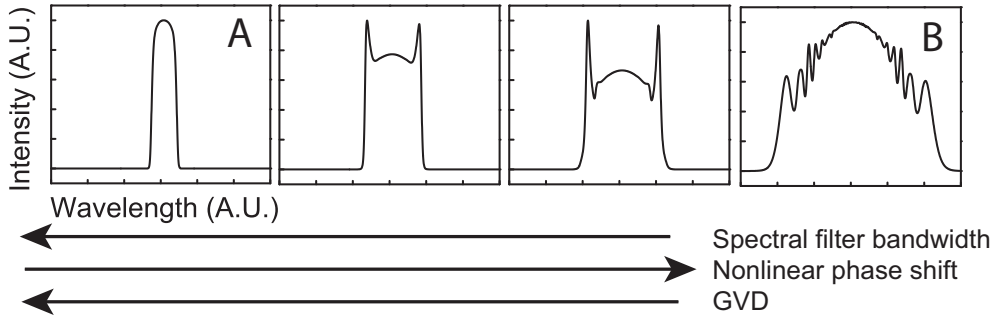

Figure 2.13: Output spectrum vs. laser parameters. Figure taken from Ref. [26].

Design guidelines

As dissipative soliton lasers are practically desirable for applications, it can be useful to translate these theoretical results into some basic design guidelines:

1) Determine the desired net GVD

The GVD is determined by the fiber lengths required in design, and hence, by the repetition rate. It also is directly related to the bandwidth of the output pulse. The bandwidth increases rapidly with decreasing GVD. The results above suggest these rough guidelines for a Yb fiber laser emitting near 1000 nm and using standard HI1060 SMF: with 50 m of total fiber, ∼5-nm bandwidth is expected (section 2.6); with 4 m of fiber, ∼15-nm bandwidth is expected (section 2.2.2); and with 2 m of fiber, ∼40-nm bandwidth is expected (section 2.4.3).

2) Determine the spectral filter bandwidth

The filter is a crucial component for both stability and performance of the dissipative soliton laser. Once the GVD is fixed, one can choose an appropriate spectral filter. The filter bandwidth should be chosen to align with the bandwidth set by the GVD. That is, it should be large enough to support high energy, but narrow enough to ensure around a factor of two filtering for stability and for reduction of the chirped pulse duration in the cavity. Again, as rough guidelines: for 50 m of fiber, 10-nm bandwidth is appropriate; for 4 m of fiber, 12-nm bandwidth is appropriate; and for 2 m of fiber, 15-nm bandwidth is appropriate.

3) Optimize the nonlinear phase shift

Once the GVD and the spectral filter bandwidth are determined, Φ_{NL} is easily optimized by adjusting the pump power. In our lab, we find that it is best to begin with a narrow filter to ensure stable mode-locking, and then increase the filter bandwidth and the pump power to optimize the performance. With a narrow filter, it will be easiest to achieve mode-locking, but the laser will also be prone to multi-pulsing at relatively low energy. The filter bandwidth and pump power

should be increased to obtain the highest stable single-pulse energy.

This brief design guide is intended to gives some initial suggestion of the parameters to use. More-precise values can easily be determined with numerical simulations.

2.3.3 Experimental confirmation

Experiments are designed as in section 2.2 (Figure 2.3) and match the simulated cavity. Two differences from the simulations are i) the spectral filter, which has a sinusoidal spectral transmission resulting from the insertion of a quartz plate between two polarizers (see Figure 2.3), and ii) the saturable absorber. The NPE is generally biased such that higher-intensity light is transmitted back into the cavity and lower-intensity light is rejected. We further use the NPE output port as the main output to optimize the efficiency of the cavity. As a consequence, additional care must be taken to perform controlled experiments, as the output coupling and the transfer function of the NPE are coupled. However, the output coupling has its main effect on the energy in the cavity, which can be measured, and the exact form of the NPE transmission function has little influence on the output pulse parameters.

Many of the parameters in fiber lasers are strongly interconnected, which makes controlled experiments a challenge. For example, in order to change the spectral filter, we must replace the birefringent filter plate for one of a different thickness, and this requires realigning the cavity, which in turn changes the bias of the NPE, which then effects the output coupling, which, finally is directly linked to another main system variable, Φ_{NL}. To change the GVD, for another example, we must

change the fiber length, which in addition to also changing the NPE, changes directly the length of fiber which contributes to Φ_{NL}. Controlled experiments are therefore performed with fixed fiber length and filter. The Φ_{NL} itself can be directly tuned through control of the pump power and the wave plates, with little effect on the other parameters, and as such will be the focus of our experimental confirmation of the trends from the simulations.

Thus, Φ_{NL} is increased with adjustments to the pump power and the wave-plates. The pulses are dechirped outside the cavity with a grating pair and the spectra and autocorrelation are measured (Figure 2.14). There is very good agreement between the experimental and simulated spectral features (compare the first two rows of Figure 2.14).

To obtain an approximate value for Φ_{NL}, we assume the temporal profile is constant in the three fiber segments, and approximate the nonlinear phase as

$$\Phi_{NL} \approx \sum_{n=1}^{3} \gamma_n (I_{peak})_n L_n. \tag{2.5}$$

We assume a constant peak power in the gain fiber and following SMF, which we calculate from a measurement of the power before the output port. The peak power in the SMF before the gain is calculated from an additional measurement of the output coupling, to determine the energy that returns through the fiber after the free-space section. For simulated pulses, the value of Φ_{NL} is calculated directly with Eq. 2.5. We then plot the experimental data points versus the theoretical values of Φ_{NL} in Figure 2.15. Because our experimental value of Φ_{NL} is an estimate, the apparently excellent quantitative agreement between the measured and simulated results should be considered fortuitous. More importantly, the qualitative trends

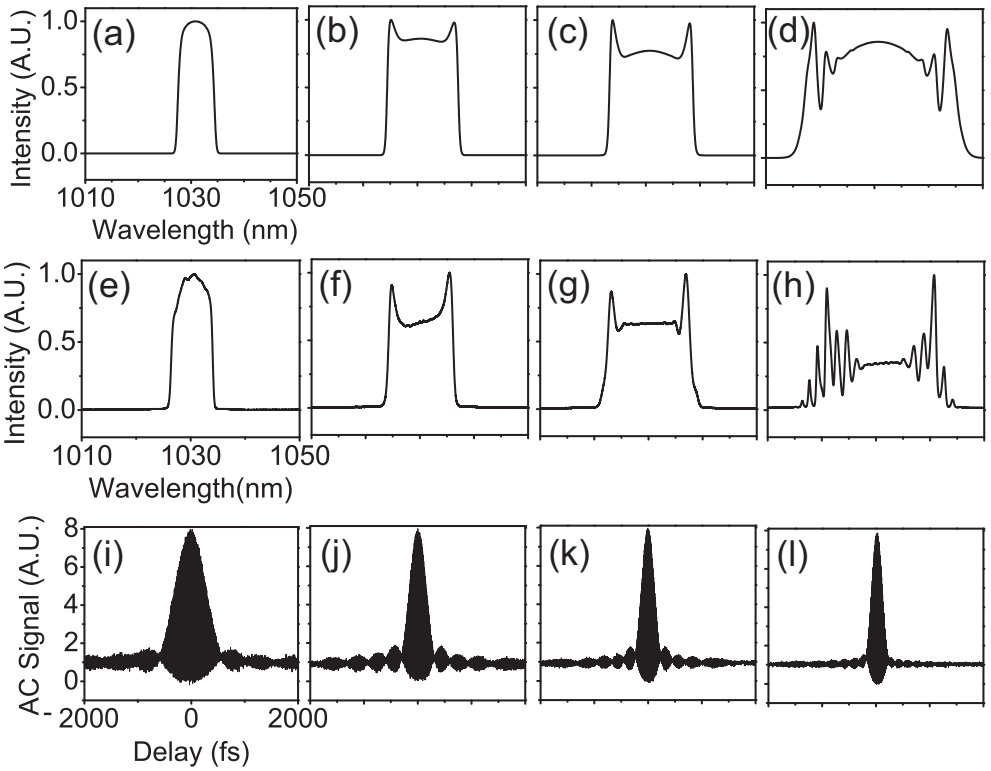

Figure 2.14: Experimental results; top: simulated output spectrum with Φ_{NL}: (a) $\sim 1\pi$, (b) $\sim 3\pi$, (c) $\sim 4\pi$, (d) $\sim 8\pi$; middle: experimental output spectrum with approximated Φ_{NL}: (e) $\sim 1\pi$, (f) $\sim 3\pi$, (g) $\sim 4\pi$, (h) $\sim 8\pi$; bottom: corresponding interferometric AC of dechirped output pulses. Figure taken from Ref. [26].

from the experiment are well-aligned to both numerical simulations and analytic theory. We conclude that we have a satisfactory understanding of pulse-shaping in dissipative-soliton lasers.

In addition, because of the very good agreement, we can conclude that the exact shape for the spectral filter and the saturable absorber transmission function have only a small effect on the main parameters of the pulse. However, there is a particular mode (see the last column for Figure 2.5 for example), the flat-top soliton, which is not observed in numerical simulations with a monotonic and approximate saturable absorber but is predicted by analytic theory. Analytic theory predicts that the quintic term of the saturable absorber must be negative for these modes

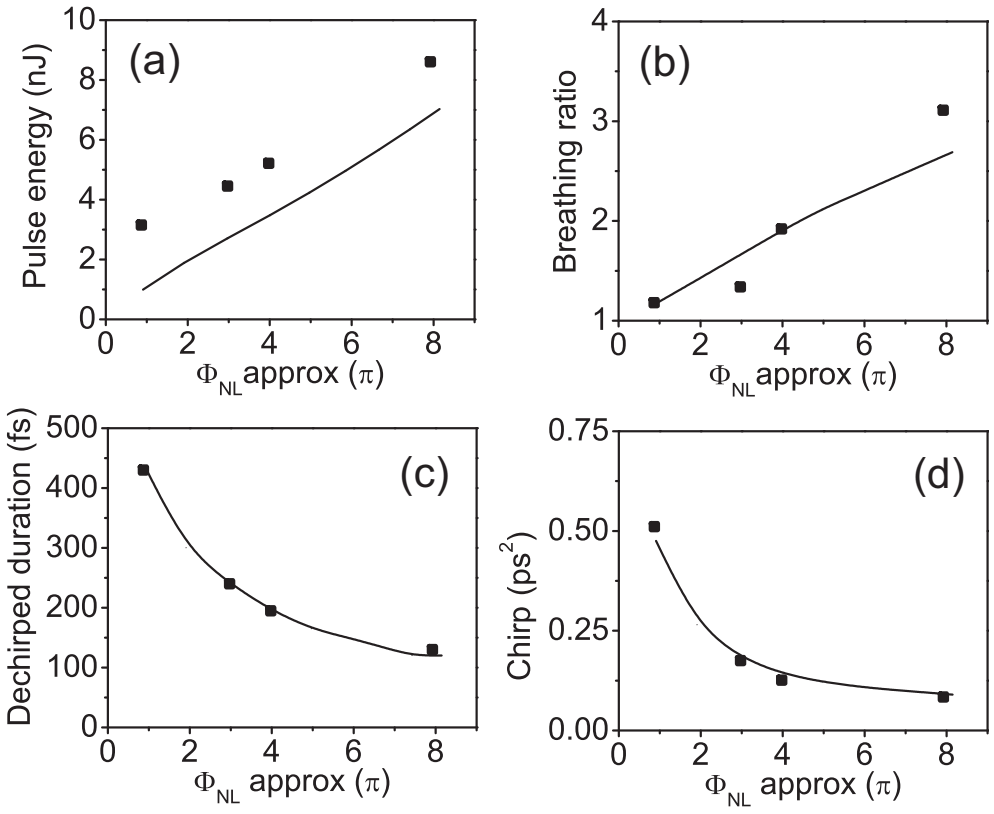

Figure 2.15: Experimental and numerically simulated laser performance vs. approximate Φ_{NL}; dots: experiment, lines: numerical simulation; (a) pulse energy before the NPE port, (b) breathing ratio, (c) dechirped pulse duration, (d) chirp. Figure taken from Ref. [26].

to be stable. In other words, the saturable absorber cannot be monotonic. A more-sophisticated model of the NPE that explicitly includes the two polarization components with cross-phase modulation accounts not only for those pulses but also for modes in Figure 2.14. However, as these flat-top pulses require a specific saturable absorber and are difficult to find in an experimental setting, we focus instead on the solutions with B<1. These are typically most-desired because they combine high energy with ultra-short duration.

2.4 Physical limits

A natural question to ask for both its intrinsic scientific significance and for its implications for applications is: what are the limits to the pulse duration and energy of dissipative-soliton lasers? We address this question theoretically (2.4.1) and then with particular results pertaining to both the energy (2.4.2) and pulse duration (2.4.3).

2.4.1 Area theorem

To understand the limiting behavior of a dissipative-soliton laser, further analysis of the underlying theory from section 2.2 can be useful. We search for an area theorem, or a simple relation that expresses the conditions that must be satisfied for a pulse solution to exist [27]. Eq. 2.3 can be rewritten in terms of the pulse energy and the full-width at half-maximum pulse durations:

$$E = F(B)G(D, \Omega, \delta) \tag{2.6}$$

and

$$T = \left(\frac{|B| \cosh^{-1}(2 + B)}{\sqrt{|B^2 - 1|}} \right) \frac{D\Omega|\delta|G(D, \Omega, \delta)}{2(\Delta + 2)\gamma}, \tag{2.7}$$

where

$$F(B) = \begin{cases} \cos^{-1}(B) & \text{for } |B| < 1 \\ \\ \cosh^{-1}(B) & \text{for } B > 1, \end{cases} \tag{2.8}$$

$$G(D,\Omega,\delta)=\frac{\sqrt{\frac{2}{3}}\left(\Delta+2\right)\sqrt{D^2\left(\Delta-8\right)\Omega^2+12\left(\Delta-4\right)}}{D\sqrt{|\delta|}\Omega\sqrt{\Omega\left(D^2\Omega^2+4\right)}}, \tag{2.9}$$

and

$$\Delta=\sqrt{3D^2\Omega^2+16}. \tag{2.10}$$

Of course, Eqs. 2.6 and 2.7 could be combined with the elimination of B, but instead we leave the expression in two parts because, as seen in sections 2.2 and 2.3, the spectral form of the dissipative soliton laser is crucial to its understanding, and this form is identified with the B parameter.

The pulse energy is a product of $G(D,\Omega,\delta)$, which is a function the system parameters, and a function of the pulse parameter B. From Eq. 2.8, we see that the nature of the energy depends critically on the value of B (Figure 2.16). When B>1, a pulse solution exists at any value of the energy, much like in the case of solitons of the nonlinear Schrdinger equation. However, when $|B|$ <1 the pulse energy is limited at B=-1, where the ansatz (Eq. 2.2) diverges and F(B)=π. This feature distinguishes the CQGLE pulse solutions from other soliton solutions; for a fixed system, a pulse has an energy maximum determined by Eq. 2.6. When Eqs. 2.6 and 2.7 are combined, we can compare the relation of changes in the pulse duration to those in the energy. For 0<B<2.217, the energy scales inversely with pulse duration. For all other values of B, energy is proportional to the pulse duration. This is a surprising result because in all previously-derived area theorems for short pulse propagation (for studied soliton solutions) the pulse duration varies inversely with the energy [27].

To test these ideas, a dissipative-soliton laser as in Figure 2.3 was constructed with a 183-cm segment of single-mode fiber before 60 cm of gain fiber, and ter-

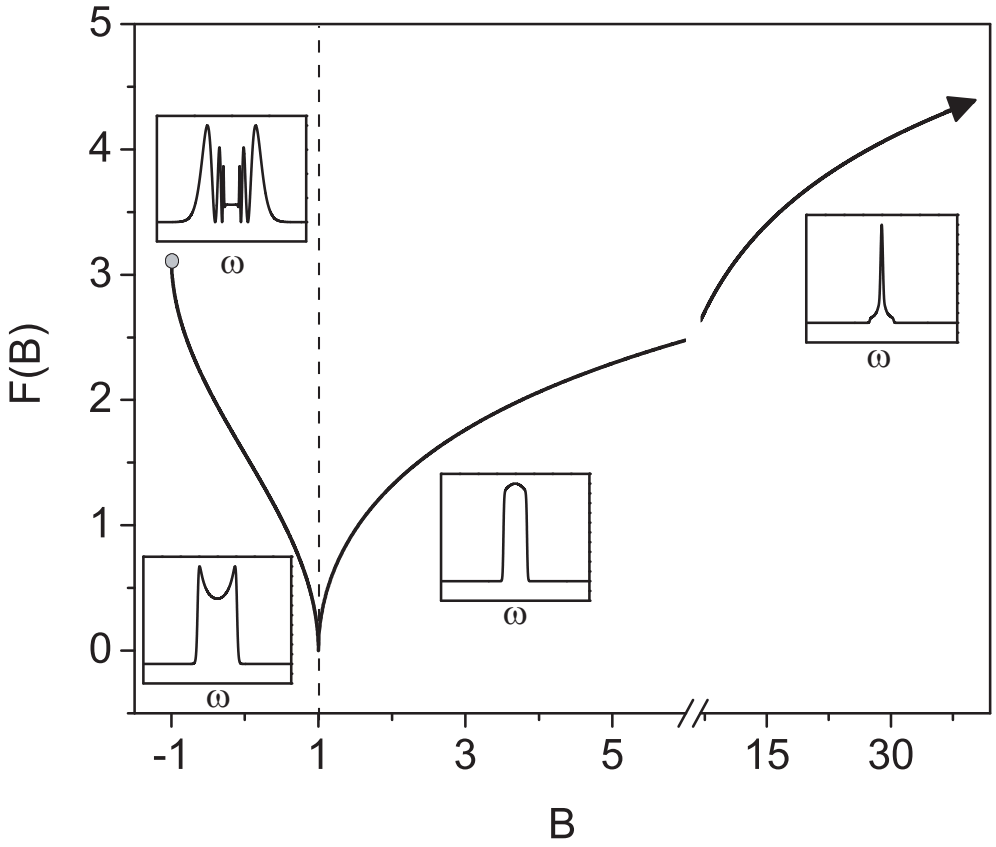

Figure 2.16: Variation of the pulse energy as a function of the pulse parameter, B. The dotted line separates solutions with $|B|$ <1 for δ >0 from those with B>1 for δ <0. Insets: spectral profiles plotted for the respective values of B. Figure taken from Ref. [27].

minating with a 125-cm segment in a unidirectional ring cavity. All parameters are held constant and we increase the pump power from zero. Initially, for a given setting of the wave plates, after the laser reaches threshold at low pump power, the laser operates in continuous-wave mode (corresponding to a plane-wave solution to Eq. 2.1). With further increase of the pump power, mode-locking occurs and a single pulse traverses the cavity. A further increase in power increases the energy and bandwidth of the pulse (Figure 2.17). This evolution is predicted by both the analytical spectra as F(B) approaches the energy limit at π (Figure 2.17), and the numerical simulations (as in section 2.2.1). The characteristic two-peaked spectrum of normal-dispersion lasers develops more structure as it broadens.

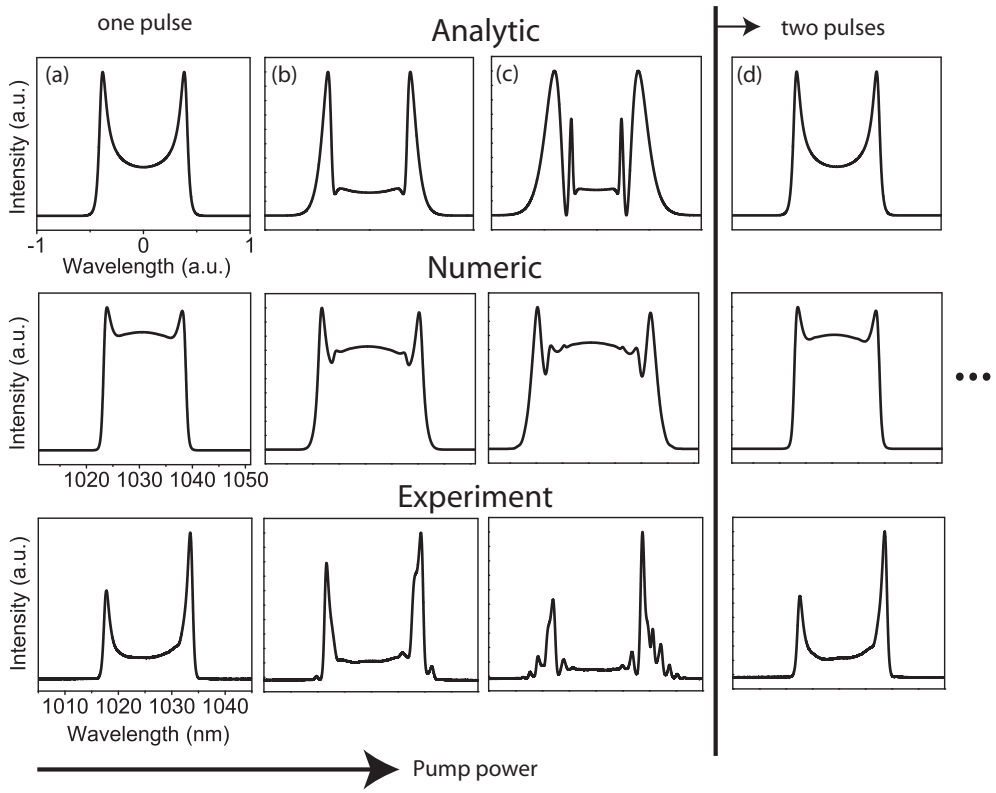

Figure 2.17: Top: theoretical spectra for increasing pulse energy, as B approaches -1; middle: simulated spectra with increasing saturation energy; bottom: measured spectra with increasing pump power. The rightmost spectra correspond to the birth of the second pulse in the cavity. Figure taken from Ref. [27].

If the pump power is increased still further, a new pulse is generated in the cavity and the spectral shape returns to the narrower spectrum of Figure 2.17(a) (Figure 2.17(d)), the lowest-energy mode of a single pulse. This pattern, represented graphically in Figure 2.18, continues until the maximum pump power is reached. Up to four pulses have been observed in the cavity. The minimum number of pulses that can satisfy the area theorem exist at any given time.

The energy quantization and area theorem are direct consequences of the analytic theory. That is, the theory "contains" this information. This contrasts with analysis based on the CGLE, where multi-pulsing is addressed as an addition to the theory [6]. While it is clear that there has to be an energy limit, defined

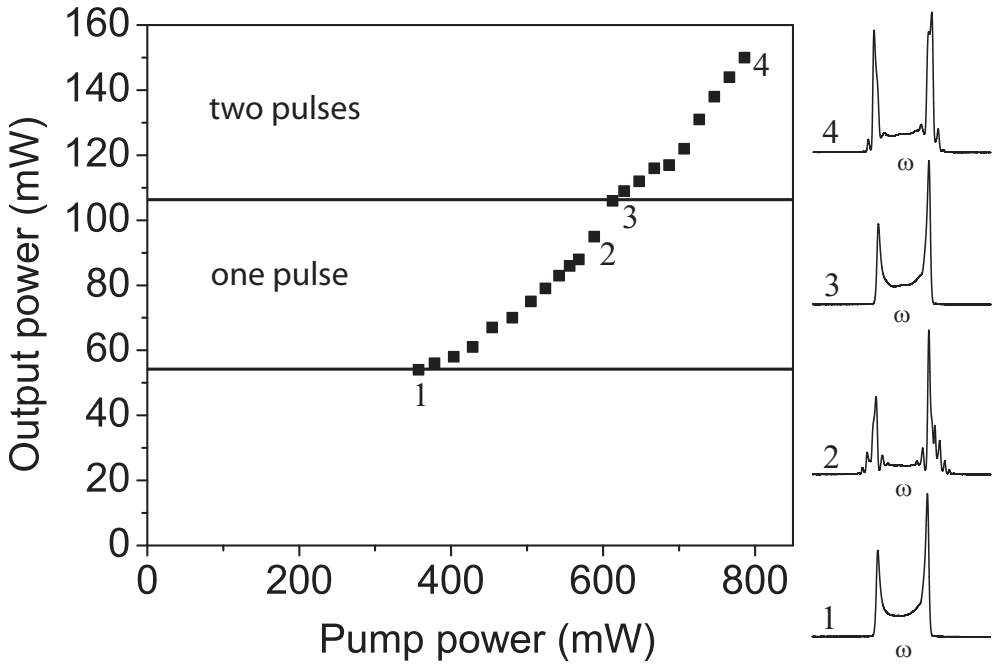

Figure 2.18: Mode-locked output power vs. pump power. The spectra on the right are for the corresponding pump levels. Figure taken from Ref. [27].

qualitatively by the area theorem in Eq. 2.6, further experiments need to be done to determine information about the exact quantitative upper energy limit. This question is addressed in the next section.

2.4.2 Pulse energy

Dissipative soliton lasers are expected to generate stable high-energy pulses because they can be mode-locked with net (normal) cavity GVD an order of magnitude higher than that of fiber lasers with dispersion maps, and pulse energy is theoretically expected to increase with increasing GVD [4, 6, 27]. In general, numerical simulations of the complete dynamics of the fiber cavity show that higher-energy solutions can always be stabilized with larger GVD.

To assess this theoretical prediction, we designed an experimental cavity with a

long length of fiber before the gain [28]. A fiber laser was built as in Figure 2.3 but with an additional pump laser to ensure enough pump power to achieve the highest energy. 15 m of SMF is followed by 0.5 m of Yb fiber, with another 0.5-m segment attached at the end of the gain fiber. The total cavity dispersion is $\sim$0.38 ps^2. The birefringent filter thickness is chosen to provide a 6-nm bandwidth, because simulations predict narrower bandwidths at large normal dispersion. The setup produces a variety of mode-locked states as the wave plates are rotated. The output pulse train is monitored with a photodetector/sampling oscilloscope combination with a bandwidth of 30 GHz. The interferometric and intensity autocorrelations are monitored for delays up to $\sim$100 ps.

Stable operation with a single pulse in the cavity occurs for powers $<$200 mW. Above this threshold, multiple pulses exist in the cavity, unless the spectrum is broad and highly structured. The highest energy obtained for a stable and self-starting single pulse is 22 nJ. However, if we relax the self-starting requirement, 26 nJ can be obtained. Diagnostics of the 26-nJ pulses show good agreement with simulations corresponding to the same cavity and energy (Figure 2.19). The dechirped pulse duration is 165 fs, which is close to the transform-limited value. The temporal side-lobes contain $\sim$4% of the energy. As in simulations and analytic theory, the spectrum exhibits the strong fringes that indicate that the pulse is at the limit of the area theorem. A small pulse that contains $\sim$0.5% of the total pulse energy occurs $\sim$4 ps from the main peak, which is the time interval expected from the spectral fringe spacing. The transmitted spectrum (Figure 2.19a dotted) of the NPE port is cleaner than the ejected spectrum with only $\sim$2% of the energy in the side lobes and negligible small remote pulses. For applications that require the cleaner pulse and spectrum, the transmitted pulse can be output via a second beam splitter. Some pulse energy will be sacrificed with this approach, which will

be illustrated below.

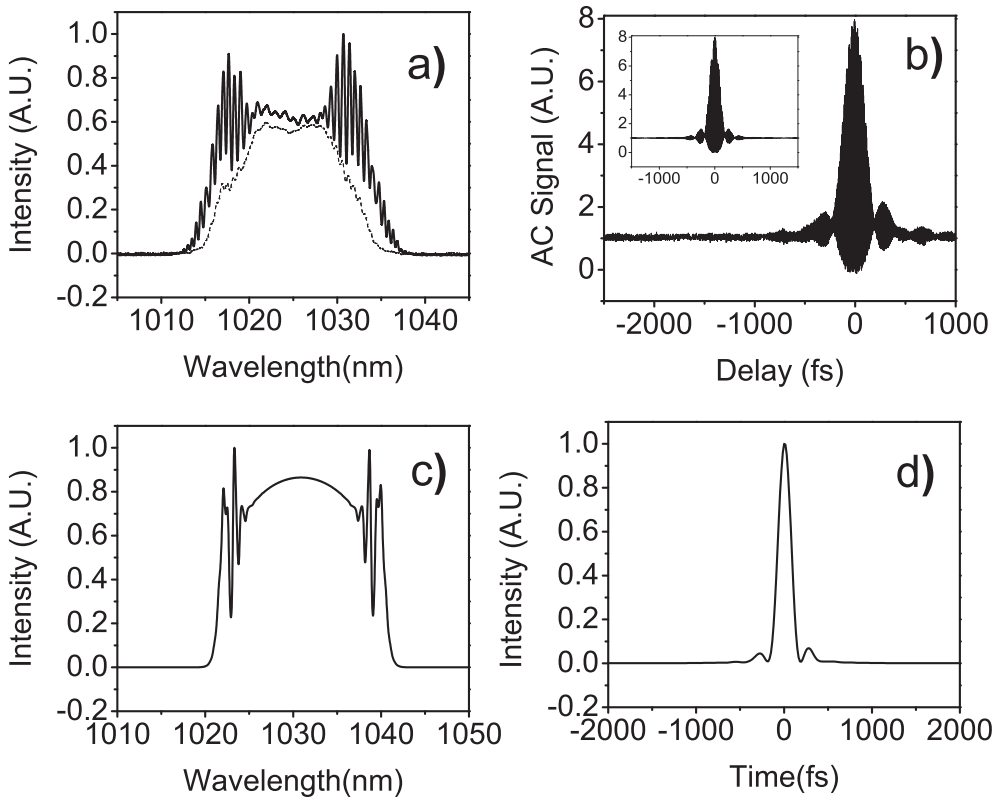

Figure 2.19: a) Spectra transmitted (dotted) and rejected (solid) from the NPE port, b) dechirped autocorrelation (∼165 fs) and the autocorrelation of the zero-phase Fourier-transform of the spectrum (∼140 fs, inset), c) simulated spectrum, d) simulated dechirped pulse (∼195 fs). Figure taken from Ref. [28].

The major conclusion is that a dissipative soliton fiber laser can generate stable pulses with very high energy despite the accumulation of nonlinear phase shifts greater than 10π. Further investigation is still needed to determine if this is an absolute limit to the stabilization of a pulse in the cavity in the face of large nonlinear phase accumulation.

2.4.3 Pulse duration

The general guidelines for achieving short pulses can be determined from the simulation results in section 2.3 [29]. The spectral bandwidth broadens with decreasing GVD, decreasing filter bandwidth, and increasing Φ_{NL}. To investigate how these parameters can be pushed to the limit in a realistic laser, we must focus on a particular cavity type. As in the rest of this chapter, we will continue to focus on Yb-doped systems with standard components because they have the greatest current interest. The conclusions can be easily generalized to other specific fiber laser systems.

From a broad survey of numerical simulations, the conclusion is that decreasing GVD or increasing Φ_{NL} are the best ways to increase spectral bandwidth, and in addition tuning the GVD allows for better pulse quality. Therefore, to achieve the shortest pulses, we need to design a cavity with the shortest lengths of fiber possible (to minimize total GVD), pump with as much power as possible (to increase Φ_{NL}), and use the appropriate spectral filter bandwidth. This then also tells us the expected practical limitations: how short the cavity can be built, and how much pump power is available.

We first search for short pulses numerically by simulating a realistically short cavity: 50 cm of SMF precedes 20 cm of gain fiber, which is followed by another 50 cm of SMF. A spectral filter with 40 nm bandwidth is used. We find the shortest pulse in this cavity by increasing the energy until the simulations fail to converge at an energy of 44 nJ. This results in a pulse at the limit of the area theorem (see section 2.4.1) with spectral fringes (Figure 2.20(a)). The pulse can be dechirped numerically to 34 fs (Figure 2.20(b)). The laser comprises ∼100 dispersion lengths. Therefore, the simulations suggest that 30 fs is a reasonable limit

to practical all-normal-dispersion fiber lasers at 1 μm wavelength. Shorter pulses may be generated if we had the freedom to further decrease the fiber dispersion, for example. Commercial fibers at 1.55 μm allow for some flexibility for Er fiber lasers which could allow for further decreases in pulse duration. The ∼30-fs limit was achieved with a pulse with 44-nJ energy, which corresponds to 7 W of pump power. However, realistic SMF lasers pumped in-core typically have 200-400 mW of output power, which corresponds to only 2-3 nJ of pulse energy. The simulations re-run with this energy give a minimum pulse duration of 70-80 fs.

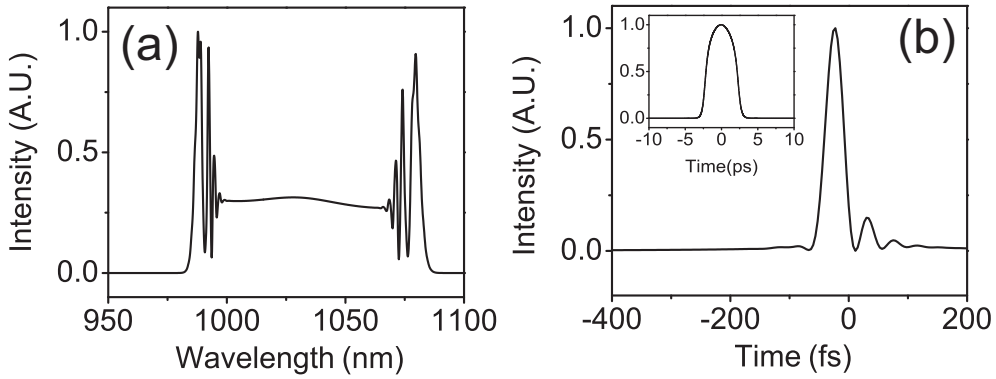

Figure 2.20: Short pulse numerical simulation: a) spectrum and b) dechirped intensity profile (inset: 4.3-ps chirped pulse directly from the laser). Figure taken from Ref. [29].

The role of third-order dispersion (TOD) begins to be noticeable in the simulations for such short pulse durations, as expected. However, removing or doubling the TOD in the fiber creates only small (<10%) changes in the 30-fs pulse. Therefore, contrary to previous short pulse mode-locking mechanisms, the compensation of higher-order dispersions in dissipative soliton lasers should not affect the performance appreciably. Limits to stability that might arise from TOD need to be considered separately.

Based on the simulation results, a dissipative soliton fiber laser was built (Figure 2.21). We increased the length of SMF after the gain segment to enhance

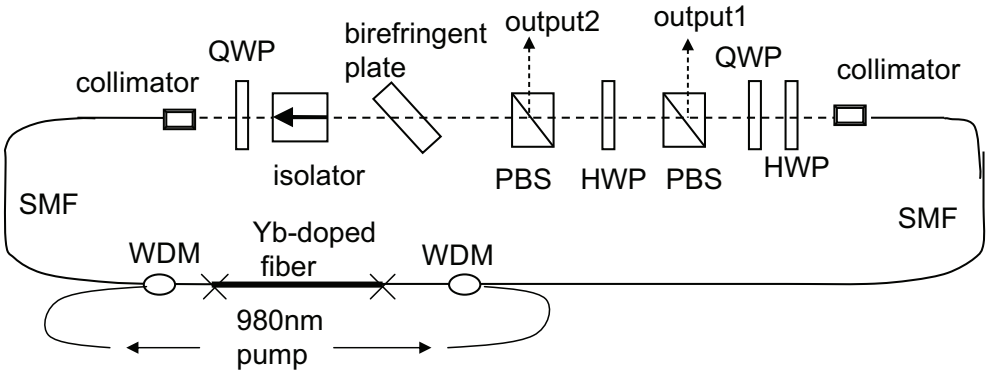

Figure 2.21: Schematic of laser: QWP: quarter-wave plate; HWP: half-wave plate; PBS: polarizing beam-splitter; WDM: wavelength-division multiplexer. Figure taken from Ref. [29].

the value of Φ_{NL} that can be reached with modest pulse energy. The fiber section consists of 44 cm of SMF followed by 17 cm of Yb-doped fiber, which is followed by 170 cm of SMF. This gives a repetition rate of 80 MHz and a total GVD of 0.053 ps^2. Two 980-nm diodes supply ∼900 mW of pump power. This design differs from the one in Figure 2.3 because it has a second pump and a second beam-splitter. The second beam-splitter is used to improve beam quality by coupling the light out after NPE cuts off the lower-intensity parts of the pulse in the first beam-splitter. A birefringent filter thickness is chosen to correspond with 15-nm bandwidth. A variety of self-starting mode-locked states are observed by adjusting the wave plates. The pulse with the shortest duration, when measured from output 1 (Figure 2.22(a) inset) has a spectrum similar to the simulation result (Figure 2.20(a)), and when measured from output 2 is much cleaner (Figure 2.22(a)), as expected. The pulse is dechirped to 70-fs duration (Figure 2.22(b)) and has 2-nJ energy. The filter plays a crucial role; without it, mode-locking does not occur.

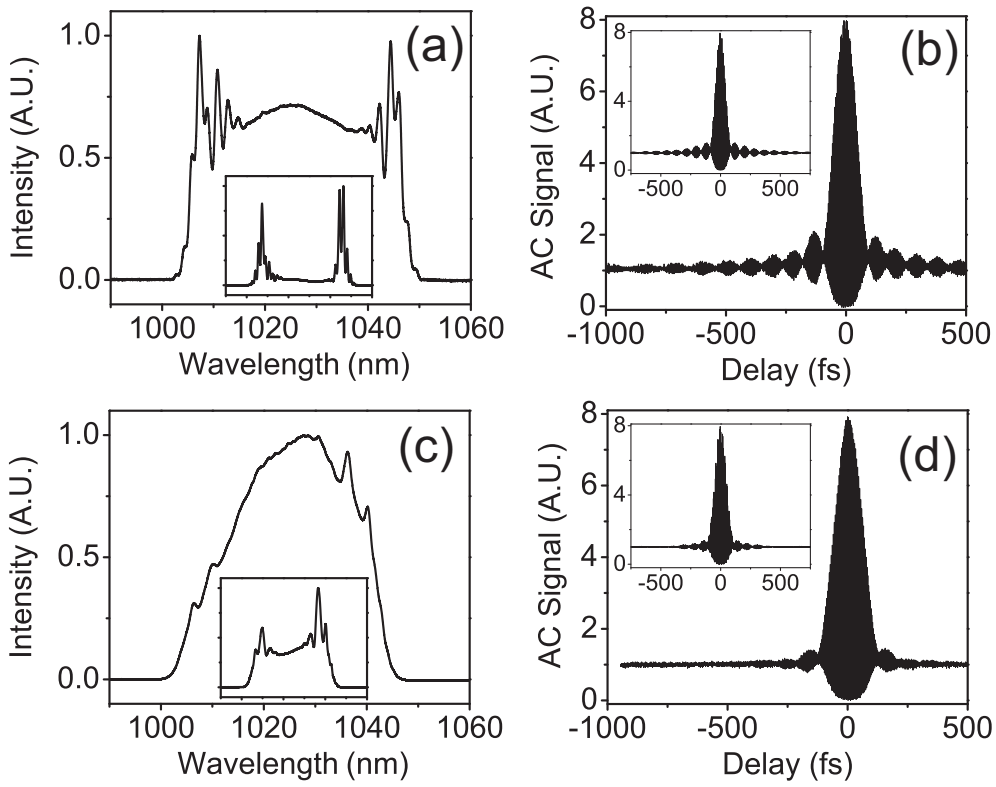

Figure 2.22: Short pulse experimental results: a) spectrum from output 2 (spectrum from output 1 inset) and b) 68-fs dechirped autocorrelation from output 2 (autocorrelation of transform-limited pulse inset). Figure taken from Ref. [29].

2.5 Practical extensions

2.5.1 Core-size scaling

It is well known that increasing the size of the fiber core reduces nonlinear effects, and therefore can increase the pulse energy available from a laser. Because the dissipative soliton laser allows for nonlinear phase shifts greater than 10π, this approach is a promising route to achieve pulse energies greater than 1 μJ directly from a fiber laser.

Double-clad fiber

Double-clad (DC) fiber, which refers to a second cladding used to guide pump light, is a common technique to increase the power in fiber systems while maintaining the single mode in the signal core [30, 31]. Particularly relevant to dissipative soliton mode-locking are 25-nJ pulses at 80 MHz produced by An et al. [32]. The pulses in this work are short (150 fs) but lack in pulse quality with energy in the wings out to 3 ps. In this section we present the results of a high performance double-clad dissipative soliton laser [33].

The design of the laser is the same as in Figure 2.3, but with the DC fiber replacing most of the SMF. The Yb-doped DC fiber (Liekki DC1200 10/125) has a 10-μm core, and the 2-m length is chosen to keep the GVD moderate. This will allow short pulse durations, (see section 2.4.3) while ensuring that the fiber is long enough to absorb most of the pump light. The multi-mode pump light is coupled into the fiber laser through a home-built pump-signal combiner with $\sim$85% coupling efficiency, and can deliver a maximum of 18 W. A 35-cm fiber collimator precedes the gain and a 15-cm fiber collimator follows it, and both are made with standard 6-μm core diameters. The splice loss caused by the fiber core mismatch is reduced with a few millimeters of $\sim$8.5-μm-core fiber placed at the intersections. This gives an estimated loss of about 0.5 dB. Experiments were performed using filters with a range of spectral bandwidths. Optimum performance was achieved with 20-nm filter bandwidth. With narrower filters, the output spectrum was narrow and the energy was limited; with broader filters, no mode-locking could be achieved.

Stable, self starting mode-locking is achieved with a repetition rate of 80 MHz with up to $\sim$8 W of pump power. The resulting pulses have 31-nJ (2.2 W) energy,

with 4.5-ps duration. These are dechirped to 80 fs outside the cavity (Figure 2.23b). The spectrum exhibits the typical features of a dissipative soliton fiber laser (Figure 2.23a). If the pump power is increased beyond 8 W, the laser sporadically switches to continuous-wave operation.

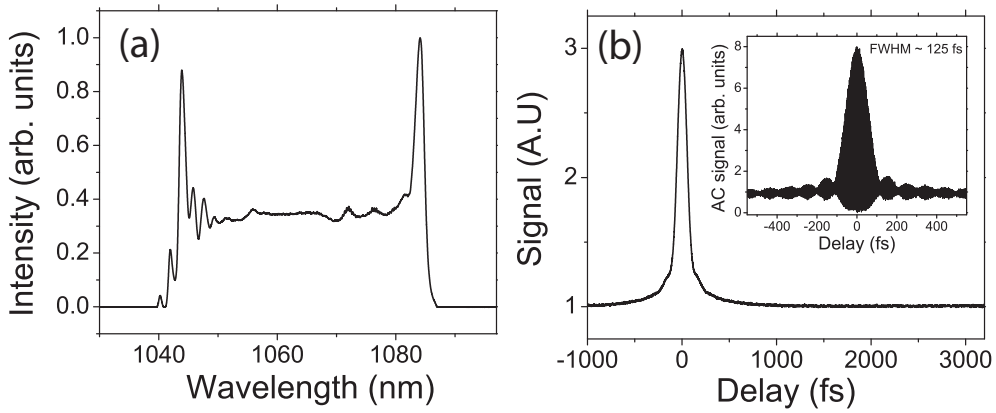

Figure 2.23: (a) Output spectrum and (b) intensity autocorrelation of the dechirped pulse. Inset: interferometric autocorrelation of the dechirped pulse. Figure taken from Ref. [33].

After dechirping, the laser generates 80-fs pulses with ∼200-kW peak power and well over 1 W of average power. This result is a landmark for fiber sources as the pulse parameters are comparable to those of solid-state sources. This is the first fiber laser to compete directly with performance of solid-state lasers.

Photonic crystal fiber

Photonic crystal fibers (PCFs) allow for very large single-mode cores. In recent years, several high-performance implementations of PCF in dissipative soliton lasers have successfully increased output powers and pulse energies of fiber sources [34–36]. In this section, we discuss the details of a dissipative-soliton laser based on PCF that reached a peak power of 1 MW [37].

The cavity design is similar to that in Figure 2.3, but without the extra fibers associated with collimators and pump coupling. Two lenses and two dichroic mirrors are used for pump steering (Figure 2.24). The Yb-doped PCF (Crystal-Fibre DC-170-40-Yb) has a mode-field diameter of 33 μm, and the 1.25-m length was chosen to optimize pump absorption. This fiber is nominally single-mode, with an estimated dispersion of 0.019 ps2/m around 1- m operation wavelength. The multimode pump allows for a maximum of 35 W of pump power at 976-nm wavelength. The birefringent filter thickness was chosen to obtain a 12-nm bandwidth.

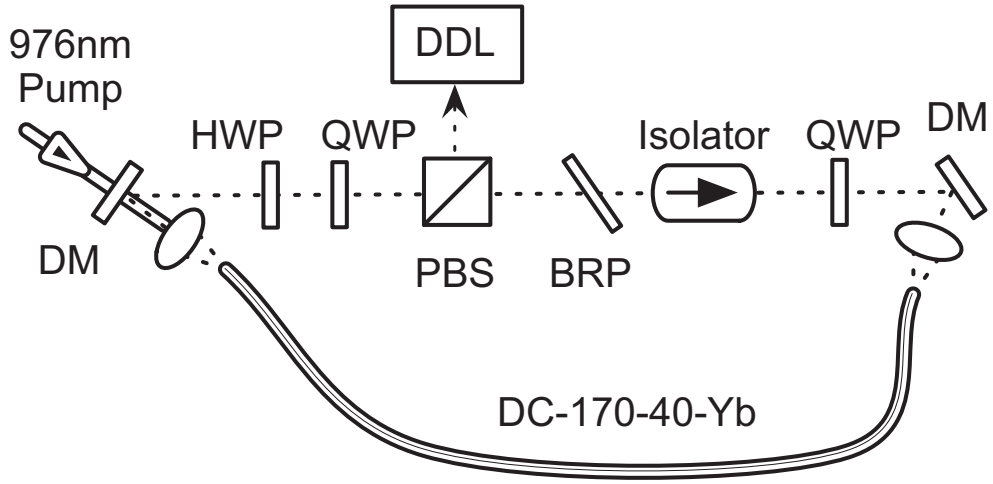

Figure 2.24: Experimental PCF ring laser design: DM, dichroic mirror; HWP and QWP, half- and quarter-wave plates; PBS, polarizing beamsplitter; BRP, birefringent plate; DDL, dispersive delay line. Figure taken from Ref. [37].

Stable, self-starting mode-locking is achieved for a variety of wave plate settings. With 24-W pump power, 142-nJ output pulses are generated, which corresponds to 12 W of average power at an 80-MHz repetition rate. The pulses are dechirped with -0.035 ps^2 of GVD, to yield 100-nJ and 115-fs pulses (Figure 2.25). The peak power is thus near 1 MW. Mode-locking is sustained over many hours and the RF spectrum shows good stability with a peak to noise contrast of 70 dB. Scaling from the double-clad result in the previous section, this laser should support 300-nJ pulses with similar pulse duration, which is in agreement with simulations,

but this current setup is limited by pump power. The average and peak powers demonstrated here exceed those of standard Ti:sapphire lasers and approach that of state-of-the-art chirped-pulse oscillators. It should be noted that fiber endface damage was observed, possibly due to self-Q-switching, which may occur as the wave plates are adjusted. Careful surface preparation and existing endcap technology can be used to alleviate this damage.

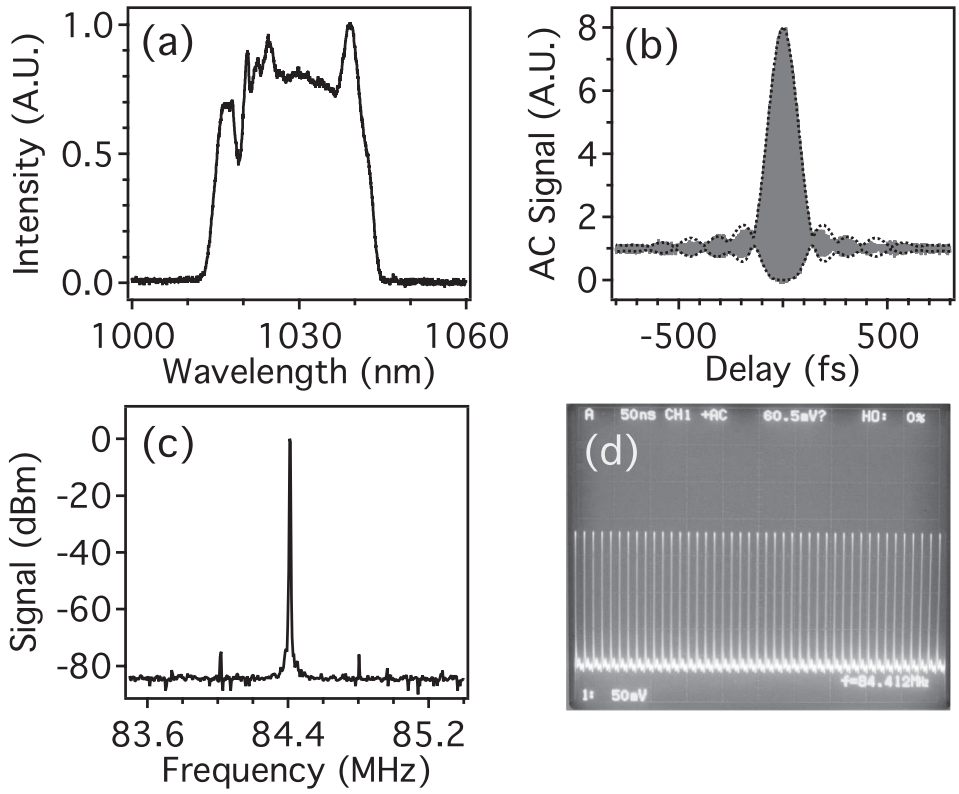

Figure 2.25: Mode-locked output: (a) spectrum, (b) dechirped interferometric autocorrelation (gray) and transform-limited envelope (dotted black), (c) RF noise spectrum, 2 MHz span, 1 kHz resolution and (d) pulse train, 50 ns/div and 400 kHz bandwidth. Figure taken from Ref. [37].

An advantage of fiber-based systems is the possibility of compact integration and elimination of all free-space sections that would require optical alignment. The use of PCF sacrifices some of these practical advantages, as splicing of PCF to ordinary fiber is not a standard capability. However, progress is being made on

this front. Large-mode-area PCFs that can be bent have been developed recently. Fiber-coupled pump combiners based on ring mirrors have been demonstrated, and new ways to interface PCF to single-mode fiber technology are in development. Integration of the laser design shown in Figure 2.24 is thus within the reach of current technology.

Chirally-coupled core fiber

Recently-developed chirally-coupled core (CCC) fibers use a secondary core wound around a large central core to create a distributed and integrated mechanism for filtering of higher-order modes (HOMs) [38]. CCC fibers have achieved effectively single-mode performance, without additional mode-filtering or mode-matching. CCC fibers offer a core size comparable to that of PCF, with the additional possibility of simple integration, owing to the use of standard large-area step-index fiber. In this section, we review an initial demonstration of the use of CCC fiber in a mode-locked laser [39].

A Yb-doped piece of CCC with core diameter of 33.5 μm and a numerical aperture (NA) of 0.06 has a mode area of $\sim 350 \mu m^2$ and V = 6.1. This large V number means that the core could support six HOMs. A helically-wrapped leaky side core in optical proximity to the main core couples out these HOMs through phase-matched interactions relating to the optical angular momentum of the HOMs, with minimal effect on the fundamental mode [38] (Figure 2.26(a)).

The oscillator is designed in a standard dissipative soliton configuration (Figure 2.3), and is shown in Figure 2.26(b). Given the low 5-dB/m pump absorption of the fiber, we used 3.9 m of CCC fiber for sufficient pump absorption. To avoid bend losses and any possible need for an external HOM filter, we loosely coil the fiber

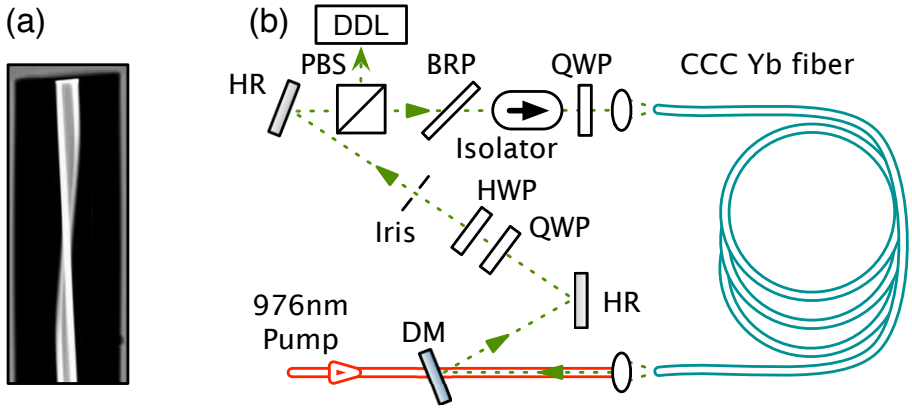

Figure 2.26: (a) Side view of angle-cleaved CCC fiber. (b) CCC fiber oscillator design: DM, dichroic mirror; PBS, polarizing beamsplitter; DDL, dispersive delay line; BRP, birefringent plate; QWP and HWP, quarter- and half-wave plate; HR, dielectric mirror. Figure taken from Ref. [39].

(30-cm diameter). In this initial demonstration, the laser is free-space pumped with a maximum of 35 W at 976-nm wavelength and an iris is placed before the output to filter out residual cladding light.

Stable, self-starting mode-locking at 53 MHz can be achieved with adjustments of the wave plates. As an initial confirmation of HOM filtering in the laser, at ~2 W of pump power, the output beam quality (a Gaussian beam with M^2 ~1.10-1.15) is comparable to that of single-mode fibers with much smaller cores, and no secondary pulses are visible 30-dB below the peak of the pulse out to 100 ps. With an 8-nm spectral filter mode-locking is stable over hours with about 15 W of coupled pump power (Figure 2.27). The pulse energy is 43 nJ (2.3 W of output power), and the pulses can be dechirped to 195-fs duration, within 10% of the transform-limit. Stable pulse energies of up to 47 nJ were obtained, but the pulses had larger wings, extending out to 1 ps from the peak. A further increase of the pump power results in additional pulses in the cavity. Small modulations on the spectrum are attributed to interference with a small amount of HOM content.

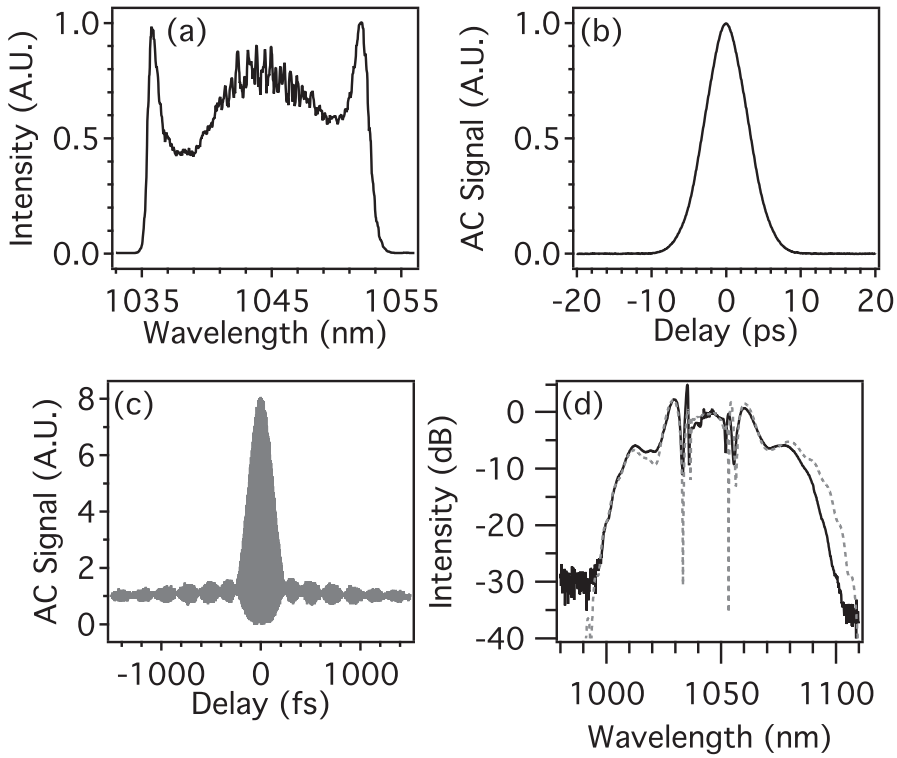

Figure 2.27: (Mode-locked output: (a) spectrum (0.1-nm res.), (b) chirped autocorrelation, and (c) dechirped interferometric autocorrelation. (d) Spectrum after propagation trough 1 m of SMF (solid) compared to simulation (dashed). Figure taken from Ref. [39].

We estimate that the HOMs carry on the order of 0.1% of the energy, which confirms the strong fundamental mode selection. In addition, we verify the peak power by launching 2-nJ dechirped pulses into 1 m of SMF with a 5-μm core diameter, and comparing the spectral broadening to simulation (Figure 2.27(d)). The excellent agreement confirms the quality of the pulses generated by the dissipative-soliton laser fabricated with CCC fiber.

The development of pump combiners and pigtailed isolators for CCC fiber is underway. We expect that in the near future these will enable construction of high-energy dissipative-soliton lasers with standard splicing technology that is currently used for single-mode fibers. As a consequence of the development of CCC fiber

and associated components, all needed elements are in place to construct integrated fiber lasers that will out-perform solid-state lasers.

2.5.2 Environmental stability

For wide adoption of fiber lasers beyond the laboratory environment, mode-locked operation must be stable against environmental perturbations. For example, thermal and mechanical perturbations can induce random birefringence in fiber, which can severely alter the performance of the laser. The use of highly-birefringent, polarization-maintaining (PM) fiber limits the light to a linear polarization in one axis, and suppresses the effects of any induced birefringence. In this section we review the application of PM fiber to a dissipative soliton laser to achieve an environmentally-robust system [40].

In a PM fiber cavity, nonlinear polarization evolution is not suitable as a saturable absorber because there is only one polarization in the fiber. As a consequence, we use a semiconductor saturable absorber mirror (SESAM) as a saturable absorber. The cavity is thus designed in a Fabry-Perot configuration, for simple implementation of a reflective SESAM (Figure 2.28). The fiber section consists of 1 m of SMF followed by 60 cm of Yb-doped gain fiber and another 40 cm of SMF. The SESAM (from BATOP GmbH) has $\sim$ 35% modulation depth, a $\sim$40-nm spectral bandwidth and a relaxation time constant of $\sim$500 fs. The birefringent filter has a bandwidth of 12 nm. Output 3 (Figure 2.28) is the main laser output, with a coupling ratio which is tuned with the quarter-wave plate, while the other outputs serve to monitor pulse evolution in the cavity.

With appropriate settings of the wave plates, mode-locking is achieved. The

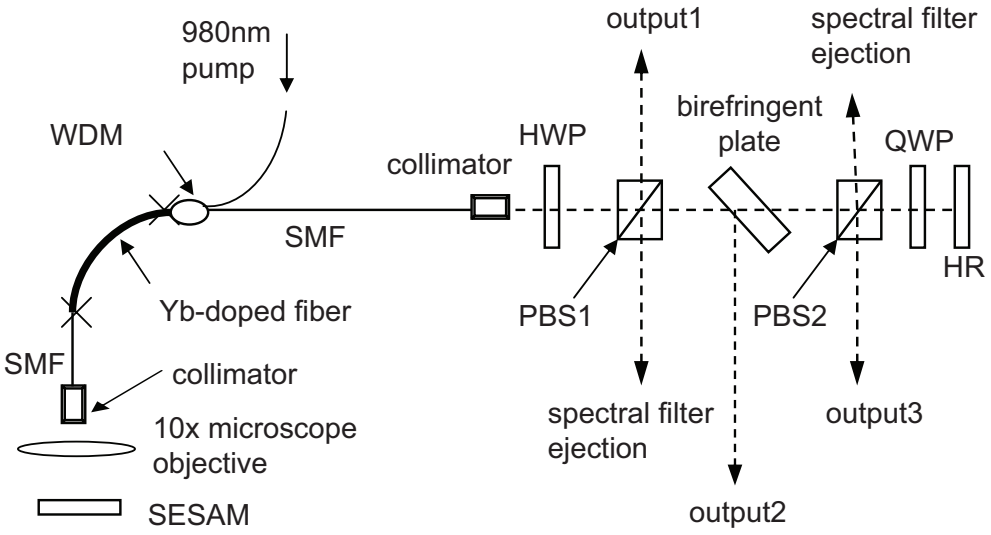

Figure 2.28: Schematic of an environmentally-stable linear dissipative soliton fiber laser: QWP: quarter-wave plate; HWP: half-wave plate; PBS: polarizing beam-splitter; WDM: wavelength-division multiplexer; HR: high reflection mirror. All components are PM components. Figure taken from Ref. [40].

wave plate settings are critical in a PM fiber cavity because the polarization state of the light must be properly aligned to the appropriate axis of the fiber to avoid deleterious secondary structure. The spectral profiles from all outputs exhibit the steep spectral sides and peaked edges that are typical of dissipative soliton lasers (Figure 2.29). Spectral fringes with ∼0.7-nm spacing indicate possible remote pulses located ∼5 ps from the main pulse on output 1, which roughly matches the polarization mode delay due to the total linear birefringence. However, output 2 and 3 do not have visible fringes (Figure 2.29(a)). This suggests that any residual energy in the other polarization states or secondary structure is ejected at output 1 (Figure 2.28).

The main output emits pulses at 33-MHz repetition rate with a pulse energy of 2.2 nJ (74 mW of average power), a pulse duration of ∼6 ps (Figure 2.29(b) inset), and a dechirped pulse duration of 310 fs (Figure 2.29(b)). This mode of operation is truly insensitive to external mechanical perturbations of the fiber and

was unchanged and sustained until intentionally interrupted. In contrast to non-PM versions of dissipative soliton lasers, only limited modes are observed with the PM cavity, all similar to that of Figure 2.29. This limitation is currently not understood, but this work successfully demonstrates the translation of a dissipative soliton laser to a environmentally stable configuration.

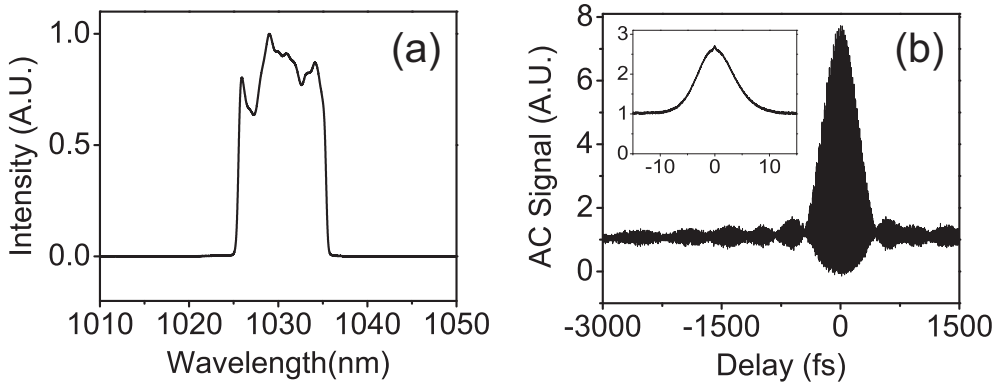

Figure 2.29: Output (a) spectrum and (b) dechirped autocorrelation of the environmentally-stable dissipative soliton laser. Inset: chirped autocorrelation. Figure taken from Ref. [40].

2.6 Giant-chirp oscillators

The results presented to this point are exclusively devoted to oscillator performance. However, many applications require more peak power than an oscillator can provide, and so require that the pulses be amplified. Large-mode-area fibers are employed to reduce nonlinear effects in chirped-pulse amplification (CPA) [41]. A typical fiber CPA system has several stages of amplification, a stretcher, a pulse-picker, and a compressor (Figure 2.30). There is clear motivation to simplify this system, to provide greater integration at lower cost. In this section, we review and advance a method to extend dissipative soliton mode-locking to a parameter regime that allows for dramatic simplification of a typical CPA system [42].

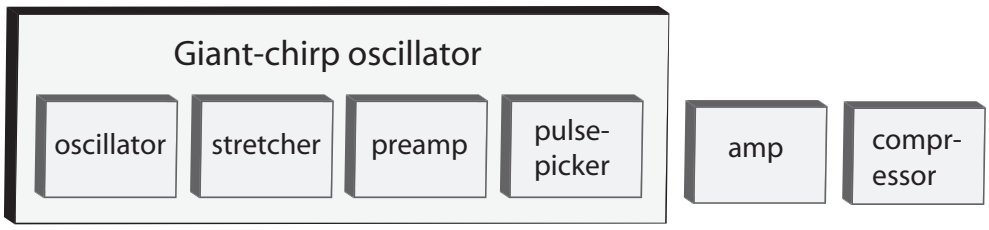

Figure 2.30: Components of fiber CPA systems. The small boxes inside the giant-chirp oscillator box represent the components of a standard CPA system that are replaced by the giant-chirp oscillator. Figure taken from Ref. [42].

We begin with an analytical investigation by rewriting Eq. 2.1 in a non-dimensionalized form,

$$\frac{\partial U(z,t)}{\partial z} = gU(z,t)+(1-i\frac{D\Omega}{2})\frac{\partial^2 U(z,t)}{\partial t^2}+(\frac{\alpha}{\gamma}+i)|U(z,t)|^2U(z,t)+\frac{\delta}{\gamma^2}|U(z,t)|^4U(z,t), \tag{2.11}$$

where now U is the product of the electric field envelope and $\sqrt{\gamma}$ and t is the product of the local time and $\sqrt{\Omega}$. We again examine the trends given by the solution of this equation with the exact particular solution Eq. 2.2. The variation of the pulse parameters as a function of GVD is shown in Figure 2.31.

With increasing GVD the pulse duration, chirp and energy all increase, the bandwidth decreases slowly, and the dechirped pulse duration increasingly deviates from the transform-limited duration. Pulses from a system with large normal GVD are therefore qualitatively identical to the pulses generated with lower GVD, but with large quantitative differences. These quantitative differences make the oscillator an ideal source for an initial stage in a CPA system. In particular, large GVD translates to long fiber, which in turn translates to low-repetition rate, removing the need for a pulse-picker. The large chirp means that there is no need for an additional stretcher. And finally, because there is no pulse-picker or

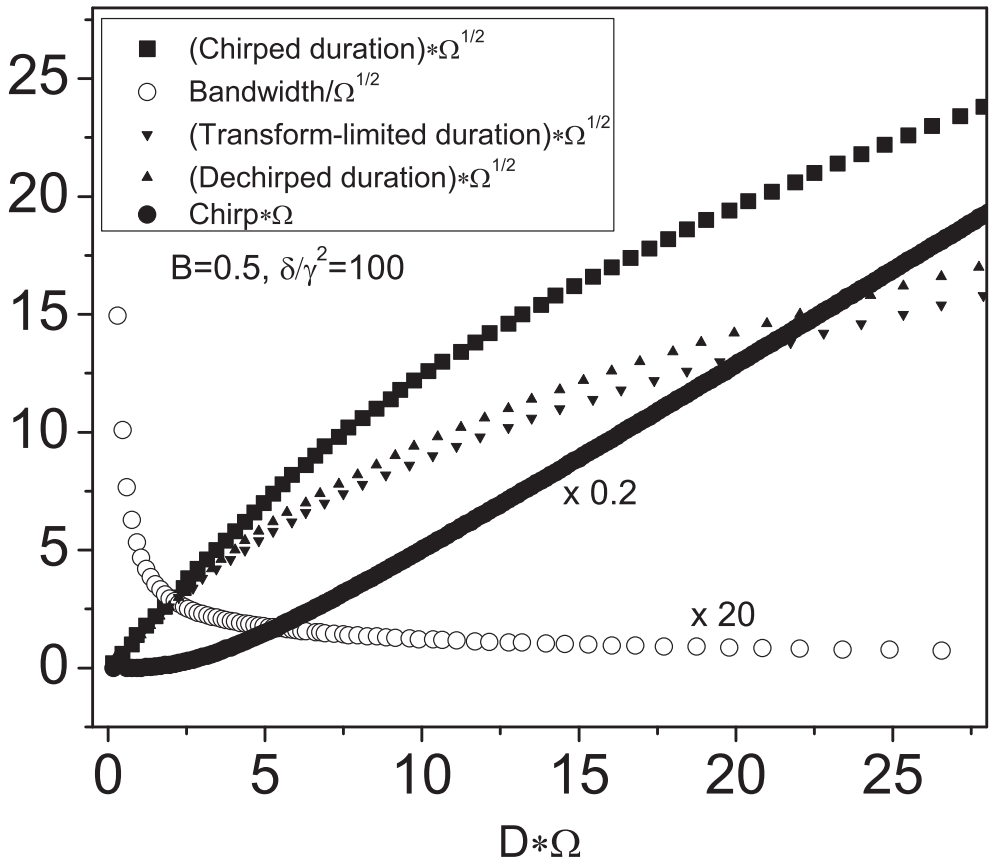

Figure 2.31: Variation of exact solution normalized pulse parameters with normalized dispersion. Figure taken from Ref. [42].

stretcher, and because the oscillator produces high energies, one or more stages of pre-amplification can be removed [42].

Scaling the repetition rate of fiber oscillators presents several challenges. Third order dispersion, nonlinear switching, relaxation oscillations and increased drift become apparent with the long fiber lengths required for low-repetition rate oscillators. In addition, it is well known that low-repetition fiber oscillators can also give rise to low-coherence noise bursts [43, 44]. For example, a fiber laser with 31-kHz repetition rate, 2.7-μJ pulse energy and 300-ns pulse duration [45], while showing no signs of noise with typical spectral and photodiode measurements of the chirped pulse, further investigation in our lab showed the pulses to be unaf-

fected by large amounts of added GVD; the phase is not coherent, making such high energy pulses unusable for applications requiring large peak power. Given the existence of such noisy pulses, it is important to clearly verify pulse coherence with a measurement such as a dechirped autocorrelation. Recent low repetition rate fiber oscillators [46, 47] do not prove the coherence of their pulses despite the similarities to the noisy pulses in Ref. [45], such as a smooth spectral profile and very large energies. Other results [48, 49], while not clearly demonstrating coherence, have properties resembling coherent normal dispersion solutions, such as steep spectral sides and modest pulse energies, but have low energy, narrow bandwidth and orders of magnitude more chirp than can be practically compensated for a useful extension of CPA.

To investigate a low-repetition rate dissipative soliton oscillator, a giant-chirp oscillator (GCO) is constructed as in Figure 2.3, but with a longer fiber before the gain, giving a net GVD of 1.4 ps^2 and a repetition rate of 3.2 MHz. A 62-m segment of SMF precedes 40 cm of Yb-doped gain fiber, and a 50-cm segment of SMF follows the gain fiber. A birefringent filter was chosen to provide a 10-nm bandwidth. A typical output of the oscillator has a spectral shape characteristic of dissipative soliton lasers (Figure 2.32(a)). The pulse is 140-ps long out of the oscillator, which is ∼300 times longer than the transform limit of ∼500 fs. This transform-limited pulse would require ∼500 m of fiber (∼10 ps^2) to reach that duration, which is about 10 times more fiber than is in the cavity. The output pulse energy is 15 nJ.

The potential utility of the giant-chirp oscillator is illustrated by a demonstration of CPA. The pulses of Figure 2.32 seed an SMF preamplifier, the output of which was fed into a large-mode area (∼1000 μm^2) PCF amplifier pumped with a

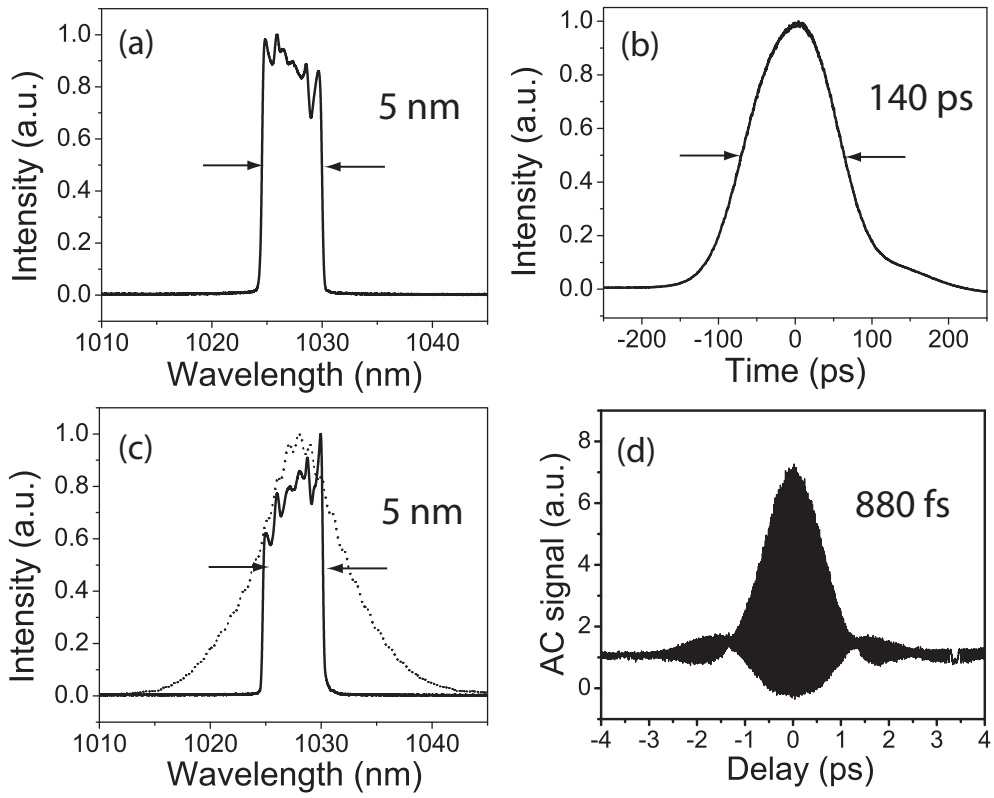

Figure 2.32: Giant-chirp oscillator: a) spectrum and b) pulse measured by a detector with 50-ps resolution. c) Solid: amplified spectrum; dotted: amplified spontaneous emission spectrum and d) autocorrelation of amplified and dechirped pulse. The pulse duration assuming an approximate deconvolution factor of 1.5 is shown. Figure taken from Ref. [42].

maximum of 25 W (e.g. see Figure 2.30). The 140-ps duration of the giant-chirp oscillator is long enough for amplification of pulses to up to 10 μJ of energy without distortion. The pulse energy is 67 nJ after the preamplifier, and 1.3 μJ after the PCF amplifier, which corresponds to 4.3 W of average power at the 3.2-MHz repetition rate. The final pulse energy is limited by the available pump power (25 W), not by the onset of nonlinear distortion. The amplified pulses are dechirped to 880-fs duration (Figure 2.32(d)) by gratings that supply 11 ps^2 of anomalous GVD. The final pulse duration is within a factor of 2 of the transform limit.

With a custom fiber GVD profile, the repetition rate could be scaled arbitrarily

with the same output pulse parameters. However, as an alternative with standard fibers, decreasing the spectral filter bandwidth can have the opposite effect to increasing the GVD, the chirp and chirped pulse duration decrease and the bandwidth increases. In the limit of a very large filter, or no external filter, this means pulses with very narrow (< 1 nm) bandwidths and large chirp, but in the limit of a narrow filter, this allows for larger bandwidths and less chirp. We demonstrate how this concept allows scaling the repetition rate to 562 kHz.

Guided by this understanding, we can optimize our design for a seed source for a CPA system. We begin by targeting a useful repetition-rate for CPA, $\sim$500 kHz. An oscillator at this repetition rate would be expected to be highly chirped because of the large amount of normal GVD. The chirp can be decreased to a dechirpable magnitude with a 2-nm spectral filter. The spectral filters used in the rest of this chapter are based on birefringent quartz plates and have a sinusoidal transmission profile. To achieve narrow filter bandwidths ($\lesssim 5$ nm), larger, costly plates must be used. Furthermore, the additional sinusoidal transmission peaks of the filter can interfere with mode-locking and promote parasitic lasing. As an alternative, we use a diffraction grating and a collimator (see section 1.3.2). The overlap of the wavelength dependant spatial beam with the Gaussian mode of the fiber results in a spectral filter profile of the same type. This Gaussian profile has the additional benefit of producing a larger solution space in numerical simulations, presumably because the filter is closer to the intrinsic dissipative soliton solution of the system (section 2.2). Other techniques can be used to produce a single peaked Gaussian spectral filter, such as the appropriate combination of birefringent plates, but we found the grating filter to be the most practical approach with components at hand.

The experimental setup is identical to previous all-normal dispersion systems with the exception of the design of the spectral filter (Figure 2.33). 362 m of single-

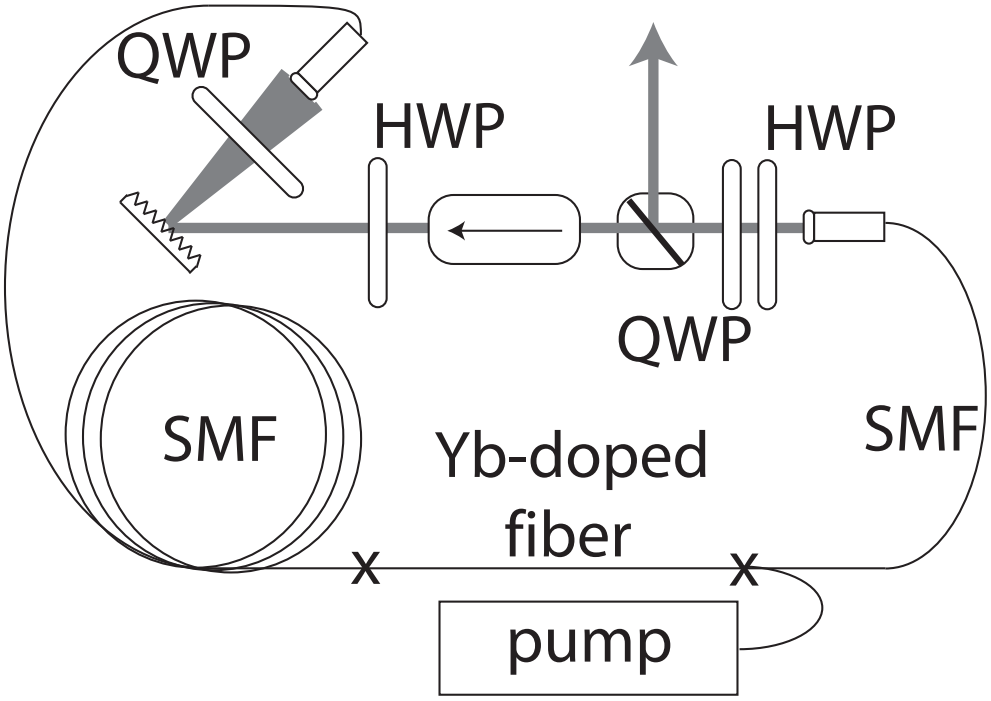

Figure 2.33: Schematic of experimental system. QWP: quarter wave plate; HWP: half wave plate; SMF: single-mode fiber.

mode fiber (SMF) precedes 60-cm ytterbium-doped gain fiber which is followed by a short 50-cm length of SMF, minimized to reduced nonlinearity. With a 2-nm bandwidth gaussian spectral filter (600 lines per mm diffraction grating at 45° incident angle placed 8.2 cm from the collimator), the cw laser efficiency is 27% and stable single-pulsed mode-locking was achieved at the fundamental repetition rate of 562 kHz (Figure 2.34). With 130-mW pump power, the output power was 14 mW, corresponding to 25-nJ pulse energy. The pulse was dechirped with 11-ps^2 of anomalous dispersion to a duration of 800 fs, 1.5 times the transform limited duration. The dechirped duration could be further reduced if TOD is removed from the dechirping setup. Because of the large net dispersion, the intrinsic spectral bandwidth is narrow, and using a narrow filter, the characteristics should be similar

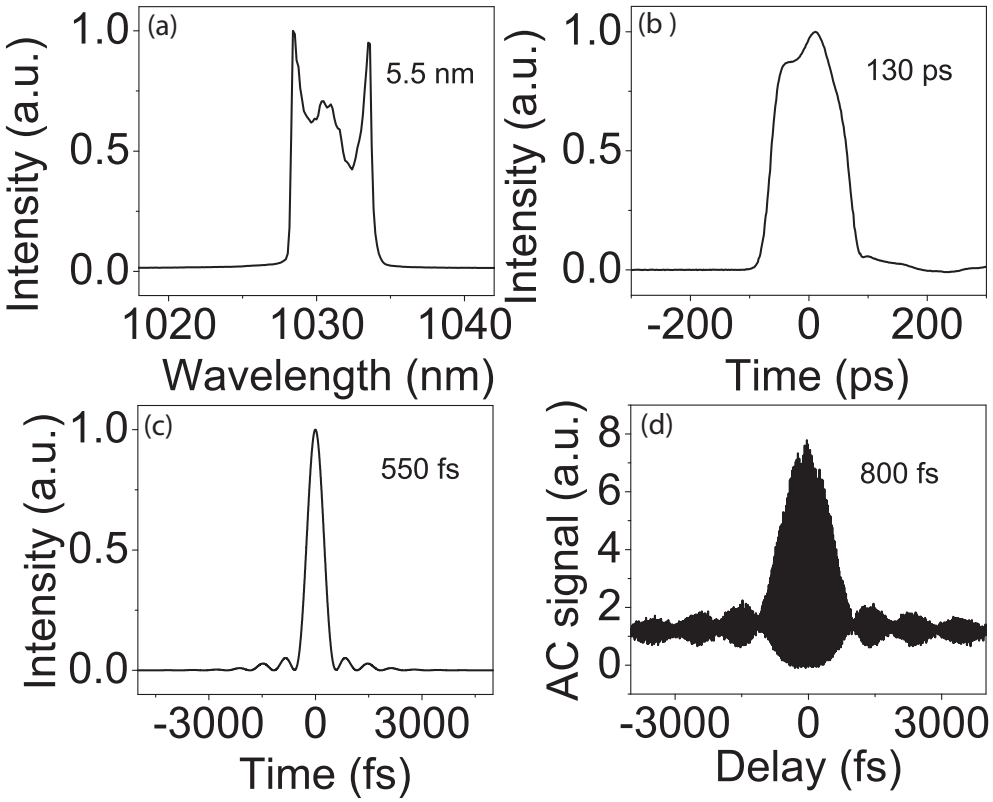

Figure 2.34: 562-kHz oscillator: output (a) spectrum; (b) pulse; (c) calculated transform-limited pulse; and (d) dechirped autocorrelation.

to a dissipative soliton at a much higher repetition rate with a larger filter. For example, the spectrum shows the characteristic steep sides and 2 peaked structure of normal dispersion mode-locking (Figure 2.34(a)), the autocorrelation has the secondary structure inherent with steep-edged spectra (Figure 2.34(d)), and the dechirped pulse is close to the transform limited-duration. The chirped pulse was measured directly with a fast optical detector and oscilloscope with a 30-ps response time, showing a chirped duration of 130 ps (Figure 2.34(b)). If desired, the repetition rate can be extended still further, but only at a sacrifice to the spectral bandwidth.

At 562-kHz repetition rate, the laser is subject to drift of the output pulse parameters as a consequence of environmental perturbations to the long lengths

of fiber in the cavity. This drift can be minimized in a number of ways including replacing the saturable absorber, using PM fiber, using a faraday rotator, but each technique comes with a trade of performance. These issues must be addressed before low repetition rate dissipative soliton oscillators can find broader use for applications.

This low-repetition rate oscillator has one of the largest pulse energies reported from a standard single-mode fiber oscillator. Further work must be done to investigate the pulse energy limitations for such dissipative soliton systems.

These experiments were performed with components available in our laboratory, and are not intended to represent the limit to this approach. For example, some applications require lower repetition rates, which will facilitate larger pulse duration and chirp, which will in turn allow for the further extension of the peak power. More chirp does come at the expense of bandwidth, and further investigation is need to determine the optimum chirp to maximize amplifier peak power. Custom fibers and operation at 1.5-μm wavelength could also be beneficial as there is a larger degree of freedom in the selection of fibers with various values of GVD.

2.7 Conclusions

The development of stable and reliable femtosecond lasers depended on the capability of introducing controllable anomalous dispersion into laser cavities. Lasers based on soliton-like pulse-shaping have dominated ultrafast science and technology over the past two decades. Fiber lasers offer major practical advantages over solid-state lasers, but the energy of soliton pulses in fiber lasers is inadequate for many photophysical applications, and as a consequence fiber lasers have found

limited use compared to solid-state lasers.

Pulse-shaping in normal-dispersion lasers is dominated by spectral filtering of a chirped pulse in the cavity. Such pulses are modeled well by solutions to the cubic-quintic Ginzburg-Landau equation, which confirms the role of the dissipative processes. Pulses that breathe weakly as they traverse the cavity are referred to as dissipative solitons. The normal-dispersion lasers provide a convenient setting for studying this new class of nonlinear wave. The dissipative-soliton solutions can accumulate remarkably large nonlinear phase shifts without distortion or wave-breaking, and this property translates into unprecedented pulse energies from a fiber laser. Lasers constructed of ordinary single-mode fibers can generate 100-fs pulses with energy as high as 30 nJ, to date. Such lasers are the first fiber lasers to compete directly with solid-state lasers in performance. Normal-dispersion lasers can also be designed to generate highly-chirped pulses at low repetition rates. Such giant-chirp oscillators hold significant promise for simplifying short-pulse fiber amplifiers.

Most of the results presented in this chapter represent the initial demonstrations of new concepts. Dissipative-soliton lasers thus offer the best performance among femtosecond fiber lasers to date, along with new regimes of operation. When these properties are combined with the simple designs that are possible through the elimination of intracavity anomalous dispersion, attractive instruments result. With further development and engineering, the dissipative-soliton lasers should have major impact on ultrafast science and technology.

BIBLIOGRAPHY

[1] W. H. Renninger and F. W. Wise, in *Fiber Lasers*, edited by O. G. Okhotnikov (Wiley-V C H, Berlin, 2012).

[2] F. O. Ilday, J. R. Buckley, W. G. Clark, and F. W. Wise, Phys. Rev. Lett. **92**, 213902 (2004).

[3] A. Chong, J. Buckley, W. Renninger, and F. Wise, Opt. Express **14**, 10095 (2006).

[4] W. H. Renninger, A. Chong, and F. W. Wise, Physical Review A **77**, 23814 (2008).

[5] R. L. Fork, O. E. Martinez, and J. P. Gordon, Opt. Lett. **9**, 150 (1984).

[6] H. A. Haus, J. G. Fujimoto, and E. P. Ippen, J. Opt. Soc. Am. B **8**, 2068 (1991).

[7] B. G. Bale, J. N. Kutz, A. Chong, W. H. Renninger, and F. W. Wise, J. Opt. Soc. Am. B **25**, 1763 (2008).

[8] J. M. Soto-Crespo, M. Grapinet, P. Grelu, and N. Akhmediev, Phys. Rev. E **70**, 66612 (2004).

[9] N. Akhmediev, J. M. Soto-Crespo, M. Grapinet, and P. Grelu, Optical Fiber Technology **11**, 209 (2005).

[10] A. Komarov, H. Leblond, and F. Sanchez, Phys. Rev. E **72**, 25604 (2005).

[11] E. Ding and J. N. Kutz, J. Opt. Soc. Am. B **26**, 2290 (2009).

[12] N. Akhmediev, J. M. Soto-Crespo, and P. Grelu, Physics Letters A **372**, 3124 (2008).

[13] W. Chang, A. Ankiewicz, J. M. Soto-Crespo, and N. Akhmediev, Phys. Rev. A **78**, 23830 (2008).

[14] A. Komarov, K. Komarov, H. Leblond, and F. Sanchez, Journal of Optics A: Pure and Applied Optics **9**, 1149 (2007).

[15] W. van Saarloos and P. C. Hohenberg, Phys. D **56**, 303 (1992).

[16] J. M. Soto-Crespo, N. N. Akhmediev, V. V. Afanasjev, and S. Wabnitz, Phys. Rev. E **55**, 4783 (1997).

[17] F. I. Khatri, J. D. Moores, G. Lenz, and H. A. Haus, Opt. Commun. **114**, 447 (1995).

[18] H. Lim, F. O. Ilday, and F. W. Wise, Opt. Lett. **28**, 660 (2003).

[19] L. M. Zhao, D. Y. Tang, and J. Wu, Opt. Lett. **31**, 1788 (2006).

[20] O. Prochnow, A. Ruehl, M. Schultz, D. Wandt, and D. Kracht, Opt. Express **15**, 6889 (2007).

[21] *Dissipative Solitons*, edited by N. Akhmediev and A. Ankiewics (Springer, Berlin Heidelberg, 2005).

[22] I. Aranson and L. Kramer, Rev. Mod. Phys. **74**, 99 (2002).

[23] E. A. Ultanir, G. I. Stegeman, D. Michaelis, C. H. Lange, and F. Lederer, Phys. Rev. Lett. **90**, 253903 (2003).

[24] Z. Bakonyi, D. Michaelis, U. Peschel, G. Onishchukov, and F. Lederer, J. Opt. Soc. Am. B **19**, 487 (2002).

[25] Y. Tanguy, T. Ackemann, W. J. Firth, and R. Jäger, Phys. Rev. Lett. **100**, 13907 (2008).

[26] A. Chong, W. H. Renninger, and F. W. Wise, J. Opt. Soc. Am. B **25**, 140 (2008).

[27] W. H. Renninger, A. Chong, and F. W. Wise, J. Opt. Soc. Am. B **27**, 1978 (2010).

[28] A. Chong, W. H. Renninger, and F. W. Wise, Opt. Lett. **32**, 2408 (2007).

[29] A. Chong, W. H. Renninger, and F. W. Wise, Opt. Lett. **33**, 2638 (2008).

[30] A. Hideur, T. Chartier, M. Brunel, S. Louis, C. Ozkul, and F. Sanchez, Applied Physics Letters **79**, 3389 (2001).

[31] B. Ortaç, A. Hideur, T. Chartier, M. Brunel, C. Özkul, and F. Sanchez, Opt. Lett. **28**, 1305 (2003).

[32] J. An, D. Kim, J. W. Dawson, M. J. Messerly, and C. P. J. Barty, Opt. Lett. **32**, 2010 (2007).

[33] K. Kieu, W. H. Renninger, A. Chong, and F. W. Wise, Opt. Lett. **34**, 593 (2009).

[34] B. Ortaç, M. Baumgartl, J. Limpert, A. Tünnermann, B. Ortac, and A. Tuennermann, Optics Letters **34**, 1585 (2009).

[35] C. Lecaplain, B. Ortaç, G. Machinet, J. Boullet, M. Baumgartl, T. Schreiber, E. Cormier, and A. Hideur, Opt. Lett. **35**, 3156 (2010).

[36] M. Baumgartl, F. Jansen, F. Stutzki, C. Jauregui, B. Ortaç, J. Limpert, and A. Tünnermann, Opt. Lett. **36**, 244 (2011).

[37] S. Lefrançois, K. Kieu, Y. Deng, J. D. Kafka, and F. W. Wise, Opt. Lett. **35**, 1569 (2010).

[38] C.-H. Liu, G. Chang, N. Litchinitser, A. Galvanauskas, D. Guertin, N. Jabobson, and K. Tankala, in *Advanced Solid-State Photonics* (Optical Society of America, Washington, 2007), p. ME2.

[39] S. Lefrancois, T. S. Sosnowski, C.-H. Liu, A. Galvanauskas, and F. W. Wise, Opt. Express **19**, 3464 (2011).

[40] A. Chong, W. H. Renninger, and F. W. Wise, Opt. Lett. **33**, 1071 (2008).

[41] D. Strickland and G. Mourou, Opt. Commun. **56**, 219 (1985).

[42] W. H. Renninger, A. Chong, and F. W. Wise, Opt. Lett. **33**, 3025 (2008).

[43] V. J. Matsas, T. P. Newson, and M. N. Zervas, Optics Communications **92**, 61 (1992).

[44] M. Horowitz, Y. Barad, and Y. Silberberg, Opt. Lett. **22**, 799 (1997).

[45] W. H. Renninger, A. Chong, and F. W. Wise, in *Conference on Lasers and Electro-Optics/Quantum Electronics and Laser Science Conference and Pho-*

tonic Applications Systems Technologies (Optical Society of America, Washington, DC, 2008), p. CTuFF6.

[46] S. Kobtsev, S. Kukarin, and Y. Fedotov, Opt. Express **16**, 21936 (2008).

[47] M. Zhang, L. L. Chen, C. Zhou, Y. Cai, L. Ren, and Z. G. Zhang, Laser physics leters **6**, 657 (2009).

[48] X. Tian, M. Tang, P. P. Shum, Y. Gong, C. Lin, S. Fu, and T. Zhang, Opt. Lett. **34**, 1432 (2009).

[49] E. J. R. Kelleher, J. C. Travers, Z. Sun, A. G. Rozhin, A. C. Ferrari, S. V. Popov, and J. R. Taylor, Applied Physics Letters **95**, 111108 (2009).

CHAPTER 3

PULSE SHAPING MECHANISMS IN NORMAL-DISPERSION MODE-LOCKED FIBER LASERS[1]

3.1 Introduction

Ultrashort pulses are stabilized in an oscillator when the effects of optical nonlinearity are exactly balanced by other processes after one cycle around the cavity. The most common way to compensate nonlinearity is through group-velocity dispersion (GVD). When the GVD is anomalous, pulses are formed by a balance between positive nonlinear and negative dispersive phase changes. Before 1993, researchers operated fiber lasers almost exclusively with large net anomalous GVD, in the soliton-like regime. At the next level of performance, stretched-pulse or dispersion-managed soliton ([2, 3]) operation exists for net anomalous or small normal GVD, and allows femtosecond pulses with up to nanojoule energies and ~ 10 kW peak power levels.

Recent work has shown theoretically ([4, 5]) and experimentally ([6, 7]) that much higher pulse energies and peak powers can be achieved in fiber lasers that operate at large normal dispersion. In the normal dispersion regime, solitons do not form, so new pulse-shaping processes are needed. The aim of this chapter is to present theoretical and intuitive understanding of the pulse-shaping processes and pulse evolutions in normal-dispersion fiber lasers, which includes but is not limited to dissipative soliton mode-locking (chapter 2). The results of numerical simulations that accurately model experiments will be presented. Pulses that propagate in normal-dispersion media are susceptible to distortion and break-up owing to op-

[1]The majority of this chapter is reprinted, with permission, from Ref. [1].

tical wave breaking [8]. To compensate nonlinear phase and avoid wave-breaking, dissipation is required and plays a key role in the pulse-shaping. Several distinct regimes of mode-locking can be labeled usefully by the pulse that forms in each one. These include

- Dissipative solitons [5, 7, 9–32]
- Passive similaritons (pulses that evolve in a self-similar fashion have been dubbed similaritons) [33–37]
- Amplifier similaritons [38–41].

In addition, we consider a pulse evolution that has been exploited experimentally in lasers with dispersion maps, but has not been understood theoretically ([34, 42]). Ilday *et al.* used the phrase "wave-breaking-free" to describe these pulses, but that conveys no insight about the pulse formation or evolution that underlies the property. The analysis shows that the pulse formation depends crucially on dissipation, while the evolution is dominated by the presence of the dispersion map. We suggest that these pulses be called stretched dissipative solitons. These mode-locking regimes will be examined numerically and compared to recent experimental works. For each regime, we will address the following questions:

- How do the relevant physical processes balance to shape the pulse?
- What identifies the regime? How is it unique?
- What are the performance advantages?

The chapter is organized as follows. Dissipative solitons in all-normal-dispersion lasers will be explained in section 3.2. This analysis is distinguished from that in

chapter 2 by using numerical simulations to determine, without approximation, what is fundamentally important to start and stabilize these pulses. Section 3.3 addresses dispersion-managed cavities with net normal GVD. We find that two distinct pulse evolutions can occur for a single set of cavity parameters. The formation of self-similar pulses in the passive normal-dispersion fiber of a laser (section 3.3.1) will be described, and contrasted with dissipative-soliton formation. The second regime in a mapped cavity is the stretched dissipative soliton. In section 3.3.2 we show that these pulses are formed similarly to dissipative solitons, but their evolution is defined by the dispersion map. Section 3.4 briefly considers normal-dispersion lasers in which self-similar evolution occurs in the amplifier, not in passive fiber. Spectral filtering is critical to stabilizing this evolution, which has the remarkable feature of being a local nonlinear attractor in the gain fiber. The different regimes will be summarized and compared in section 3.5.

3.2 Dissipative soliton fiber lasers

In 2006 Chong *et al.* introduced a new femtosecond mode-locking regime based on cavities with only normal-dispersion components [9] (chapter 2). This was a major departure from prior approaches to femtosecond pulse generation, all of which relied on dispersion compensation. The pulses depend on the balance of both amplitude and phase modulations, and are thus considered dissipative solitons, accurately modeled with a quintic Ginzburg-Landau master equation [5]. To date, the best performance from single-mode fiber lasers has been achieved with this mode-locking mechanism. 100-fs pulses with energies of ∼30 nJ and peak power levels of ∼300 kW can be generated by lasers based on SMF [7], and megawatt peak power can be reached in large-mode area fiber ([27,30–32]). Furthermore, the dissipative

soliton regime has been extended to large net dispersion (> 1 ps^2), which allows for high energy pulses with large and linear chirp [20]. This giant-chirp oscillator can significantly reduce the complexity of chirped-pulse amplification systems. In this section, the key mechanisms in normal dispersion mode-locking will be revealed in the context of an all-normal dispersion dissipative soliton (DS) laser. Specifically, we find that amplitude and phase modulations have equal importance, and that large nonlinear phase shifts are compensated by propagation of a chirped pulse in normal-dispersion fiber. The simulations are designed to model a realistic laser based on Yb:fiber operating at 1 μm. Details and parameters of the simulations are in the Appendix.

To begin to understand DS mode-locking, the fiber sections are modeled as if they are lumped into a single segment of gain fiber, which is the simplest realistic model for a dissipative soliton fiber laser (Figure 3.1). The resulting pulse

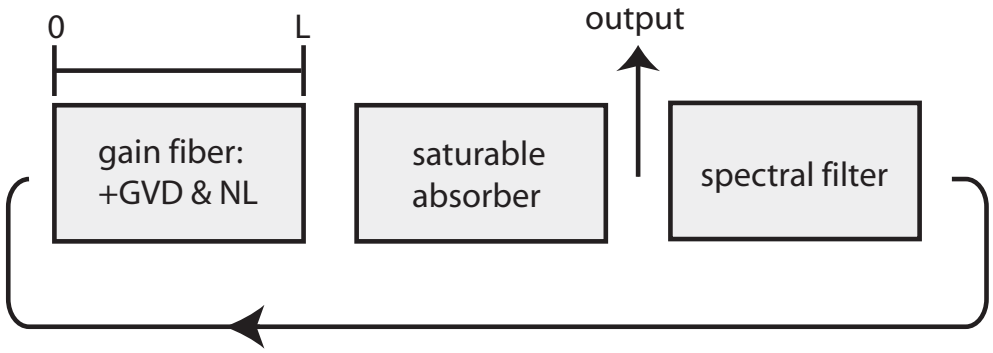

Figure 3.1: Schematic of the simplest all-normal dispersion dissipative soliton laser.

parameters and evolution are those of a typical DS laser (Figure 3.2). In the fiber, the spectrum develops structure (Figure 3.2(a)) and the pulse duration increases (Figure 3.2(b)). The saturable absorber slightly reduces the pulse duration. The spectral filter cuts away the spectral structure, and because the pulse is chirped,

restores the pulse to its original duration. Further insight is gained by examining the temporal magnitude and phase. The temporal phase is the same at the end of each segment, which implies that the saturable absorber and the spectral filter have little effect on it. However, if we look into the fiber section (Figure 3.2(c)) we see that the temporal phase evolves in such a way that it begins and ends with the same profile. Thus, for this pulse shape, normal dispersion compensates a self-focusing nonlinear phase shift.

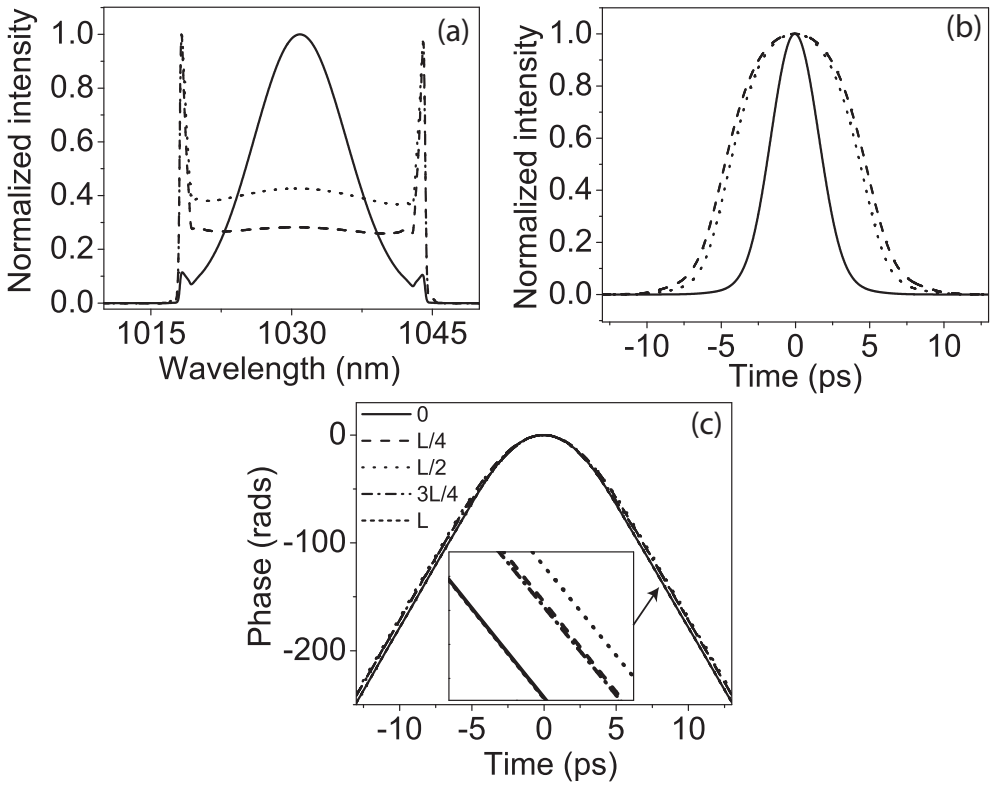

Figure 3.2: Evolution of the (a) spectrum and (b) temporal profile of a DS plotted after the filter (solid), after the fiber (dashed), and after the saturable absorber (dotted); (d) evolution of the temporal phase in the fiber section.

To demonstrate that this picture is not an artifact of combining the fiber sections, and to verify and generalize this conclusion, we also simulate a cavity that artificially separates GVD, nonlinearity and the saturating gain into independent sections of the oscillator, in that order (Figure 3.3). In this case, as before, the

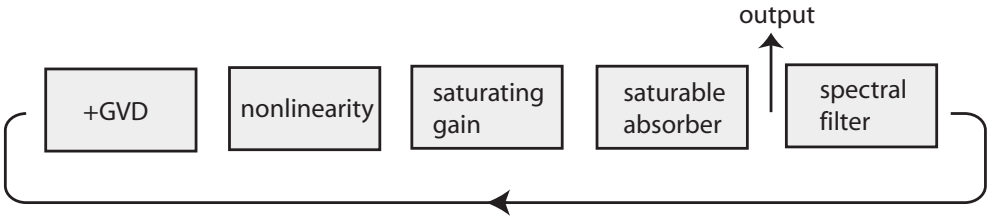

Figure 3.3: Schematic of an all-normal dispersion dissipative soliton laser with physical processes separated for clarity.

spectrum gains structure in the nonlinear section (Figure 3.4(a)) and the pulse duration increases due to the GVD (Figure 3.4(b)). The saturable absorber shortens the pulse. Also, as in Figure 3.2, the spectral filter cuts away the spectral structure, and because the pulse is chirped, decreases the pulse back to its original duration. The primary difference in this scenario is that the temporal phase evolves in the normal dispersion fiber (Figure 3.4(c)). However, as in Figure 3.2, the change in the phase due to the normal GVD cancels the nonlinear phase shift (Figure 3.4(d)). The spectral filter also contributes to the temporal phase, but it is negligible compared to that from the nonlinearity and the normal GVD (Figure 3.4(d)).

Based on the simulations, we can say that linear phase accumulation is balanced by spectral filtering and saturable absorption to create the pulse amplitude, and simultaneously GVD balances the nonlinear phase accumulation in a DS. These balances are illustrated in Figure 3.5. Remarkably, a chirped pulse that propagates through normal-GVD material can accumulate a linear phase that is negative, *i.e.*, that one would ordinarily associate with propagation at anomalous GVD. This feature is critical to the generation of high-energy pulses.

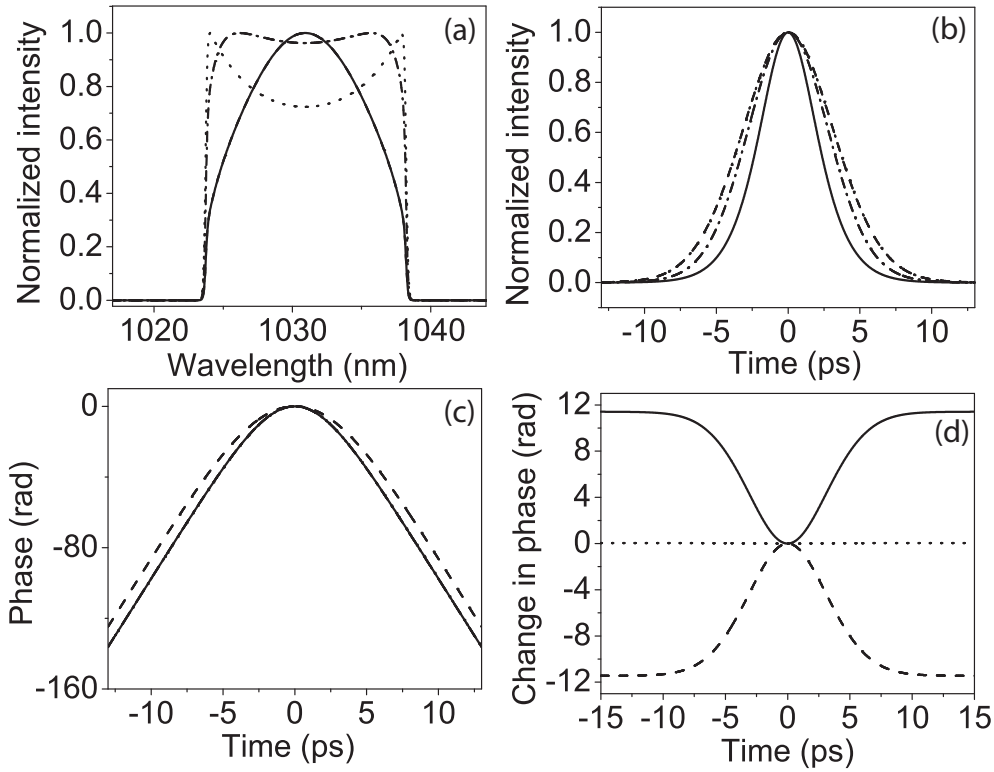

Figure 3.4: Evolution of the: (a) spectrum, (b) pulse, and (c) temporal phase of the solution to a normal dispersion oscillator plotted after the filter (solid), after the GVD (dashed), after the nonlinearity (dotted), and after the saturable absorber (dashed-dotted). (d) Change in phase due to the GVD (solid), nonlinearity (dashed), and spectral filter (dotted).

3.3 Dispersion-managed fiber lasers

In a dispersion-managed cavity, several distinct operating regimes exist. Dispersion-managed solitons occur for net GVD near zero, and for large normal GVD two distinct regimes can co-exist for a single set of cavity parameters. One of these regimes features parabolic pulses that evolve self-similarly in a long segment of passive fiber [33]. In section 3.3.1 we will investigate how nonlinearity is managed in this regime, comparing and contrasting with dissipative soliton mode-locking. The second pulse evolution found at large normal GVD was first observed experimentally by Ilday *et al.*, who described it generically as "wave-breaking-free."

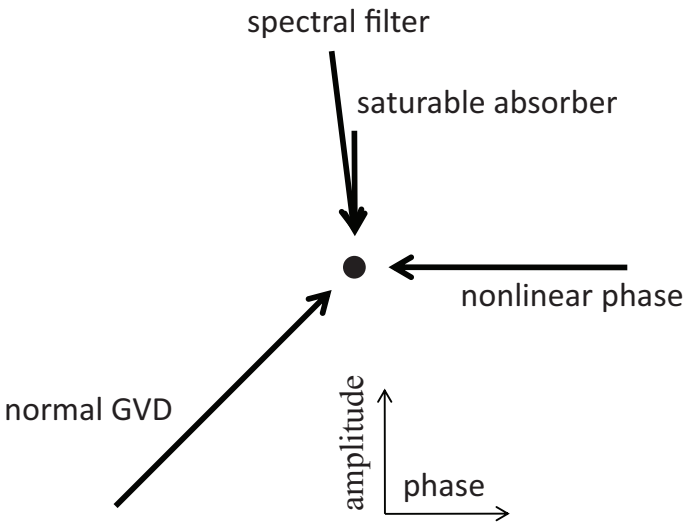

Figure 3.5: Qualitative illustration of the amplitude and phase balances in a DS laser.

This mode was later exploited by Buckley *et al.* to achieve 100-fs pulses with energy above 10 nJ for the first time. It features highly down-chirped pulses with large breathing ratios, and supports stable pulses with peak powers of ∼100 kW ([34,42]). However, a theoretical understanding has not been reported to date. In section 3.3.2 we will present the first theoretical results that exhibit this evolution. These demonstrate that the pulses are shaped by the same mechanisms as dissipative solitons, but have additional evolution defined by the particular dispersion map.

We simulate a realistic dispersion-managed cavity as in Ref. [34], *e.g.* (Appendix A.2). SMF precedes a Yb-doped gain fiber, which is followed by a saturable absorber, an output coupler and gratings that supply anomalous GVD, in that order (Figure 3.6). We consider only linear anomalous-GVD segments. It is typically desirable to avoid soliton formation in high-energy lasers, which motivates the use of linear anomalous-GVD segments. As a practical matter, in 1-μm systems the anomalous GVD is commonly provided by diffraction gratings. In most cases, the

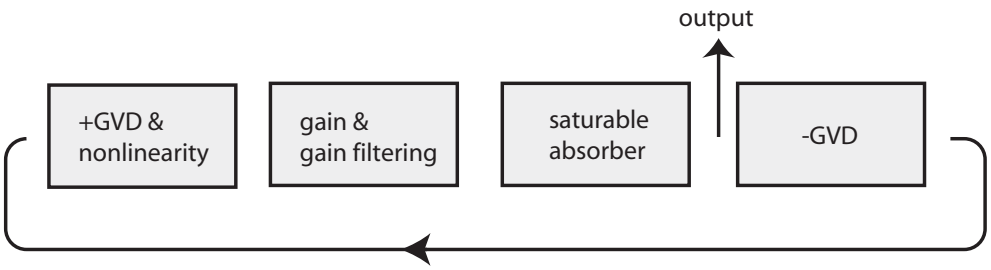

Figure 3.6: Schematic of a typical 1-μm dispersion-managed fiber laser.

conclusions we find can be generalized to 1.55-μm systems, where the ready availability of anomalous-dispersion fiber makes nonlinear anomalous-dispersion segments more common. By varying the initial conditions of the simulations slightly (different white noise or Gaussian initial conditions), the two solutions shown in Figure 3.7(a) can be seen.

3.3.1 Passive self-similar fiber lasers

The solid line in Figure 3.7 is the well-known self-similar pulse solution [33]. The pulses have minimal spectral evolution. They are always positively chirped, with a nearly-parabolic pulse profile. The pulse duration increases monotonically in the passive fiber, and the maximum duration occurs at the transition from normal to anomalous dispersion. The temporal breathing ratio ranges from 10 to 50 under typical conditions. The dispersive delay is primarily responsible for returning the pulse to the original duration after a round-trip of the cavity. The self-similar pulses can tolerate large nonlinear phase shifts without distortion or wave-breaking. As there has been some confusion in the literature, we emphasize that these similaritons are the asymptotic solutions of the nonlinear Schrodinger equation with only nonlinearity and normal GVD. These are distinct from the similaritons that form

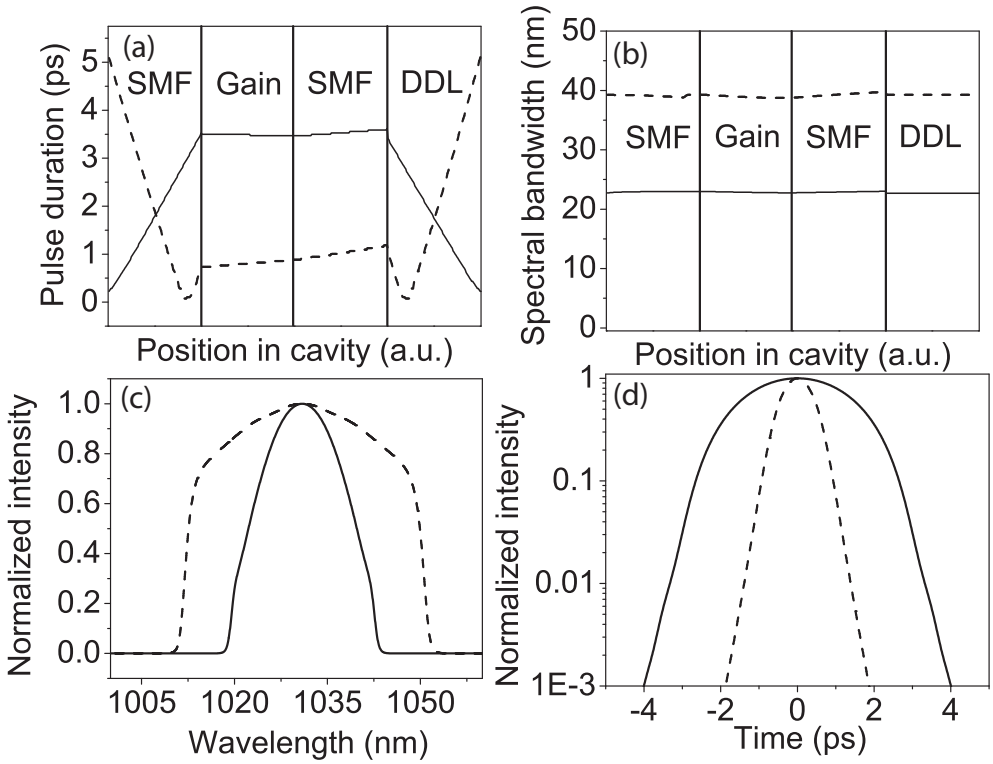

Figure 3.7: Evolution of the (a) pulse duration (the full-width at half of the maximum) and (b) spectral bandwidth (the full-width at a fifth of the maximum) and output (c) spectra and (d) chirped pulses for self-similar (solid) and stretched dissipative soliton (dashed) mode-locked pulses given identical cavity parameters. DDL: dispersive delay line.

in the presence of gain, and which constitute nonlinear attractors [43]. The first similariton laser [33] was *not* a similariton amplifier with the cavity feedback.

On initial inspection, it would seem that the self-similar propagation has little relation to dissipative-soliton formation. The initial similariton laser was designed to minimize the effects of gain filtering, which would in turn minimize perturbation of the self-similar propagation. To address these questions, we performed a series of simulations with the parameters varied continuously but with fixed average parameters, and we found that a continuous transition can be made from dissipative soliton formation to self-similar evolution. (The parameters of the simulations are in Appendix A.2.1.) Thus, we conclude that the self-similar regime does rely on

dissipation. It is desirable to have a more-detailed understanding of how the temporal amplitude and phase of the pulse balance around the cavity, and this is also provided by the simulations.

The results for the end-points of the series (*i.e.*, the "pure" dissipative soliton and the passive similariton) are shown in Figure 3.8. Although the average parameters of the systems are identical, clear differences remain in the converged solutions. The bandwidth of the DS laser is larger and the spectrum more square (Figure 3.8(a)). In the DS laser, the increase of the pulse duration from the normal dispersion is compensated by the filter and the saturable absorber, whereas in the mapped cavity the anomalous dispersion also plays a major role (Figure 3.8(b)). As expected, the self-similar pulse becomes more parabolic (Figure 3.8(d)) than the DS pulse (Figure 3.8(c)).

To compare the performance of these two systems, the pump power is increased in both the DS and the self-similar cavities with the same net parameters until the maximum energy is reached. As is expected in DS lasers ([5, 18]), the spectrum of the high energy output becomes broad and structured, and features prominent peaks at the edges (Figure 3.9(a), solid line). The self-similar spectrum, although narrower than the DS spectrum, broadens while it maintains a smooth parabolic profile (Figure 3.9(a), dashed line). Because the bandwidth approaches that of the gain filter, the self-similar pulse has a significant pulse cutting contribution due to the spectral filter (Figure 3.9(b), dashed line). The respective pulse evolutions (Figure 3.9(b)) clearly distinguish the two regimes. Because of the dispersion map, the self-similar pulse is longer and more parabolic (Figure 3.9(d)) than the DS pulse (Figure 3.9(c)).

The numerical solutions confirm the basis of the term self-similar. Figure 3.9(f)

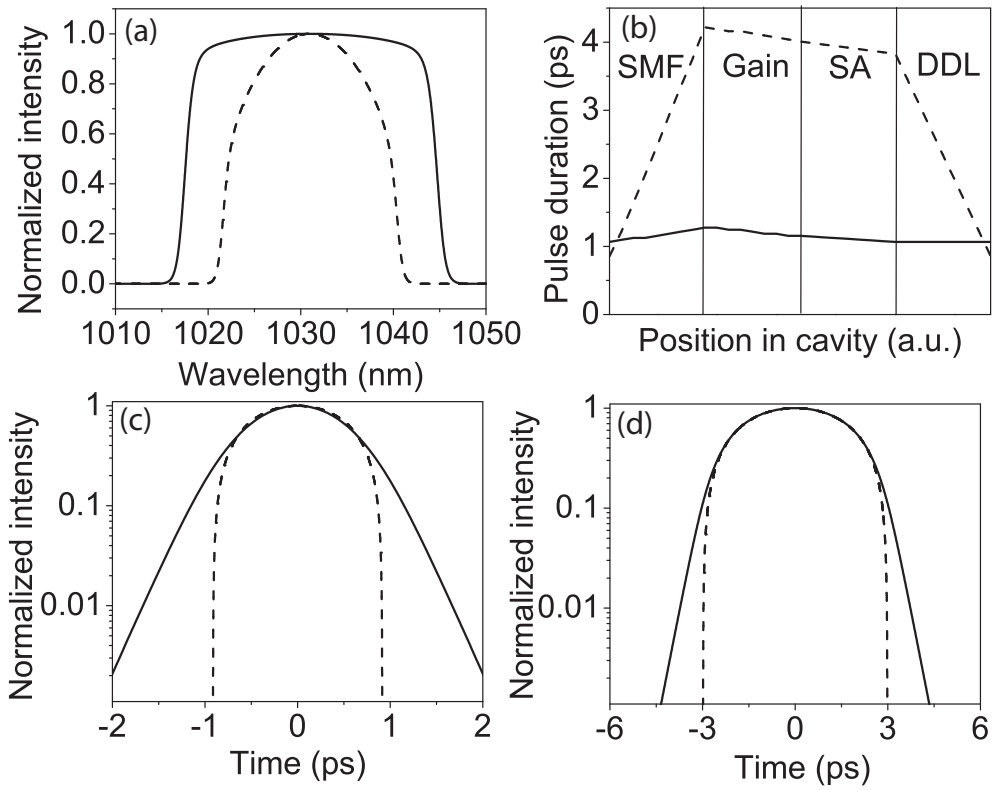

Figure 3.8: (a) Spectrum after the first SMF and (b) temporal evolution of the DS (solid) and self-similar (dashed) pulses. (c) Pulse after the first SMF for the DS and the (d) self-similar pulses; the dotted lines represent parabolic fits.

shows the evolution of the pulse through the fiber section in the self-similar laser. The pulse evolves self-similarly in a parabolic form, while the form of the DS pulse changes continuously and is not self-similar (Figure 3.9(e)). The maximum output energy for the DS pulse is 30 nJ and for the self-similar pulse is 57 nJ. This difference stems from the extended duration of the self-similar pulse due to the additional dispersion map in the cavity, which decreases the peak power. As another measure of performance, the nonlinear phase $\phi^{NL} = \int \gamma(z) P_o(z) dz$ is useful for quantifying the peak power that each mechanism can accommodate. $\phi^{NL} = 10$ for the self-similar mode and $\phi^{NL} = 20$ for the DS mode. While in this case the energy tolerated by the self-similar mode is greater, it occurs with less total phase shift. This is important because in a real cavity, to operate in

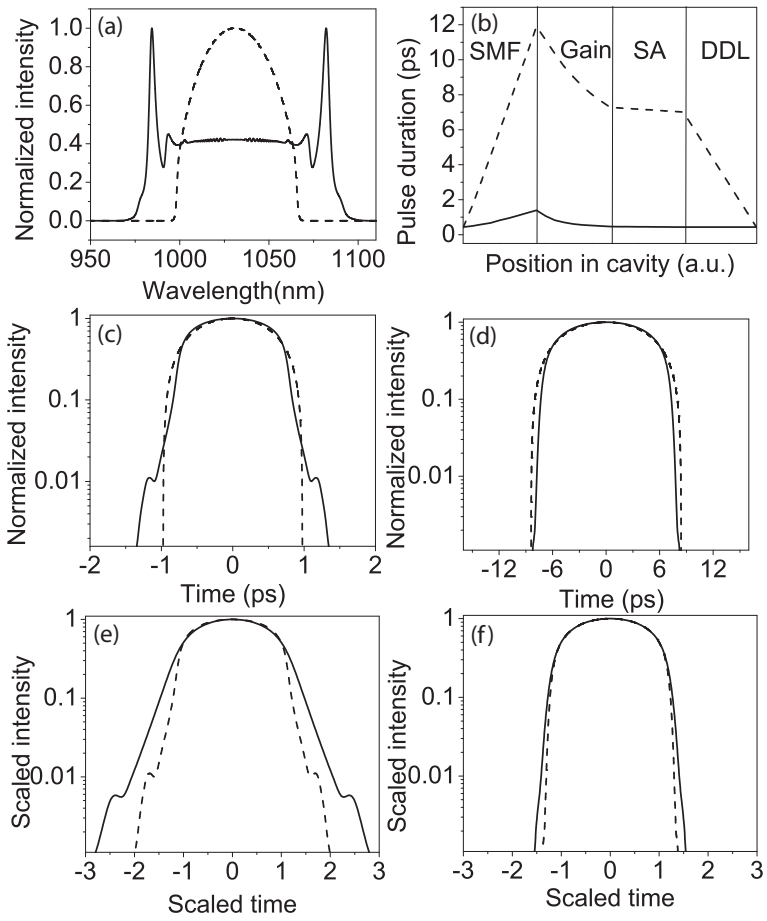

Figure 3.9: (a) Spectrum after the first SMF and (b) temporal evolution of the DS (solid) and self-similar (dashed) pulses. Pulse after the first SMF for the (c) DS and the (d) self-similar pulses; the dashed lines represent parabolic fits. Temporal evolution of the pulse in the first section of the fiber of the (e) DS laser and the (f) self-similar laser; the dashed (solid) line represents propagation through half (all) of the fiber.

the self-similar mode with sufficient pulse breathing, more fiber is necessary, which in turn carries more nonlinearity. As a consequence, the maximum energies for self-similar and DS mode-locking regimes will be comparable.

To illustrate how the basic physical processes balance each other to form a stable self-similar pulse, we examine the evolution of the high energy self-similar pulse shown in Figure 3.9. The spectrum broadens and approaches a parabolic form on propagation in the long passive fiber, and is returned to its original form after the

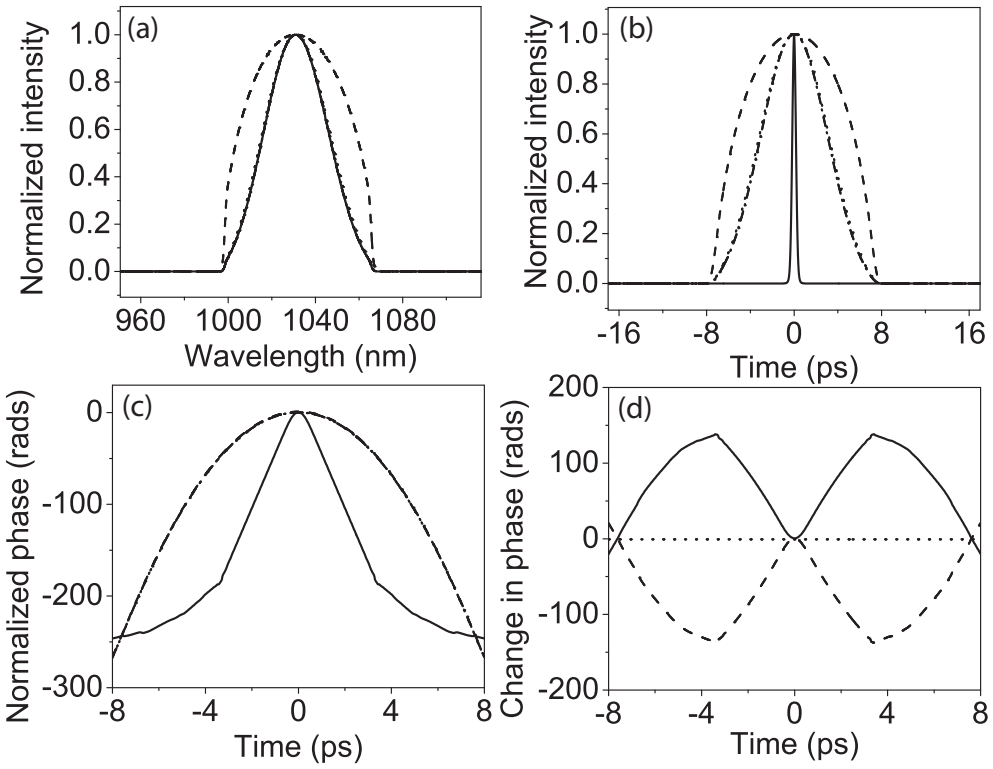

Figure 3.10: Evolution of the: (a) Spectrum, (b) pulse, and (c) temporal phase of the solution to a normal dispersion oscillator plotted after the filter (solid), after the GVD (dashed), after the nonlinearity (dotted), and after the saturable absorber (dashed-dotted). (d) Change in phase due to the SMF (dashed), anomalous GVD (dashed), and spectral filter (dotted).

gain filter (Figure 3.10(a)). The temporal profile also broadens as the pulse propagates in the fiber, and the positive pulse chirp increases. The anomalous-dispersion segment compensates most of the pulse broadening, with small contributions from the gain filter and the saturable absorber (Figure 3.10(b)). The large temporal phase accumulation in the fiber is canceled by the dispersive delay (Figure 3.10(c)), with a negligible contribution from the filter (Figure 3.10(d)).

The balancing of amplitude and phase modulations in a self-similar laser are illustrated in Figure 3.11. The saturable absorber and the spectral filter play very similar roles as in the DS laser, but the roles of dispersion and nonlinearity play out differently. Of course, the strong evolution in the self-similar laser contrasts with

the nearly-static solutions in a DS laser. In a self-similar laser the nonlinearity interacts with the normal dispersion to linearize the spectral phase such that the temporal phase can then be compensated by anomalous dispersion. This can only happen if the pulse shape is near parabolic, as was predicted and demonstrated in [33]. One consequence of this parabolic pulse is its self-similar evolution. This means that attempts to model the self-similar solution must take into account the evolution itself. However, because the amplitude balances are the same as in the DS pulse and because the total GVD balances with the nonlinear phase, we can expect master-equation treatments with averages parameters to be useful in modeling self-similar lasers.

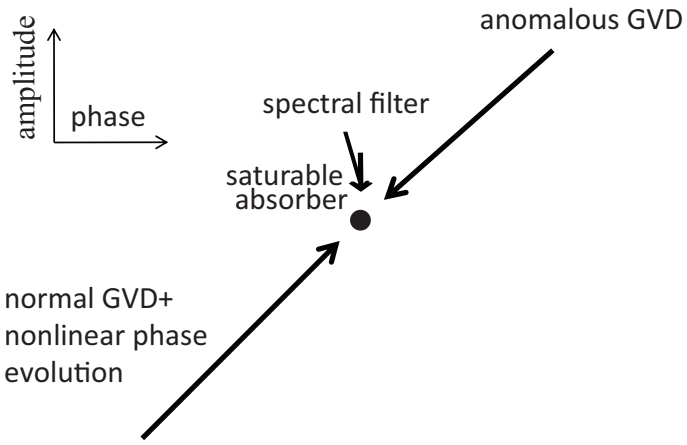

Figure 3.11: Qualitative illustration of the amplitude and phase balances in a passive self-similar laser.

3.3.2 Stretched dissipative soliton fiber lasers

Perhaps surprisingly, another set of solutions exists in the dispersion-mapped cavity designed to support self-similar pulses in the passive fiber [44]. The solution corresponding to the dashed line in Figure 3.7 exhibits the features of the curious regime reported in Refs. [34] and [42]. The pulse duration decreases in the

normal-dispersion section and increases in the dispersive delay. The evolution in each segment is mostly monotonic as in a self-similar laser, but the variation of the pulse duration is reversed somehow. The pulses depend strongly on dissipative effects such as the gain filter and the saturable absorber. The pulses are predominantly down-chirped and can reach the transform limit in the first part of the grating section. Thus, much less dispersion is required to dechirp these pulses outside the cavity than is needed for similaritons. In order to isolate this regime from self-similar propagation, we searched for a parameter which would ensure its existence. We found that the nonlinearity in the first segment of SMF can be varied to determine whether this or the passive self-similar mode exists. We find that this mode will always converge instead of a self-similar pulse in the limit of this nonlinearity becoming small.

We isolate this new regime and exaggerate some of its key features by setting the nonlinearity in the first fiber to zero and by varying the pulse energy (details are in Appendix A.2.2). Two transform-limited pulse duration minima occur in the evolution. At high energy, the minima occur near each other, at the transition from normal to anomalous dispersion. With decreasing energy, the minima shift to the center of the dispersive sections (Figure 3.12(a)). The spectrum can be cut by the gain filter, and grows back in the nonlinear section of fiber after the gain (Figure 3.12(b)). A crucial point is that the function of the anomalous dispersion and the first section of fiber can be viewed as simply increasing the magnitude of the negative chirp; these sections can be removed and the solution in the gain and the SMF will remain nearly identical to a dissipative soliton in an all-normal-dispersion laser [5]. In this simulation, this statement is exact because the dispersions of the first SMF and the dispersive delay are equal and opposite. This regime therefore is an extension of normal dispersion mode-locking toward

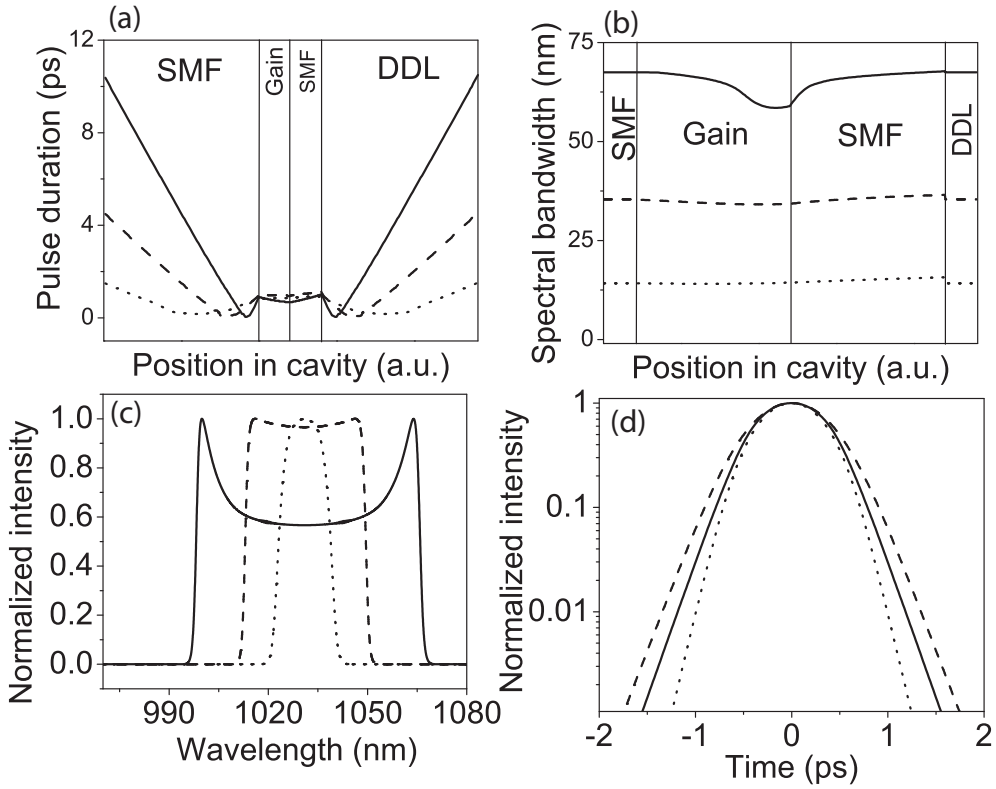

Figure 3.12: Evolution of (a) pulse duration and (b) spectral bandwidth, and output (c) spectra and (d) pulses of an SDS laser for 1 nJ (dotted line), 4 nJ (dashed line), and 12 nJ (solid line) intra-cavity pulse energies.

zero net cavity dispersion. The pulses are dissipative solitons with an evolution defined by the additional dispersion map. Thus, it seems most informative to refer to these pulses as stretched dissipative solitons (SDS). Ilday *et al.* had dubbed these pulses "wave-breaking-free" to refer to a consequence of their evolution, before the evolution itself was understood [42]. This was a generic label, as self-similar pulses and dissipative solitons also avoid wave-breaking at large nonlinear phase shifts. The analysis based on the CQGLE of Refs. [5] and [18] can be used to understand this regime. For example, higher-energy solutions have less chirp, and push the point in the gratings where the pulse is transform-limited closer to the output of the laser. Also, as in the all-normal-dispersion case, the spectrum has steep sides and can have peaks on the edges (Figure 3.12(c)). The SDS regime allows for

large pulse energy as is typical for normal dispersion systems; the largest energy shown here is 12 nJ (Figure 3.12 solid line). In addition, the pulse duration can be very short (*e.g.*, 45 fs for the 12 nJ case) because of the low values of net GVD possible [19], hence the $>$ 100 kW peak powers seen in Ref. [34]. The temporal breathing in this regime can also be very large; a breathing ratio of ~ 30 has been observed experimentally and in the simulated 12-nJ case the breathing ratio is ~ 200.

3.4 Amplifier-similariton fiber lasers

Recently, a fourth normal dispersion mode-locking mechanism was introduced in which parabolic amplifier similaritons are stabilized in an oscillator [38–41]. Spectral filtering is found to be critical to stabilizing the amplifier similaritons in the cavity. The pulse undergoes large (20 times) spectral breathing as it traverses the

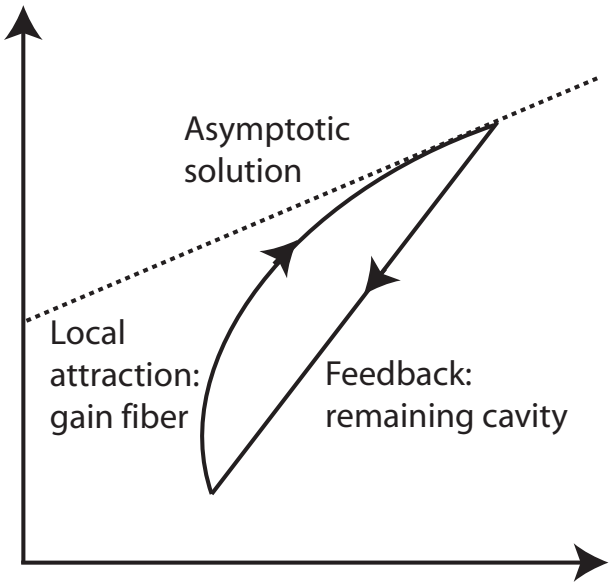

Figure 3.13: Illustration of the local attraction in an amplifier similariton fiber laser.

cavity. Unlike the other three regimes, the amplifier similariton fiber laser relies on a local nonlinear attraction to stabilize the pulse (Figure 3.13). An arbitrary pulse inserted into a gain fiber is nonlinearly attracted to an asymptotically-evolving parabolic pulse. The output pulse parameters are entirely determined by the energy of the input pulse and the parameters of the fiber. The challenge is for the pulse to reach this solution in a fiber length compatible with efficient laser design, and filtering can facilitate this. Shorter, nearly-transform-limited pulses can reach the amplifier similariton solution in shorter propagation lengths [43]. Oktem *et al.* built a laser in which the parabolic pulse evolves into a soliton in an anomalous

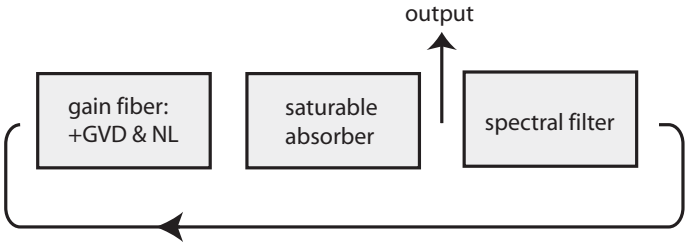

Figure 3.14: Cartoon schematic of an amplifier similariton fiber laser.

dispersion fiber after the gain, which allows for a short transform-limited pulse to return to the input of the gain fiber [38]. Renninger *et al.* showed that a strong spectral filter after the gain fiber can stabilize amplifier similaritons with feedback, so an anomalous-dispersion segment is not needed [39] (Figure 3.14). For fixed chirp, a pulse with a narrower spectrum is shorter and close enough to the transform limit to provide a self-consistent cavity. The resultant pulse after the gain segment is highly parabolic and the spectral profile is distinguished from that in other mode-locking regimes (Figure 3.15). Aguergaray *et al.* built a Raman oscillator with kilometers of gain fiber, which provides enough propagation length for the asymptotic solution to be achieved [40]. Demonstration of stable propagation of amplifier similaritons in three diverse cavities illustrates the robustness of this regime.

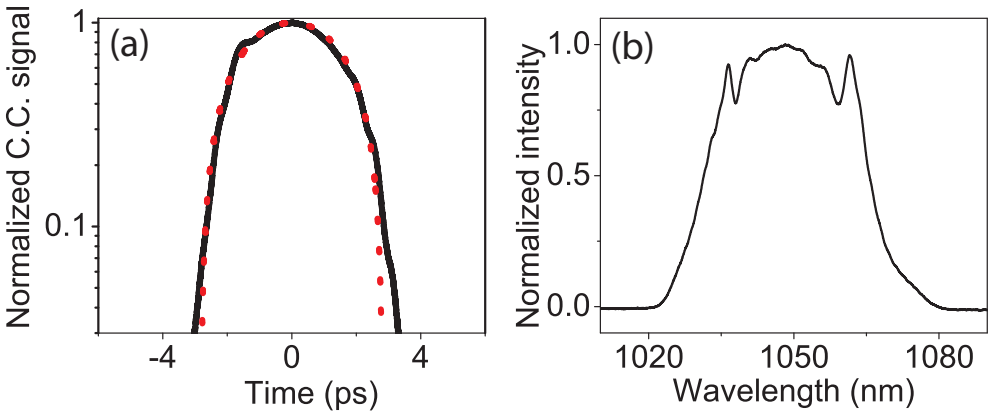

Figure 3.15: (a) Cross-correlation (C.C.) of the pulse (with dotted parabolic fit) and (b) spectrum after propagation through the gain fiber.

The differences between this regime and the others mentioned are related to the fact that the pulse relies on a local attraction in the gain fiber. As one consequence, the behavior and performance of the laser are decoupled from the average cavity parameters. In Ref. [39], the pulses are much shorter than would be expected from a master mode-locking model with the average cavity parameters. As a result, the laser should offer flexibility in design for specific performance, and future work will address this point experimentally.

3.5 Discussion of results

In this section, we will compare and contrast the four operating regimes (Table 3.1). High-performance short-pulse fiber lasers rely on an exact balance of large accumulated nonlinear phase shifts during one cycle around the cavity. In the normal-dispersion regime, dissipation plays a crucial role in establishing this balance. Dissipative effects such as spectral filtering and saturable absorption enable the stabilization of a chirped pulse in the presence of nonlinearity and normal dispersion. Dissipative solitons, SDS and passive self-similar lasers rely on this

	DS	SDS	Passive SS	Active SS
Average cavity parameters	✓	✓	✓	
Dispersion map		✓	✓	
Self-similar/parabolic			✓	✓

Table 3.1: Comparison of important features: DS: dissipative soliton, SDS: stretched dissipative soliton, SS: self-similar.

complete balance. Because the effects are important through the traversal of the entire cavity, the average cavity parameters determine the pulse parameters. Master mode-locking models ([4,5]) are useful for determining pulse properties for these regimes. Amplifier similariton lasers, however, rely on a local nonlinear attractor and therefore will be less amenable to such analyses. This opens up interesting possibilities that may go against conventional laser wisdom, such as operation at net zero dispersion or ultrashort pulse durations at large normal dispersion.

The SDS and passive self-similar regime require dispersion-managed cavities. From a physical perspective, this means that the mode-locking mechanism is more complicated, as the evolution of the pulse is important. As an example, mathematically these two regimes are bistable in the same cavity, which leads to a wealth of interesting nonlinear dynamical behavior. From a practical perspective a dispersion-managed cavity allows for a precise tunability of the net dispersion at the cost of some complexity and loss in the design. However, tuning the net dispersion can allow the generation of dissipative solitons with shorter duration than can be reached in all-normal-dispersion cavities.

Dispersion managed solitons can also exist in a dispersion managed cavity. In fact, the temporal evolution of these pulses resembles that in Figure 3.12(a) (dotted line), but the mode-locking mechanism is distinctly different. Dispersion-managed

solitons exist from net anomalous dispersion to slightly normal dispersion when there are minimal dissipative perturbations. In the normal dispersion regime, particularly near zero dispersion, dissipative effects such as gain filtering play a major role. There is extensive literature on dispersion-managed solitons, so we have restricted our discussion to high-energy mode-locking regimes, which exploit (and in fact depend on) dissipative mechanisms.

In the initial development of dissipative soliton lasers, the acronym ANDi fiber laser, for all-normal dispersion fiber laser, was used. This name was given in reference to the design of the system more than to the pulse-shaping mechanisms. Because amplifier similariton fiber lasers can also exist in an all-normal dispersion cavity, we refer instead to the relevant physical mechanisms: dissipative soliton mode-locking or amplifier similariton mode-locking.

Both active and passive self-similar pulses have been stabilized in fiber lasers. In the passive case, this coincides with temporal breathing, which leads to longer durations and large pulse energy. In addition, a parabolic pulse and spectrum can be attractive for applications owing to good pulse quality. In the active case, the nonlinear attraction of the gain fiber is responsible for the mode-locking of the laser. In this case, dissipation plays a supporting role by facilitating creation of a self-consistent cavity.

Pulse quality is a critical feature for applications of mode-locked lasers. With proper design, the pulses from almost all of the regimes can be compressed to within 5% of the transform limit. The exception is the giant-chirp oscillator ([20]). This is a property of the solution of the equation that models the cavity with very large group-velocity dispersion. Pulses from a giant-chirp oscillator can be dechirped to ~ 2 times the transform-limit. Another issue that affects pulse quality is the

spectral shape of the output of most normal-dispersion lasers. The square, or steep-sided, spectral shape has a sinc function Fourier transform. As a consequence, the transform-limited pulses have low-intensity wings in their temporal profile. These typically contain $\sim 5\%$ of the pulse energy. The exception is the amplifier similariton regime, where the spectra approach a parabolic form that yields dechirped pulses with less energy in the wings.

For many applications, the square or peaked spectral shapes produced by normal-dispersion lasers will be perfectly acceptable. This is the case in nonlinear microscopy, *e.g.*, where the peak power is the most-important parameter. However, a smoother spectral shape may be needed for other applications. In this case, a smoother spectrum can be obtained by taking the output after the filter. The structured spectra of normal-dispersion lasers would appear to be a concern for subsequent amplification. In chirped-pulse amplification, spectral modulations can grow as nonlinear phase is accumulated. Ilday *et al.* have shown that the spectral structure can be smoothed by the amplification process [45]. Finally, nonlinear and dispersive propagation of pulses from normal-dispersion lasers is quantitatively different from the propagation of Gaussian pulses. One must account for this is the design of a pulse compressor, *e.g.*.

For the shortest pulses, for the mode-locking mechanisms where the average cavity parameters are important, the laser must be operated as close as possible to net zero dispersion. Consequently, the passive self-similar and SDS regimes are preferable. For short-pulse operation in the amplifier similariton laser, the bandwidth is only limited by the gain bandwidth. Initial demonstrations already include promising results (~ 55 fs). For energy, however, little is known about the preferred operation regime. To date, dissipative soliton mode-locking achieves the

highest performances with $>$ 100-nJ pulse energies.

3.6 Conclusions

A numerical investigation into fiber lasers mode-locked with net normal dispersion reveals several distinct regimes, including active and passive similariton mode-locking, along with dissipative and stretched-dissipative soliton mode-locking. Each regime balances the linear and nonlinear phase accumulations as well as the amplitude modulations. Wave-breaking is avoided with a unique combination of normal dispersion and dissipation in each regime. A dissipative soliton is a chirped pulse that can balance nonlinear phases by spectral filtering and saturable absorption. A stretched dissipative soliton provides the same balance but with additional temporal evolution defined by a linear dispersion map. Remarkably, a passive similariton solution can exist in a stretched dissipative soliton cavity, but with a very different evolution. In this regime, the spectral filer and saturable absorber still play important roles in creating the pulse, but anomalous dispersion also becomes important. A parabolic pulse evolving self-similarly linearizes the nonlinear phase in the normal dispersion fiber, which is compensated by a dispersion delay. Because of the clear similarities to dissipative soliton mode-locking, master equation models can be used to model passive similariton lasers, but for a complete understanding the evolution must also be taken into account. Finally, the amplifier similariton regime is distinguished from the other three regimes because it relies on local nonlinear attraction in the gain fiber of the laser. As a consequence, the behavior and performance is decoupled from the average cavity parameters, and this will allow flexibility in design for specific performance.

BIBLIOGRAPHY

[1] W. H. Renninger, A. Chong, and F. W. Wise, Selected Topics in Quantum Electronics, IEEE Journal of **18**, 389 (2012).

[2] K. Tamura, E. P. Ippen, H. A. Haus, and L. E. Nelson, Opt. Lett. **18**, 1080 (1993).

[3] M. H. Ober, M. Hofer, and M. E. Fermann, Opt. Lett. **18**, 367 (1993).

[4] H. A. Haus, J. G. Fujimoto, and E. P. Ippen, J. Opt. Soc. Am. B **8**, 2068 (1991).

[5] W. H. Renninger, A. Chong, and F. W. Wise, Physical Review A **77**, 23814 (2008).

[6] F. W. Wise, A. Chong, and W. H. Renninger, Laser & Photon. Rev. **2**, 58 (2008).

[7] K. Kieu, W. H. Renninger, A. Chong, and F. W. Wise, Opt. Lett. **34**, 593 (2009).

[8] D. Anderson, M. Desaix, M. Karlsson, M. Lisak, and M. L. Quiroga-Teixeiro, J. Opt. Soc. Am. B **10**, 1185 (1993).

[9] A. Chong, J. Buckley, W. Renninger, and F. Wise, Opt. Express **14**, 10095 (2006).

[10] L. M. Zhao, D. Y. Tang, and J. Wu, Opt. Lett. **31**, 1788 (2006).

[11] J. M. Soto-Crespo, N. N. Akhmediev, V. V. Afanasjev, and S. Wabnitz, Phys. Rev. E **55**, 4783 (1997).

[12] J. W. Lou, M. Currie, and F. K. Fatemi, Opt. Express **15**, 4960 (2007).

[13] O. Prochnow, A. Ruehl, M. Schultz, D. Wandt, and D. Kracht, Opt. Express **15**, 6889 (2007).

[14] J. An, D. Kim, J. W. Dawson, M. J. Messerly, and C. P. J. Barty, Opt. Lett. **32**, 2010 (2007).

[15] A. Chong, W. H. Renninger, and F. W. Wise, Opt. Lett. **32**, 2408 (2007).

[16] B. Ortaç, O. Schmidt, T. Schreiber, J. Limpert, A. Tünnermann, and A. Hideur, Opt. Express **15**, 10725 (2007).

[17] B. Ortaç, M. Plötner, J. Limpert, and A. Tünnermann, Optics Express **15**, 16794 (2007).

[18] A. Chong, W. H. Renninger, and F. W. Wise, J. Opt. Soc. Am. B **25**, 140 (2008).

[19] A. Chong, W. H. Renninger, and F. W. Wise, Opt. Lett. **33**, 2638 (2008).

[20] W. H. Renninger, A. Chong, and F. W. Wise, Opt. Lett. **33**, 3025 (2008).

[21] B. G. Bale, J. N. Kutz, A. Chong, W. H. Renninger, and F. W. Wise, Optics Letters **33**, 941 (2008).

[22] A. Chong, W. H. Renninger, and F. W. Wise, Opt. Lett. **33**, 1071 (2008).

[23] K. Kieu and F. W. Wise, Optics Express **16**, 11453 (2008).

[24] B. G. Bale, J. N. Kutz, A. Chong, W. H. Renninger, and F. W. Wise, J. Opt. Soc. Am. B **25**, 1763 (2008).

[25] M. Schultz, H. Karow, O. Prochnow, D. Wandt, U. Morgner, and D. Kracht, Optics Express **16**, 19562 (2008).

[26] N. Akhmediev, J. M. Soto-Crespo, and P. Grelu, Physics Letters A **372**, 3124 (2008).

[27] B. Ortaç, M. Baumgartl, J. Limpert, A. Tünnermann, B. Ortac, and A. Tuennermann, Optics Letters **34**, 1585 (2009).

[28] W. H. Renninger, A. Chong, and F. W. Wise, J. Opt. Soc. Am. B **27**, 1978 (2010).

[29] K. Özgören and F. Ilday, Optics Letters **35**, 1296 (2010).

[30] S. Lefrançois, K. Kieu, Y. Deng, J. D. Kafka, and F. W. Wise, Opt. Lett. **35**, 1569 (2010).

[31] M. Baumgartl, B. Ortaç, C. Lecaplain, A. Hideur, J. Limpert, and A. Tünnermann, Optics Letters **35**, 2311 (2010).

[32] C. Lecaplain, B. Ortaç, G. Machinet, J. Boullet, M. Baumgartl, T. Schreiber, E. Cormier, and A. Hideur, Opt. Lett. **35**, 3156 (2010).

[33] F. O. Ilday, J. R. Buckley, W. G. Clark, and F. W. Wise, Phys. Rev. Lett. **92**, 213902 (2004).

[34] J. R. Buckley, F. W. Wise, F. O. Ilday, and T. Sosnowski, Opt. Lett. **30**, 1888 (2005).

[35] C. K. Nielsen, B. Ortaç, T. Schreiber, J. Limpert, R. Hohmuth, W. Richter, and A. Tünnermann, Optics Express **13**, 9346 (2005).

[36] A. Ruehl, O. Prochnow, D. Wandt, D. Kracht, B. Burgoyne, N. Godbout, and S. Lacroix, Optics Letters **31**, 2734 (2006).

[37] B. Ortaç, A. Hideur, C. Chedot, M. Brunel, G. Martel, and J. Limpert, Applied Physics B **85**, 63 (2006).

[38] B. Oktem, C. Ulgudur, and F. O. O. Ilday, Nat. Photon. **4**, 307 (2010).

[39] W. H. Renninger, A. Chong, and F. W. Wise, Phys. Rev. A **82**, 21805 (2010).

[40] C. Aguergaray, D. Méchin, V. Kruglov, and J. D. Harvey, Opt. Express **18**, 8680 (2010).

[41] B. G. Bale and S. Wabnitz, Opt. Lett. **35**, 2466 (2010).

[42] F. Ilday, J. Buckley, H. Lim, F. Wise, and W. Clark, **28**, 1365 (2003).

[43] M. E. Fermann, V. I. Kruglov, B. C. Thomsen, J. M. Dudley, and J. D. Harvey, Phys. Rev. Lett. **84**, 6010 (2000).

[44] T. Schreiber, B. Ortaç, J. Limpert, and A. Tünnermann, Optics Express **15**, 8252 (2007).

[45] P. Mukhopadhyay, K. Ozgoren, I. Budunoglu, and O. Ilday, IEEE Journal of Selected Topics in Quantum Electronics **15**, 145 (2009).

CHAPTER 4

AMPLIFIER SIMILARITON FIBER LASERS

4.1 Initial demonstration[1]

4.1.1 Introduction

Short-pulse fiber lasers based on soliton formation in anomalous-dispersion cavities [2], dispersion-managed solitons in cavities with a dispersion map [3], and all-normal-dispersion (ANDi) cavities [4–6] have been demonstrated. The latter system supports dissipative solitons in the cavity [7], and allows performance comparable to solid-state lasers [8] (also see chapter 2). In addition, ANDi designs allow for simple instruments at a lasing wavelength of 1 μm, an ideal wavelength for optical bandwidth and efficiency.

Self-similar pulses ("similaritons") are parabolic pulses that convert nonlinear phase into a linear frequency chirp that can be compensated with standard dispersive devices. Specifically, similaritons are solutions of the nonlinear Schrodinger equation with gain,

$$\frac{\partial A}{\partial z} = \frac{g}{2}A - i\frac{\beta_2}{2}\frac{\partial^2 A}{\partial t^2} + i\gamma(|A|^2)A, \tag{4.1}$$

with the form

$$A(z,t) = A_0(z)\sqrt{1-(t/t_0(z))^2}e^{i(a(z)-bt^2)} \tag{4.2}$$

for $t \leq t_0(z)$. Similaritons were first demonstrated theoretically and experimentally in single-pass fiber amplifiers [9–11], and they continue to attract much attention

[1]The majority of this section is published in Ref. [1].

[12]. Self-similar evolution of a pulse in the passive fiber of a laser has been observed, and leads to major performance increases in pulse energy over previously-studied evolutions [13].

Solitons in passive fiber and self-similar pulses in fiber amplifiers are the most well-known classes of nonlinear attractors for pulse propagation in optical fiber, so they take on major fundamental importance. Solitons are static solutions of the nonlinear Schrodinger equation, and are therefore naturally amenable to systems with feedback. The demonstration of a laser that supports similaritons in its amplifier would be remarkable as a feedback system with a local nonlinear attractor that is not a static solution. The spectrum of the self-similar pulse broadens with propagation, so an immediate challenge is the need to compensate this in a laser cavity. A design with a long normal-dispersion gain fiber, a filter, and a linear anomalous-dispersion segment was proposed [14], but has not been realized experimentally. Oktem *et al.* reported a major step forward in this context: a laser with similariton evolution in the amplifier and soliton evolution in an anomalous-dispersion segment [15]. The soliton formation is thought to stabilize the similariton solution. Thus, self-similar pulse evolution has been observed only in lasers with dispersion maps. An unanswered question is whether amplifier similaritons can form in an ANDi laser, where satisfying the periodic boundary condition will be much more challenging. Such a pulse evolution would isolate the amplifier similariton in a system with feedback. Dissipation presumably would be a crucial process in that evolution.

In this section, we demonstrate self-similar pulse formation in the amplifier of an ANDi laser. Theory and experiments show that a range of inputs to the amplifier evolve to the self-similar solution, which verifies the existence of the nonlinear

attractor in that segment of the oscillator. This local nonlinear attractor suppresses effects from the average cavity parameters that are unavoidable in lasers with dispersion maps. The solutions exhibit large (up to 20 times) spectral breathing, but the pulse chirp is always less than expected from the cavity dispersion. This new pulse evolution can be obtained over a broad range of parameters, which allows tuning the pulse duration, bandwidth, and chirp. For example, amplifier similaritons underlie the generation of the shortest parabolic pulses to date from a laser, in addition to the shortest pulses from any ANDi laser. The ability to generate high-energy chirped parabolic pulses or ultrashort pulses from a simple device will be attractive for applications.

4.1.2 Numerical simulations

Numerical modeling illustrates the main features of a laser that can support amplifier similaritons, indicated schematically at the top of Figure 4.1(a). A gain fiber with normal group-velocity dispersion (GVD) dominates the parabolic pulse shaping. This is followed by a saturable absorber, which is assumed to be conversion of nonlinear polarization evolution (NPE) into amplitude modulation in the standard way. The cavity is a ring: after the filter, the pulse returns to the gain fiber. Propagation in the gain fiber, neglecting modal birefringence, is modeled with the coupled equations for the orthogonal electric field polarization states, A_x and A_y:

$$\begin{aligned} \frac{\partial A_x}{\partial z} &= \frac{g}{2}A_x - i\frac{\beta_2}{2}\frac{\partial^2 A_x}{\partial t^2} + i\gamma(|A_x|^2 + \frac{2}{3}|A_y|^2)A_x \\ \frac{\partial A_y}{\partial z} &= \frac{g}{2}A_y - i\frac{\beta_2}{2}\frac{\partial^2 A_y}{\partial t^2} + i\gamma(|A_y|^2 + \frac{2}{3}|A_x|^2)A_y, \end{aligned} \tag{4.3}$$

where z is the propagation coordinate, t is the local time, $\beta_2 = 23$ fs^2/mm is the group-velocity dispersion, and $\gamma = 0.0044$ (W m)$^{-1}$ is the cubic self-focusing

nonlinear coefficient for the fiber. The linear gain coefficient is defined as:

$$g = \frac{g_0}{1 + \frac{\int [|A_x|^2 + |A_y|^2] dt}{E_{sat}}}, \tag{4.4}$$

where $g_0 = 6.9$ is the small-signal gain corresponding to a ∼30 dB fiber amplifier, $E_{sat} = 170$ pJ is the saturation energy, and the integral is calculated before propagation through the 2-m gain fiber. The polarization-dependent elements are treated with a standard Jones matrix formalism in the (x,y) basis. The NPE is implemented with a half-wave and a quarter-wave plate, a polarizer, and another quarter-wave plate, with orientations (with respect to the x-axis) $\theta_{q1} = 2.21$ rads, $\theta_h = 2.28$ rads, $\theta_{pol} = \pi/2$, and $\theta_{q2} = 0.59$ rads, respectively. The filter is a Gaussian transfer function with 4-nm full-width at half-maximum (FWHM) bandwidth. Finally, as in a practical oscillator a linear loss of 70% is imposed after the filter. The initial field is white noise, and the model is solved with a standard symmetric split-step algorithm.

A typical stable evolution is shown in Figure 4.1(a). The two polarization modes evolve almost identically, so the sums of the temporal and spectral intensities are plotted. The pulse duration and bandwidth increase in the gain fiber as the pulse evolves toward the asymptotic attracting solution in the fiber. The filter and saturable absorber reverse these changes. The filter provides the dominant mechanism for seeding the self-similar evolution in the amplifier. This implies that only the initial pulse profile is important, and no additional nonlinear attraction is required, in contrast to soliton evolution in the results of Oktem *et al.*. Dissipative solitons and dispersion-managed parabolic pulses [13] have nearly constant bandwidth, and the pulse duration increases due to the accumulation of linear phase. In contrast, the amplifier similariton increases in duration as a consequence of its increase in bandwidth, which is an intrinsic property of the exact asymptotic solution [9]. A key feature of amplifier similaritons is that the pulses evolve

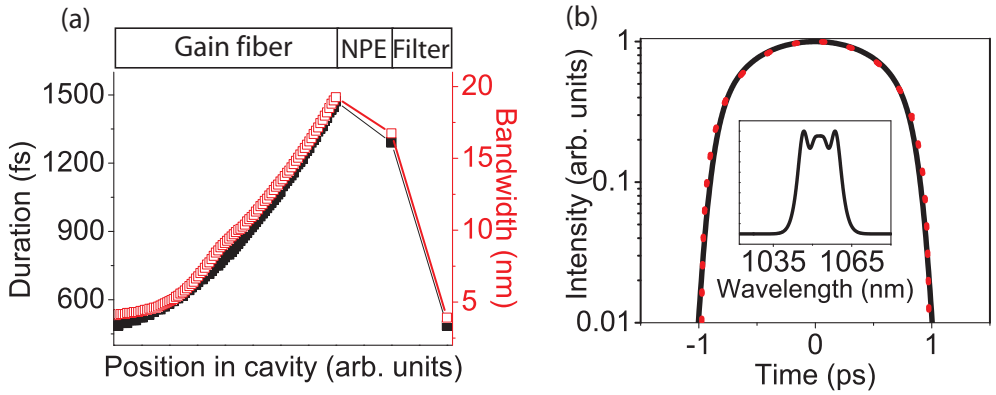

Figure 4.1: (a) Evolution of the FWHM pulse duration (filled) and spectral bandwidth (open) in the cavity. The components of the laser are shown above the graphs. (b) The output pulse at the end of the gain fiber (solid) and a parabolic pulse with the same energy and peak power (dotted). Inset: spectrum. The orthogonally polarized pulse and spectrum (not shown) are essentially identical.

toward a parabolic asymptotic solution: each polarization component is parabolic at the end of the gain fiber (Figure 4.1(b)). The associated spectra exhibit some structure, as expected for a parabola with finite chirp (Figure 4.1(b) inset). No stable solution was found with a single-field equation and a saturable absorber with transmission that increases monotonically with intensity; the coupling of the polarizations evidently provides some stabilizing function.

The pulse evolution can be quantified with the metric, $M^2 = \int[|u|^2 - |p|^2]^2 dt / \int |u|^4 dt$, where u is the pulse being evaluated and p is a parabola with the same energy and peak power. In the gain fiber, the pulse evolves from a Gaussian profile (M=0.14) after the spectral filter to a parabola (Figure 4.2(a)). To verify that the pulse is converging to a parabola, the pulse at the end of the 2-m gain fiber is taken as the initial condition for propagation through an additional 3 m of identical gain fiber, and the pulse remains parabolic (Figure 4.2(a)). To further confirm that the pulse is converging to the exact asymptotic solution demonstrated in Refs. [9–11], p from the M^2 metric is replaced with the pulse representing the

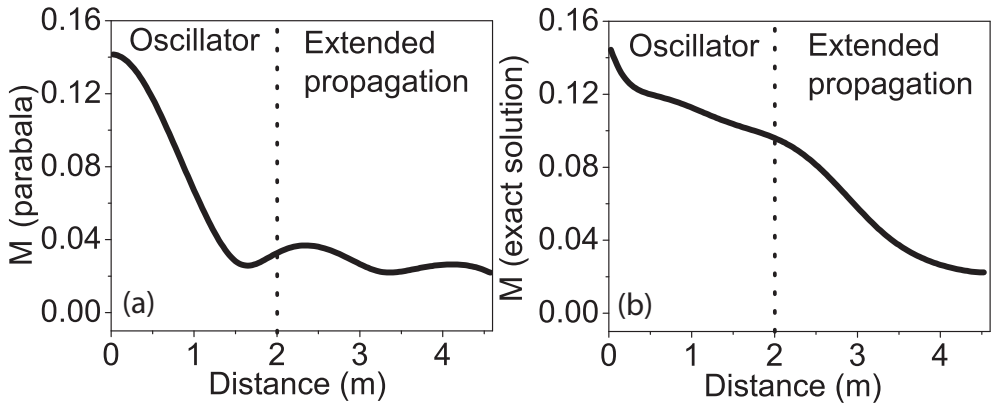

Figure 4.2: Evolution of the (a) M parameter comparing the pulse to a parabola and the (b) M parameter comparing the pulse to the exact solution of Ref. [9] in the oscillator. An additional 3 m of propagation was added to each plot to emphasize convergence.

asymptotic solution for this fiber. Indeed the pulse evolves toward the attractor in the gain fiber (Figure 4.2(b)). The resulting pulses exhibit a parabolic shape and large spectral breathing as is expected from the parabolic attractor. The numerical simulations clearly show the formation of the amplifier similariton inside the laser.

4.1.3 Experimental results

We designed a Yb fiber laser with parameters similar to those of the simulations. The schematic is identical to dissipative soliton lasers ([7]) with the exception of a diffraction grating (300 lines per millimeter) placed before a collimator, which replaces the birefringent plate as a spectral filter. The wavelength-dependent diffraction along with the Gaussian dependence of the fiber acceptance angle yield a 4-nm Gaussian spectral filter when the collimator is 11 cm from the grating. Along with the three wave-plates required for NPE, we add a half-wave plate before the grating to optimize the transmission. The zeroth-order grating reflection is used as a secondary output for analysis. The Yb-doped double-clad gain fiber is 1.8 m long

and is pumped with a multi-mode pump diode. 28 cm of single-mode fiber (a collimator pigtail) precedes the gain fiber and a pump/signal combiner and collimator follow it, which together add 128 cm of SMF. All fibers have normal GVD.

Self-starting mode-locking is achieved by adjustment of the wave plates. The chirped pulse from the grating reflection is measured directly by cross-correlation with the dechirped pulse from the NPE output, which is 60 times shorter than the chirped pulse (Figure 4.3(a)). The pulse is parabolic and the spectrum (Figure 4.3(c)) agrees well with the theoretical prediction for an amplifier similariton (Figure 4.1(b), inset). The shape of the spectrum is an immediate indication that this is a new regime of modelocking, as it lacks the characteristic steep edges of dissipative solitons in normal-dispersion lasers [5, 7]. The spectral bandwidth breathes by a factor of ∼10 as the pulse traverses the cavity. The pulse from the NPE output (Figure 4.3(d)) can be dechirped to a duration of 65 fs (Figure 4.3(b)), with minimal secondary structure. The pulse chirp (0.05 ps^2), inferred from the dispersion required to dechirp it to the transform limit, is less than the GVD of the cavity (0.08 ps^2). This is another feature of this regime, as prior ANDi lasers have generated pulses with chirp comparable to, or much greater than, the cavity GVD.

4.1.4 Discussion and extensions

The narrow filter is crucial for the formation of similaritons in the amplifier. The challenge is for the pulse to reach the asymptotic solution in a fiber length that is compatible with efficient laser design. We offer the following argument: for fixed chirp, a pulse with a narrower spectrum is shorter and closer to the transform limit; such a pulse can reach the single-pass amplifier similariton solution in a shorter

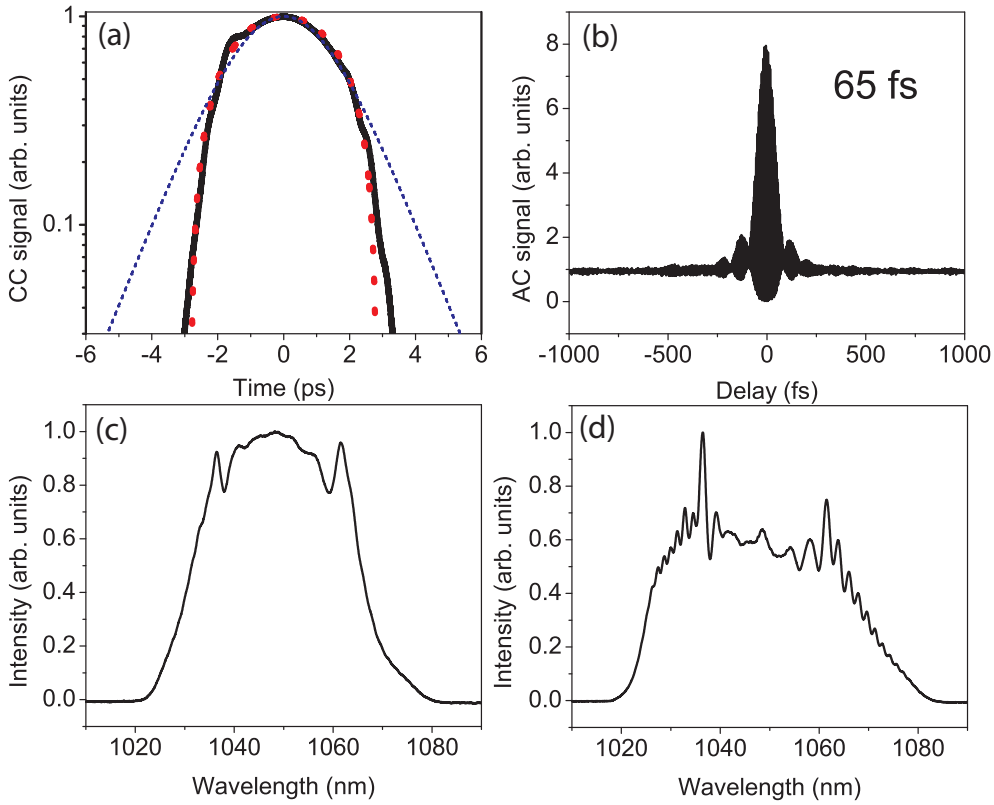

Figure 4.3: Experimental (a) cross-correlation of the pulse from the grating reflection (solid) with a parabolic (dotted) and sech^2 (dashed) fit; (b) interferometric auto-correlation of the dechirped pulse from the NPE output; and spectra from the (c) grating reflection and (d) NPE output.

segment of gain. A pulse propagating in normal-dispersion gain fiber will always be attracted to the similariton solution, but if the pulse is too long, the effect is negligible and the resulting pulse will not be parabolic.

In contrast to prior pulsed lasers, the local attraction of the pulse to the amplifier similariton solution decouples the output pulse from other elements of the cavity. This property allows a variety of pulse evolutions and performance parameters. For example, with a narrower (2 nm) spectral filter, the pulse still evolves to an amplifier similariton with large bandwidth. The resulting solution has a very large spectral breathing ratio (∼20), and yields 5-nJ pulses that dechirp to 80 fs (Figure 4.4(a,b)). A well-known limitation to similaritons in fiber amplifiers is

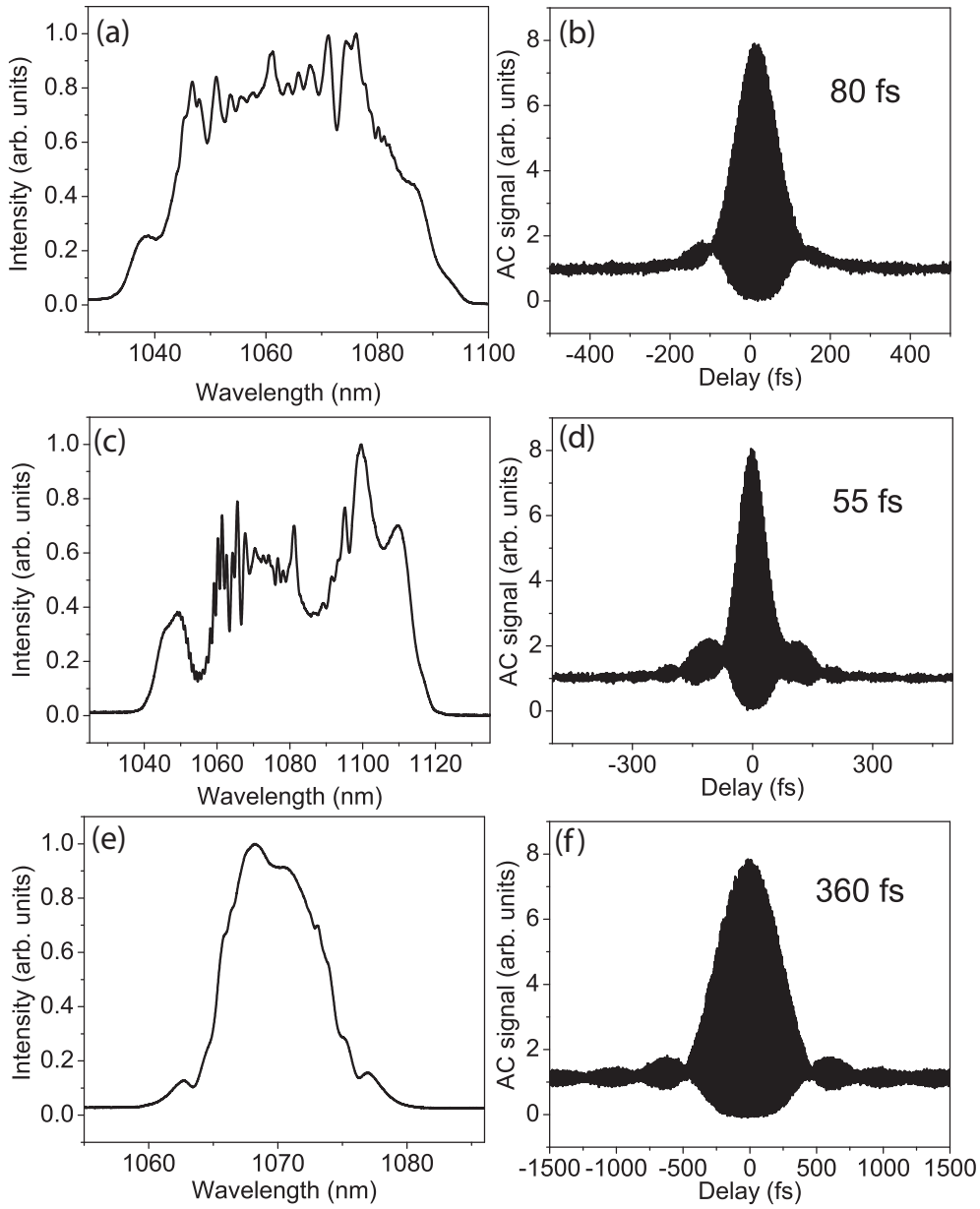

Figure 4.4: Output spectrum and dechirped auto-correlation for modes with (a,b) large spectral breathing, (c,d) short pulse duration, and (e,f) long cavities.

the gain bandwidth; as the spectrum approaches the gain bandwidth the chirp is no longer monotonic, which disrupts the self-similar evolution. With larger pump powers the spectral bandwidth increases, but the pulse quality is degraded. For example, with a 4-nm filter a 3-nJ pulse dechirps to 55 fs (Figure 4.4(c,d)), a remarkably short pulse considering the large normal GVD of the cavity. Finally,

amplifier similariton mode-locking is possible even with the addition of long lengths of fiber before the gain. For example, with 63 m of fiber and a 2-nm spectral filter, a 15-nJ pulse that can be dechirped to 360 fs is generated (Figure 4.4(e,f)). These results extend the performance of recently-developed giant-chirp oscillators [16] to shorter pulses, which is needed.

The phenomena described here can be distinguished clearly from other pulse-propagation regimes. The pulses in Ref. [13] are self-similar in the passive fiber. The laser requires a dispersion-managed cavity and spectral filtering is avoided as much as possible. The spectrum of the passive similariton has characteristic steep sides, with minimal breathing. The passive similariton is not a nonlinear attractor, so there is no local attractor and the average cavity parameters influence the pulse evolution. Finally, parabolic self-similar mode-locking as in Ref. [13] was found to exist for a narrow region of parameter space [17]. All of these features contrast with the observations presented above for the amplifier similariton laser. Of course, dissipative solitons can be generated in a laser with only normal dispersion and a filter, as is the case here. However, dissipative solitons are characterized by a small spectral breathing ratio (<5), and the pulses are not parabolic [7]. Furthermore, the multi-pulsing threshold decreases with decreasing filter bandwidth, which severely restricts the stable mode-locking states that can be accessed with a narrow filter. The amplifier similariton regime allows much higher pulse energies and much shorter pulse durations to be obtained with the narrow filter. Giant-chirp oscillators are possible based on dissipative solitons [16]. These employ larger-bandwidth filters, so spectral breathing is small. The pulses exhibit the steep-sided spectra that are characteristic of dissipative solitons, and acquire frequency chirps that can be many times larger than expected from the cavity dispersion, again all in contrast to the long-cavity results of Figure 4.4(e,f)

above.

Finally, the pulses in Ref. [15] are characterized by soliton evolution in an anomalous dispersion section of fiber. This requires dispersion management and fiber with anomalous dispersion in the cavity, which can limit the efficiency and simplicity of the operating regime. In contrast, similaritons in an ANDi fiber laser are stabilized with only a filter, which allows for a simple design with minimal components and without restriction on the lasing wavelength.

4.1.5 Conclusions

In summary, we have demonstrated self-similar pulse propagation in the gain segment of a normal-dispersion fiber laser. Strong spectral filtering is adequate to satisfy the periodic boundary condition of the laser. Thus, the evolution is dominated by the presence of the local nonlinear attractor in the cavity. This regime offers flexibility to design for distinct performance parameters. These include the shortest pulses generated by an ANDi laser and pulses with small and linear chirp, both of which will be valuable for applications.

Note added. Recently, Aguergaray *et al.* demonstrated the evolution of an amplifier similariton in a picosecond Raman fiber oscillator [18]. Stable operation in a system with Raman gain and kilometers of fiber illustrates that amplifier similariton mode-locking is robust for a large range of parameter space.

Portions of this work were supported by the National Science Foundation (Grant No. ECS-0901323) and the National Institutes of Health (Grant No. EB002019). The authors acknowledge useful discussions with F. O. Ilday.

4.2 Dispersion-mapped amplifier similariton fiber lasers[2]

4.2.1 Introduction

Major advances in fiber laser research are driven by the need to compensate for optical nonlinearities imposed on the pulse by the small confinement area of single-mode optical fiber [3, 4, 7, 13]. To date, dissipative soliton systems lead in performance, with 31-nJ, 80-fs pulses from a single-mode fiber laser [8], and 534-nJ, 100-fs pulses from a photonic-crystal fiber laser that sacrifices some of the practical advantages of single-mode fiber systems [20].

In parallel with high-performance oscillator design, new amplifier pulse propagation physics was developed in the form of the self-similar propagation of parabolic pulses. Building on previous work on parabolic pulses [21, 22], a team from Auckland showed theoretically that self-similar pulses (similaritons) can occur in a fiber with gain, and Fermann et al. verified this experimentally [9–11, 23]. Finot et al. studied the asymptotic characteristics of parabolic pulses [24], verified the robustness of the attractor to large input fluctuations [25], and also studied the extension of this regime to Raman amplifiers [26]. The limits of parabolic amplification have been addressed theoretically and have been shown to be ultimately limited by gain bandwidth, higher-order dispersion, and stimulated Raman scattering [27]. Self-similar parabolic pulses were also later shown to be an asymptotic solution in dispersion-decreasing passive fibers [28, 29]. As a practical advancement, this new wave-form has been used to achieve high performance in amplifier systems [30–32].

Recently, self-similar evolution of the pulse in the gain segment of a fiber laser

[2]The majority of this section is published in Ref. [19].

was demonstrated in a laser with an anomalous-dispersion segment [15], in an all-normal-dispersion fiber laser [1], and in a Raman fiber laser [18]. In Ref. [1] it was shown that a narrow-band spectral filter is sufficient to stabilize the evolution, which yields high-energy and ultra-short pulses at large normal dispersion (chapter 4). In parallel with the experimental developments, Bale and Wabnitz showed that the pulse evolution can be completely characterized by solutions to the ordinary differential equations for the pulse characteristics in the fiber, along with scalar transfer functions for the spectral filter [33]. By scaling the fiber core size, 10-nJ and 42-fs pulses were generated following the design of Ref. [1], and these achieve a peak power of 250 kW [34]. With the large peak power that can be obtained from a rigorously single-mode fiber laser, amplifier similariton mode-locking promises to be very useful in applications.

In this section, we report an investigation of an amplifier similariton fiber laser with a dispersion map. Despite large changes in both the magnitude and sign of the total cavity group-velocity dispersion (GVD), the pulse parameters remain nearly constant. A narrow-band spectral filter is critical to facilitate the evolution toward the amplifier similariton solution. Strong nonlinear attraction to this asymptotic solution in the amplifier section of the laser underlies the pulse's independence from the global cavity parameters. The freedom from global parameters allows for several scientifically-significant cavity designs which will, in addition, be important for applications:

- Large anomalous GVD: The dispersion-mapped amplifier similariton (DMAS) laser is a new mode of operation at large anomalous net GVD, which complements the well-known soliton operation. As a practical consideration, the DMAS laser generates shorter pulses with higher energy than soliton op-

eration at large anomalous dispersion. As a consequence, the DMAS laser can eliminate length restrictions when designing oscillators at 1550-nm laser wavelength, e.g.

- Large normal dispersion: With appropriately-tuned net positive GVD, a DMAS laser can be designed to emit transform-limited pulses. The DMAS laser joins soliton lasers as sources of transform-limited pulses. In the DMAS laser, this occurs at the opposite sign of net GVD, and shorter pulses with greater energy are produced.
- Net zero GVD: The master equation, which governs prior mode-locked lasers, predicts an instability near zero GVD when the self-phase modulation exceeds the self-amplitude modulation, as is commonly the case. The DMAS laser, which is not governed by an average-parameter model, does not suffer from the same instabilities, and can be operated at net zero GVD. Because timing jitter is expected to be minimal at net zero GVD, the DMAS laser may be a route to low-noise frequency combs.

All modes of operation produce sub-100 fs pulses with nanojoule energies and should readily scale (as in Ref. [34]) to greater than 200-kW peak powers, even with single-mode fibers.

4.2.2 Numerical simulations

To assess the viability of a DMAS laser, numerical simulations were performed. The pulse propagation within a general fiber is modeled with the following nonlinear Schrödinger equation with gain:

$$\frac{\partial A(z,\tau)}{\partial z} + i\frac{\beta_2}{2}\frac{\partial^2 A(z,\tau)}{\partial \tau^2} = i\gamma|A(z,\tau)|^2 A(z,\tau) + g(E_{pulse})A(z,\tau). \tag{4.5}$$

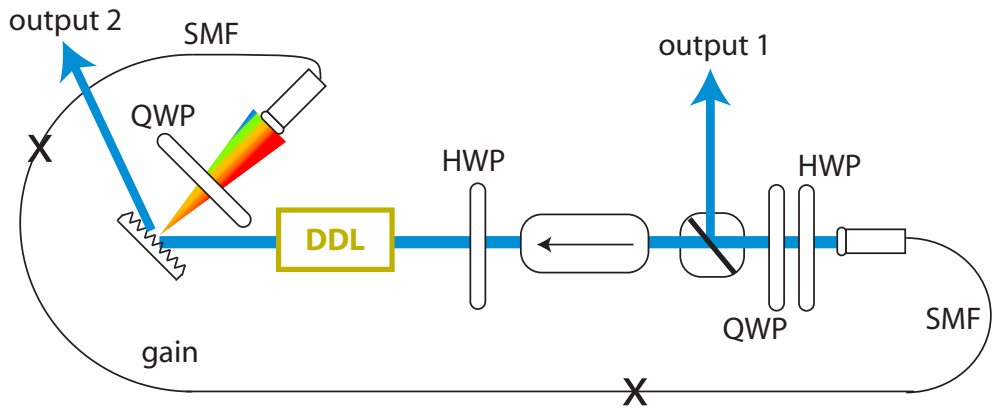

Figure 4.5: Schematic of the dispersion-mapped amplifier similariton fiber laser: QWP, quarter-wave plate; HWP, half-wave plate; DDL, dispersive delay line (diffraction grating pair).

A is the electric field envelope, τ is the local time, z is the propagation coordinate, β_2 represents the GVD, and γ represents the Kerr self-focusing nonlinearity. A 35-cm segment of single-mode fiber precedes 200 cm of Yb-doped gain fiber, and a 150-cm segment follows it (Figure 4.5), where all fibers have $\beta_2 = 230$ fs^2/cm and $\gamma = 0.0047$ (W m)$^{-1}$. In the Yb-doped gain fiber there is an additional saturating gain with $g = g_o/(1 + E_{pulse}/E_{sat})$, where g_o corresponds to 30 dB of small-signal gain, $E_{pulse} = \int_{-T_R/2}^{T_R/2} |A|^2 dt$, where T_R is the cavity round trip time and $E_{sat} = 240$ pJ. The fiber is followed by a monotonic saturable absorber with transmittance $T = 1-l_o/[1+P(\tau)/P_{sat}]$ where l_o=1.0 is the unsaturated loss, $P(\tau)$ is the instantaneous pulse power and $P_{sat} = 4.0$ kW is the saturation power. Increasing the saturable absorber modulation depth from 70% to 100% allows for the stabilization of pulses numerically without resorting to a full model incorporating nonlinear polarization evolution, as in Ref. [1]. Thus, the saturable absorber is important in this system for stabilizing the pulses from noise. The saturable absorber is followed by a linear segment of anomalous dispersion which is varied to set the net GVD of the cavity. The gain is assumed to have a Gaussian spectral profile with a 40-nm bandwidth, the output coupling is 60%, and a Gaussian filter with 4-nm bandwidth

is placed after the dispersive delay. The governing equations are solved with a standard symmetric split-step propagation algorithm [35] (the linear terms are solved exactly in the Fourier domain and the nonlinear terms are solved with a fourth-order Runge-Kutta algorithm) and are run until the energy converges to a constant value.

The net GVD was varied from large normal (no anomalous dispersion section) to equally-large anomalous GVD and results for selected values are presented (Figure 4.6). All of the simulated output pulses (output 1 in Figure 4.5) have $\sim$ 1-nJ

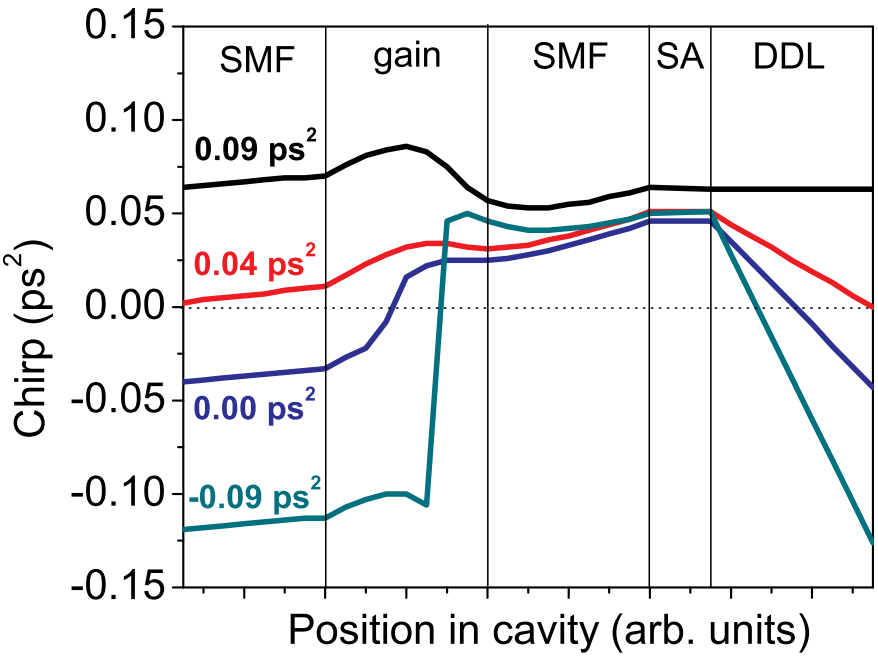

Figure 4.6: Simulated evolution of the pulse chirp for four different values of net cavity GVD: SA, saturable absorber; DDL, dispersive delay line.

pulse energy, $\sim$ 0.05-ps^2 chirp, and 50-100 fs dechirped pulse duration, which is a clear indication that the dispersive delay has little effect on the similariton formation in the gain fiber. Mode-locking mechanisms are primarily distinguished

by the pulse evolution through the cavity, and the parameter that most clearly illustrates the effects of the dispersion map is the pulse chirp (i.e., the quadratic spectral phase). In the cavity with large normal GVD, starting after the gain, the chirp increases in the normal dispersion fiber sections and then is pulled back toward ~ 0.05 ps^2 in the gain fiber (Figure 4.6). For the other dispersion values, starting after the gain, the chirp increases slightly in the fiber section, decreases in the dispersive delay, slightly increases again in the next fiber section, and is then pulled back toward ~ 0.05 ps^2. The clear and powerful nature of the nonlinear attractor responsible for DMAS mode-locking is illustrated completely by the evolution of the chirp in the gain section (Figure 4.6). Regardless of how much GVD is necessary to produce a pulse with ~ 0.05 ps^2 of chirp, the pulse nonlinearly grows the appropriate phase as it is attracted to the self-similar solution in the gain, as is most evident from the large anomalous dispersion (-0.09 ps^2) case. We note that the pulse chirp can be tuned continuously from positive to negative by tuning the GVD of the cavity; the 0.04-ps^2 result is included because it yields a transform-limited output pulse.

4.2.3 Experimental results

The DMAS oscillator is designed and built as in Ref. [1], but with the addition of a grating pair for the dispersive delay line (Figure 4.5). As in Ref. [1], a diffraction grating (300 lines per millimeter) along with the Gaussian dependence of the fiber collimator acceptance angle yield a 4-nm Gaussian spectral filter. The power, spectrum, and interferometric autocorrelation of pulses from output 1 (Figure 4.5) are measured after dechirping the pulses with a grating pair. The pulse train is measured with a 30-GHz detector to ensure that only one pulse is in the cavity

at a time. Mode-locking exists at many settings of the wave-plates, and is robust and self-starting at all values of the net GVD. In addition, the net GVD can be tuned continuously through zero without loss of mode-locking. At large anomalous net GVD, a typical example has 0.7-nJ output energy and 83-fs dechirped duration with 0.06-ps^2 chirp (Figure 4.7). Although the cavity has large anoma-

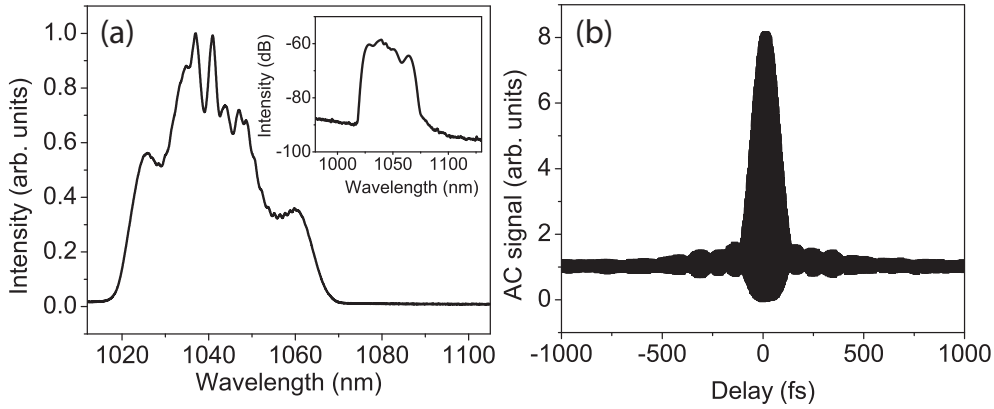

Figure 4.7: (a) Output spectrum and (b) dechirped autocorrelation of the pulses from a laser with large net anomalous dispersion. Inset: output spectrum with a logarithmic scale.

lous dispersion, there are no spectral sidebands (Figure 4.7 inset), which clearly distinguishes these pulses from the only other known mode-locking regime with this net GVD, the soliton. Other distinguishing features include the temporal and spectral shapes, the short pulse duration (considering the high magnitude of net GVD) and the fact that the pulse has chirp. The ability to produce short pulses at any net dispersion can facilitate laser designs at 1550-nm, for example. Standard single-mode fibers have anomalous dispersion, and can still be used to generate ultrashort and high-energy pulses.

To find a transform-limited output pulse, we set the net GVD to the value predicted by simulations (Figure 4.6) and varied the intra-cavity grating spacing while monitoring the autocorrelation from output 2 (Figure 4.5) until the pulse duration was minimized. A typical example, found with net GVD of 0.03 ps^2,

has 1.9-nJ pulse energy, 61-fs dechirped pulse duration, and 0.06-ps^2 chirp from output 1 (Figure 4.8(a,b)). 250-pJ and 77-fs pulses are emitted directly from output 2 (Figure 4.8(c,d)). In this example the transform-limited output pulse has lower energy, but this energy can be increased simply by swapping the output coupler with the dispersive delay, and taking the transform-limited output from the beam splitter (see Figure 4.5). It should be noted that the system is very stable and the intra-cavity grating separation can be varied smoothly without loss of mode-locking.

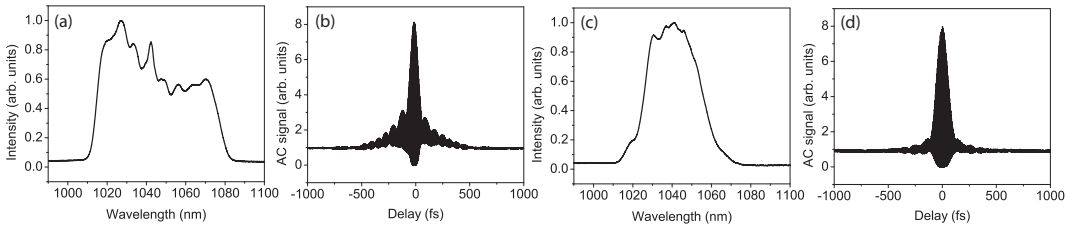

Figure 4.8: (a) Output spectrum and (b) dechirped autocorrelation of the pulses from output 1 and (c) output spectrum and (d) direct autocorrelation from output 2 from a laser operating at net dispersion of 0.03 ps^2.

Recent work shows a large reduction in the free-running carrier-envelope offset-frequency linewidth, and frequency noise power spectral density, of a fiber laser operating near zero GVD [36]. These results motivate the design of new fiber lasers that can be mode-locked with net zero GVD. When tuned to zero net GVD, the DMAS laser emits 0.8-nJ pulses with 67-fs dechirped duration and 0.06-ps^2 chirp (Figure 4.9). We note that the main features (bandwidth, chirp, spectral shape, and energy) of the three operating regimes are similar. With further tuning of the wave-plates and the pump power aimed at optimizing performance, 3.5-nJ pulses with 56-fs pulse duration can be achieved (data not shown).

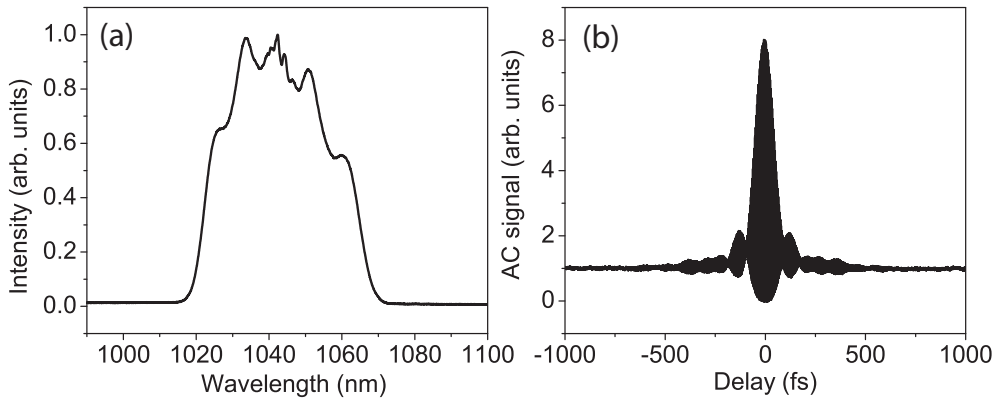

Figure 4.9: (a) Output spectrum and (b) dechirped autocorrelation of pulses from a laser with zero net cavity dispersion.

4.2.4 Conclusion

In conclusion, amplifier similaritons are generated in a fiber laser with a dispersion map. The pulse evolution is stabilized by a narrow-band spectral filter, which leads to a strong nonlinear attraction in the gain segment of the fiber laser. The output pulse parameters only change slightly as a function of the net GVD, which demonstrates the power of the local nonlinear attraction in the gain fiber. This freedom from global parameters allows for several practical advantages. At large net anomalous GVD, the DMAS laser can free up length design restrictions when designing oscillators at 1550-nm wavelengths. At large normal dispersion, the DMAS laser can be designed with a transform-limited output. Finally, at zero GVD, where the timing jitter is predicted to be minimal, the DMAS laser can be useful as a route to low-noise frequency combs. All modes of operation produce sub-100 fs pulses with nanojoule energies and should readily scale to greater than 200-kW peak power even with single-mode fiber designs.

The authors would like to thank Brandon Bale for useful discussions about numerical simulations. Portions of this work were supported by the National Sci-

ence Foundation (Grant No. ECS-0701680) and the National Institutes of Health (Grant No. EB002019).

4.3 Bandwidth extended amplifier similariton mode-locking[3]

From research led by Andy Chong and Hui Liu, this section describes an extension to amplifier similariton mode-locked fiber lasers which involves the addition of a highly-nonlinear fiber in the cavity for the creation of ultrashort pulses. Bandwidths approaching 200 nm and pulses as short as 21 fs (the shortest from a fiber laser to date) are generated in initial experiments. This demonstration introduces a class of fiber lasers with clear potential for few-cycle pulse generation.

The spectral bandwidth of a similariton grows exponentially in an amplifier. However, the self-similar evolution is disrupted when the pulse bandwidth approaches the gain bandwidth of the amplifier, and this limits the pulse energy and duration that can be achieved [38]. It may be possible to extend or continue self-similar pulse evolution beyond an amplifier. For example, a fiber with lower dispersion and/or higher nonlinear coefficient than the gain fiber can induce substantial spectral broadening. The linearly-chirped parabolic pulse produced by the amplifier will maintain close to a parabolic shape and linear chirp in the passive fiber.

The cavity (shown conceptually in Figure 4.10 and with experimental detail in Figure 4.11) contains 30 cm of SMF ($\beta_2 = 230$ fs^2/cm), 80 cm of Yb-doped gain

[3]The research summarized in this section is published in full in Ref. [37].

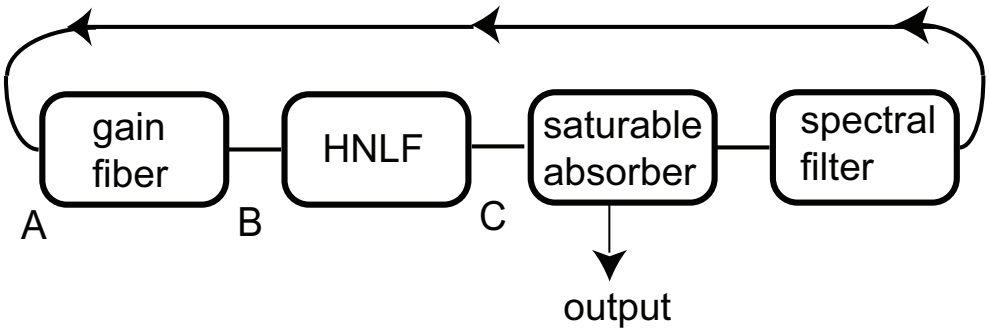

Figure 4.10: Conceptual schematic of the laser. HNLF: Highly nonlinear fiber.

fiber (gain coefficient = 6.8/m), and another 20 cm of SMF. The gain fiber and SMF have a nonlinear coefficient of 4.5×10^{-4}/(W m). Without the PCF, the laser is an established self-similar laser [1]. A 1.6-m segment of PCF (NL-1050-NEG-1 from NKT Photonics A/S) with 2.2-μm mode-field diameter is employed in the experimental setup. The PCF has $\beta_2 = 130$ fs^2/cm and nonlinear coefficient 9 times larger than that of the gain fiber. A 300 l/mm grating and a collimator create a Gaussian spectral filter with 4-nm bandwidth. The laser employs NPE as the saturable absorber, implemented by the quarter- and half-wave plates and polarizer, and is mode-locked by adjusting the wave plates. An example of the

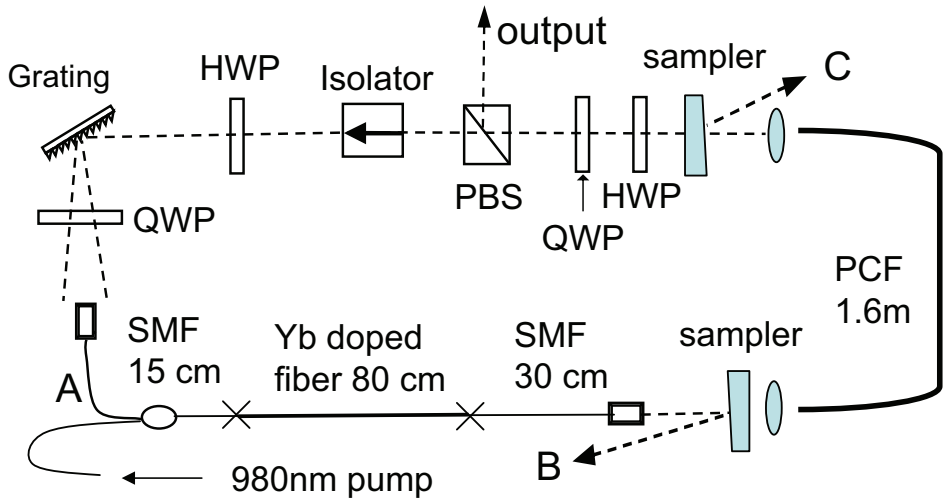

Figure 4.11: Fiber laser schematic. QWP: quarter-waveplate; HWP: half-waveplate; PBS: polarizing beam-splitter.

broadest spectra that we have observed is shown in Figure 4.12. Significant energy extends over nearly 200 nm at the base of the spectrum. The pulse energy is 1 nJ. We used multiphoton intrapulse interference phase scan (MIIPS) [39] to characterize and dechirp the output pulse. After phase correction by MIIPS the FWHM pulse duration is 21 fs, which corresponds to 6 cycles of the field. While 20% of the energy is in the secondary structure, these pulses were nevertheless used to produce high-resolution images by third-harmonic generation microscopy [39].

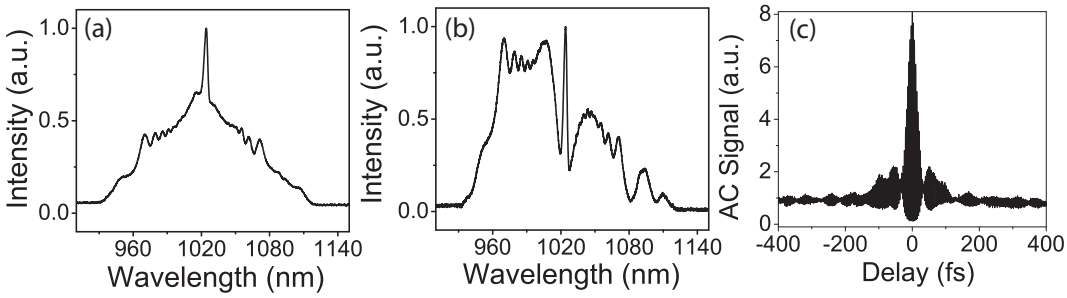

Figure 4.12: Experimental (a) spectrum after the PCF, (b) output spectrum, and (c) output autocorrelation signal after phase correction by MIIPS for a 21-fs pulse.

In conclusion, to avoid limitations caused by the gain bandwidth in amplifier similariton fiber lasers, the spectrum can be broadened in a separate nonlinear segment, and filtering produces the seed pulse to the amplifier that allows a self-consistent solution. This technique opens a promising route to the development of few-cycle fiber lasers, and clearly illustrates the benefits of a mode-locked laser based on a local nonlinear attractor.

BIBLIOGRAPHY

[1] W. H. Renninger, A. Chong, and F. W. Wise, Phys. Rev. A **82**, 21805 (2010).

[2] I. N. Duling, Electron. Lett. **27**, 544 (1991).

[3] K. Tamura, E. P. Ippen, H. A. Haus, and L. E. Nelson, Opt. Lett. **18**, 1080 (1993).

[4] A. Chong, J. Buckley, W. Renninger, and F. Wise, Opt. Express **14**, 10095 (2006).

[5] A. Chong, W. H. Renninger, and F. W. Wise, J. Opt. Soc. Am. B **25**, 140 (2008).

[6] F. W. Wise, A. Chong, and W. H. Renninger, Laser & Photon. Rev. **2**, 58 (2008).

[7] W. H. Renninger, A. Chong, and F. W. Wise, Physical Review A **77**, 23814 (2008).

[8] K. Kieu, W. H. Renninger, A. Chong, and F. W. Wise, Opt. Lett. **34**, 593 (2009).

[9] M. E. Fermann, V. I. Kruglov, B. C. Thomsen, J. M. Dudley, and J. D. Harvey, Phys. Rev. Lett. **84**, 6010 (2000).

[10] V. I. Kruglov, A. C. Peacock, J. M. Dudley, and J. D. Harvey, Opt. Lett. **25**, 1753 (2000).

[11] V. I. Kruglov, A. C. Peacock, J. D. Harvey, and J.M. Dudley, J. Opt. Soc. Am. B **19**, 461 (2002).

[12] J. M. Dudley, C. Finot, D. J. Richardson, and G. Millot, Nat Phys **3**, 597 (2007).

[13] F. O. Ilday, J. R. Buckley, W. G. Clark, and F. W. Wise, Phys. Rev. Lett. **92**, 213902 (2004).

[14] J. Dudley, A. C. Peacock, V. I. Kruglov, B. C. Thomsen, J. D. Harvey, M. E. Fermann, G. Sucha, and D. Harter, in *OFCC* (OSA, ADDRESS, 2001), p. WP4.

[15] B. Oktem, C. Ulgudur, and F. O. O. Ilday, Nat. Photon. **4**, 307 (2010).

[16] W. H. Renninger, A. Chong, and F. W. Wise, Opt. Lett. **33**, 3025 (2008).

[17] T. Schreiber, B. Ortaç, J. Limpert, and A. Tünnermann, Optics Express **15**, 8252 (2007).

[18] C. Aguergaray, D. Méchin, V. Kruglov, and J. D. Harvey, Opt. Express **18**, 8680 (2010).

[19] W. H. Renninger, A. Chong, and F. W. Wise, Opt. Express **19**, 22496 (2011).

[20] M. Baumgartl, F. Jansen, F. Stutzki, C. Jauregui, B. Ortaç, J. Limpert, and A. Tünnermann, Opt. Lett. **36**, 244 (2011).

[21] D. Anderson, M. Desaix, M. Karlsson, M. Lisak, and M. L. Quiroga-Teixeiro, J. Opt. Soc. Am. B **10**, 1185 (1993).

[22] K. Tamura and M. Nakazawa, Opt. Lett. **21**, 68 (1996).

[23] V. I. Kruglov, A. C. Peacock, and J. D. Harvey, Phys. Rev. Lett. **90**, 113902 (2003).

[24] C. Finot, G. Millot, and J. M. Dudley, Opt. Lett. **29**, 2533 (2004).

[25] C. Finot and G. Millot, Opt. Express **12**, 5104 (2004).

[26] C. Finot, G. Millot, C. Billet, and J. Dudley, Opt. Express **11**, 1547 (2003).

[27] D. B. Soh, J. Nilsson, and A. B. Grudinin, J. Opt. Soc. Am. B **23**, 10 (2006).

[28] T. Hirooka and M. Nakazawa, Opt. Lett. **29**, 498 (2004).

[29] C. Finot, B. Barviau, G. Millot, A. Guryanov, A. Sysoliatin, and S. Wabnitz, Opt. Express **15**, 15824 (2007).

[30] J. Limpert, T. Schreiber, T. Clausnitzer, K. Zöllner, H. Fuchs, E. Kley, H. Zellmer, and A. Tünnermann, Opt. Express **10**, 628 (2002).

[31] D. N. Papadopoulos, Y. Zaouter, M. Hanna, F. Druon, E. Mottay, E. Cormier, and P. Georges, Opt. Lett. **32**, 2520 (2007).

[32] Y. Deng, C.-Y. Chien, B. G. Fidric, and J. D. Kafka, Opt. Lett. **34**, 3469 (2009).

[33] B. G. Bale and S. Wabnitz, Opt. Lett. **35**, 2466 (2010).

[34] B. Nie, D. Pestov, F. W. Wise, and M. Dantus, Opt. Express **19**, 12074 (2011).

[35] G. P. Agrawal, *Nonlinear Fiber Optics*, 3rd ed. (Academic Press, New York, 2001).

[36] L. Nugent-Glandorf, T. A. Johnson, Y. Kobayashi, and S. A. Diddams, Opt. Lett. **36**, 1578 (2011).

[37] A. Chong, H. Liu, B. Nie, B. G. Bale, S. Wabnitz, W. H. Renninger, M. Dantus, and F. W. Wise, Opt. Express **20**, 14213 (2012).

[38] A. C. Peacock, R. J. Kruhlak, J. D. Harvey, and J. M. Dudley, Optics Communications **206**, 171 (2002).

[39] I. Saytashev, B. Nie, A. Chong, H. Liu, S. Arkhipov, F. W. Wise, and M. Dantus, in *Society of Photo-Optical Instrumentation Engineers (SPIE) Conference Series*, Vol. 8226 of *Society of Photo-Optical Instrumentation Engineers (SPIE) Conference Series* (SPIE, Bellingham WA, 2012).

CHAPTER 5

FUTURE DIRECTIONS

In this chapter, future directions aimed at improving the performance of femtosecond mode-locked fiber lasers are presented. There are several directions in which fiber laser research can head where progress is likely to both be made and to have high impact. First, a brief summary is given of each of these directions. Then, in section 5.1, a new approach to mode-locking is outlined, which if successfully implemented, could offer another order-of-magnitude increase to the peak power of femtosecond fiber lasers.

- Early mode-locked fiber lasers were based on Erbium-doped fibers, primarily because they operate at 1550-nm wavelength, where telecommunications systems operate. Recent work, and the results presented in this thesis are based on Yb-doped systems with amplifiers operating at around 1030-nm wavelength. Yb-doped systems offer slightly higher efficiencies as well as larger gain bandwidths, which allows for higher performance pulsed-operation. While high quality mode-locked fiber sources exist at these two specific wavelengths, other wavelengths are often required for applications, and tunability is desired. In particular, for many applications in nonlinear optics, medicine, and sensing, integrated and robust laser sources around 2-μm wavelength are needed. As an alternative to designing a technique for tuning the wavelength from a well-established lasing medium, new lasing media are constantly being developed. A promising example is thulium- and holmium-doped systems, which operate at around 2-μm wavelength. Research into high peak power sources has just begun in this direction with soliton mode-locking [1], and even signs of mode-locking in the normal dispersion regime [2, 3]. Future

progress in this direction will involve bringing 2-μm wavelength sources up to the performance seen at 1030-nm by incorporating the mechanisms identified in this thesis. Tm/Hm-doped systems also come with the additional benefit from a mode-locking perspective of a larger gain bandwidth, which when incorporated with the appropriate mode-locking mechanism like amplifier similaritons, could allow for the shortest absolute pulse duration from a fiber laser.

- The importance of low timing and intensity noise in fiber lasers is clear, particularly in relevant applications, such as research on frequency-combs (e.g. see [4]). Recent numerical analysis in our lab has determined that there is a strong link between the system parameters in a fiber laser (the spectral filter, saturable absorber, group-velocity dispersion, pulse energy...etc) and its noise performance. Future research could build on this conclusion experimentally in order to develop guidelines for how to make quieter fiber lasers. Research on frequency combs and imaging systems would greatly benefit from this enhancement.

- As mentioned briefly in section 2.5.2, for wide-adoption of fiber lasers beyond a controlled laboratory environment, they must be robust against environmental perturbations. One way to decrease environmental disturbance is to make the cavity without a free-space section (i.e. make it all fiber). This route requires the use of fiber based components to replace all of the otherwise free-space parts. In Ref. [5], for example, the authors use a fiber isolator, a directional coupler for the output, polarization controllers which bend the fiber to manipulate the fiber birefringence as a way to replace the wave-plates, and a section of polarization-maintaining fiber to form an all-fiber birefringence filter. These components allow for operation in the

dissipative soliton regime. This route succeeds at making the laser more robust, but because the saturable absorber is dependant on the birefringence of the fiber, environmental perturbations can still cause performance decreasing fluctuations. A remaining so-called "holy grail" in fiber laser research is to replace the environmentally sensitive saturable absorber, NPE, with a fiberized saturable absorber which is insensitive to environmental stress. Kieu et al. made a large step in this direction with the development of an all-fiber dissipative soliton laser with a fiber format saturable absorber based on carbon nanotubes [6]. While this technique has been successful at 1550-nm wavelength, at 1-μm wavelength, the performance of the absorber degrades with time. The origin of the degradation is still unknown. Further research in this direction will have great impact in the field as a new generation of high performance systems will see immediate broader use.

- As is clear from the results in section 2.5.1, increasing the size of the fiber core increases the pulse energy available from a fiber-based system. While this technique has been successfully implemented in dissipative soliton systems to enhance the already high pulse energies (section 2.5.1), amplifier similariton mode-locking has yet to benefit from such scaling. That is, all of the results from chapter 4 could immediately gain a factor of > 30 in pulse energy through the use of either photonic-crystal or chirally-coupled-core fiber.

In summary, through work individually in the directions above, an ultimate goal in fiber laser research would be to build a large-mode area, all-fiber, low-noise fiber source based on dissipative soliton or amplifier similariton mode-locking which can operate with several different gain media. This result would virtually ensure the replacement of solid-state sources for applications where a short pulse optical source is necessary.

5.1 Mode-locking with dispersion-decreasing fiber

As evidenced by this thesis, amplifier similariton mode-locking is highly successful for the achievement of high performance mode-locking. However, looking towards the future, it is clear that because the pulse shaping mechanism occurs in the bandwidth-limited gain fiber, at least part of the performance will ultimately be limited by the gain bandwidth. Therefore, it would be ideal to have a section of fiber in the cavity which could mode-lock the laser in a similar manner, but without the limitation.

As early as 2004, self-similar parabolic pulses were also shown to be an asymptotic solution in dispersion-decreasing passive fibers (DDF) [7, 8]. If the equations which govern a pulse propagating in a dispersion-decreasing passive fiber are properly scaled, an equation with the exact form as that for amplifiers results. That is,

$$\begin{aligned} &\frac{\partial u}{\partial \xi} = \frac{\Gamma}{2}u - i\frac{\beta_{20}}{2}\frac{\partial^2 u}{\partial t^2} + i\gamma(|u|^2)u, \\ &\text{where} \\ &\beta_2(z) = \frac{\beta_{20}}{1+\Gamma z}, \quad u = A\sqrt{1+\Gamma z}, \quad \text{and} \quad \xi = \frac{\beta_{20}\ln(z\Gamma+1)}{\Gamma}. \end{aligned} \tag{5.1}$$

With our knowledge of the self-similar solution to an amplifier (chapter 4), it is straightforward to then calculate the parabolic solution and its evolution in the case of a dispersion decreasing fiber. The answer can be found to be:

$$A(z,t) \sim \sqrt{P(z)}\left(1-\left(\frac{t}{\tau(z)}\right)^2\right)^{1/2} e^{i\theta(z,t)},$$

where

$$\begin{aligned} P(z) &= \frac{1}{4}\left(\frac{2E_{in}^2\Gamma^2}{\gamma\beta_{20}(1+\Gamma z)}\right)^{1/3}, \\ \tau(z) &= 3\left(\frac{E_{in}\gamma\beta_{20}(1+\Gamma z)}{2\Gamma^2}\right)^{1/3}, \quad \text{and} \\ \theta(z,t) &= -\frac{\Gamma}{6\beta_{20}}t^2 + f(z). \end{aligned} \tag{5.2}$$

Using the method of steepest descent, one can also calculate the corresponding spectrum and its evolution:

$$\begin{aligned} A(z,f) &= \sqrt{\frac{6\pi P\beta_{20}}{\Gamma}}\sqrt{1-\left(\frac{f}{\frac{\tau(z)}{\frac{\pi 6\beta_{20}}{\Gamma}}}\right)^2}\, e^{i\pi/4}e^{-i\frac{\pi^2 6\beta_{20}}{\Gamma}f^2}, \\ |A(z,f)|^2 &= \frac{6\pi P\beta_{20}}{\Gamma}\left(1-\left(\frac{f}{\frac{\tau(z)}{\frac{\pi 6\beta_{20}}{\Gamma}}}\right)^2\right), \quad \text{where} \\ \Delta f &= \frac{\tau(z)\Gamma}{\pi 6\beta_{20}} \quad \text{and} \\ \phi''(\omega) &= -\frac{3\beta_{20}}{\Gamma}. \end{aligned} \tag{5.3}$$

And finally converting to the most useful parameters one can calculate:

$$\begin{aligned} \Delta\lambda_{FWHM} &= \sqrt{2}\frac{\lambda_c^2}{2\pi c}\left(\frac{E_{in}\gamma\Gamma}{2\beta_{20}^2}\right)^{1/3}(1+\Gamma z)^{1/3}, \\ \phi''(\omega) &= -\frac{3\beta_{20}}{\Gamma}, \\ \Delta t_{FWHM} &= 3\sqrt{2}\left(\frac{E_{in}\gamma\beta_{20}}{2\Gamma^2}\right)^{1/3}(1+\Gamma z)^{1/3}, \quad \text{and} \\ \phi''(t) &= -\frac{\Gamma}{3\beta_{20}}. \end{aligned} \tag{5.4}$$

A major result of the dispersion-decreasing fiber solution is that both its pulse duration and bandwidth evolution like $z^{\frac{1}{3}}$ instead of exponentially like in the case of an amplifier. This is a result of the necessary scaling of the propagation equation (Eq. 5.1). As a consequence, for a given propagation length the bandwidth in this case will increase at a slower rate than in the case of an amplifier. However, from these expressions, it is clear that there is much more tunability in initial and final pulse parameters, because unlike with the gain in an amplifier, we can tune the Γ parameter of the dispersion-decreasing fiber.

To illustrate the potential of using a DDF for fiber laser mode-locking here we will present an example design for a high performance mode-locked result. First we assume that there is no freedom to tune the values of λ_c, β_{20} and γ as these are typically set by the desired lasing medium and the fiber material. This leaves us with the freedom to tune Γ, E_{in}, and z. For a given Γ, the higher the E_{in} is the higher the initial bandwidth has to be. Because we are working in an oscillator and we want the highest possible energy, we will target the highest possible initial bandwidth. Assuming this will be set by the gain medium, we now can have any energy as long as Γ is properly chosen. Finally, z or the length of the DDF is chosen such that there is significant propagation to attract to the self-similar solution. Because bandwidth growth is a signature of nonlinear propagation, we assume z must be large enough for the bandwidth to grow by at least a factor of two.

An example GVD profile as a function of distance for a design target of 100 nJ is shown in Figure 5.1. 200 m of the DDF is required to achieve the necessary nonlinear evolution. To verify the robustness of the nonlinear attraction and to test the analytic results presented here, numerical simulations are performed for a

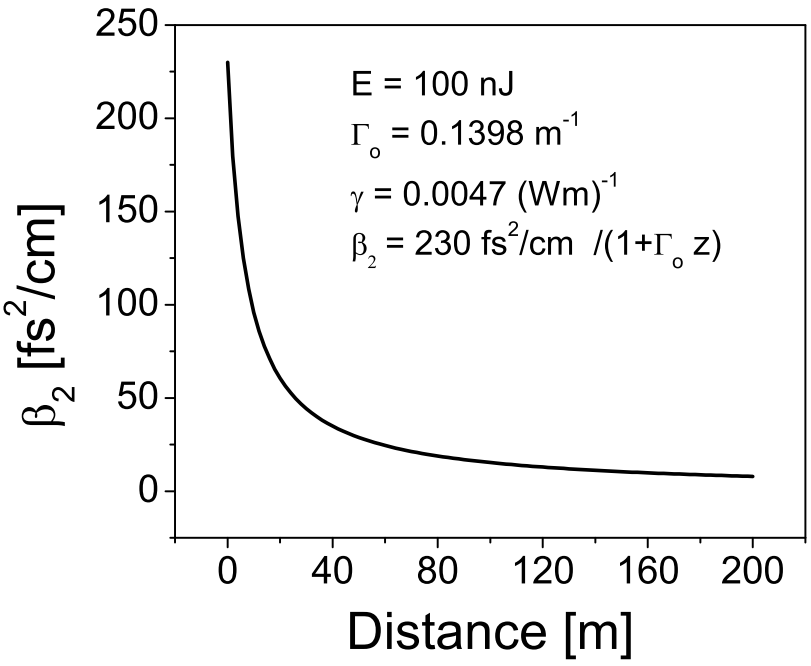

Figure 5.1: GVD profile as a function of distance for a DDF designed to mode-lock a 100-nJ fiber laser.

single pass through this fiber. The initial condition is a 40-nm Gaussian spectral profile with 0.5-ps^2 chirp. The evolution of the pulse through this fiber is shown in Figure 5.2. The pulse duration and spectral bandwidth evolve as expected like $z^{\frac{1}{3}}$. Figure 5.2(c) as in chapter 4 shows the closeness-to-a-parabola parameter. It is clear from these results that the pulse is evolving as predicted from Eq. 5.4. In addition the output pulse (Figure 5.3(a)) is parabolic. The results shown here suggest that with realistic parameters it may be possible to use a DDF to mode-lock a high performance fiber laser and possibly gain another order of magnitude increase in pulse energy performance. There are major obstacles to be tackled before this can be achieved, however. For example, simulation of only a single pass through the DDF is greatly time consuming owing to the number of points required to store all of the data for the amplitude and the phase of the highly

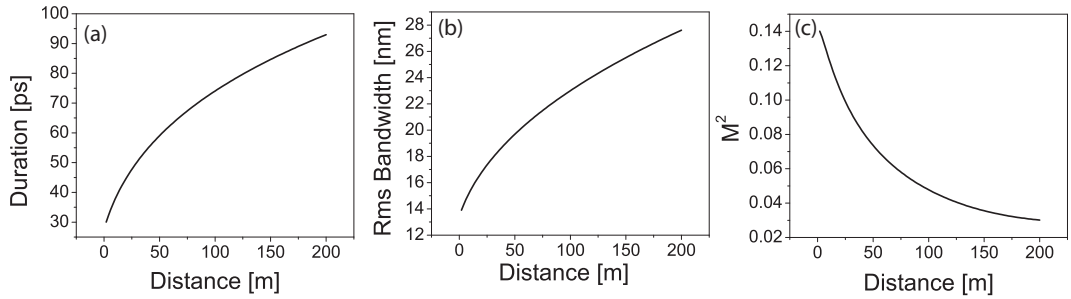

Figure 5.2: Evolution of the (a) pulse duration, (b) spectral bandwidth, and (c) parabolic closeness factor in a 200-m DDF.

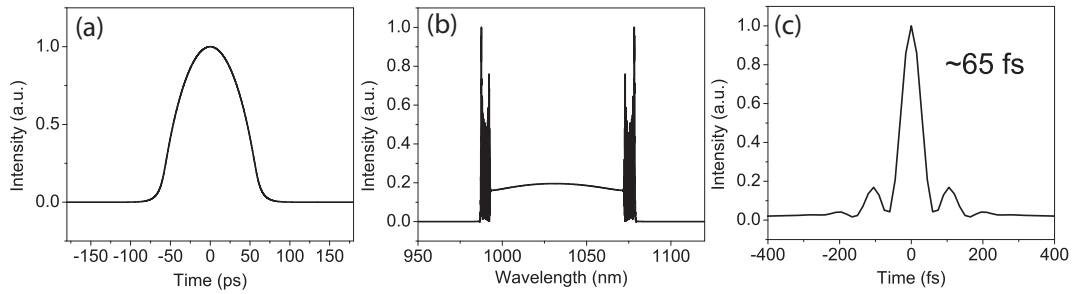

Figure 5.3: Output (a) pulse, (b) spectrum, and (c) dechirped pulse from a 200-m DDF.

chirped pulse, in addition to the number of points in the propagation direction required to ensure a smooth representation of the DDF. Therefore, new techniques will need to be developed to simulate on oscillator with this fiber. Also, TOD has been known to destabilize the evolution of a pulse in a dispersion decreasing fiber; this issue must be simulated and tested for various lengths of fiber. Finally, fabrication of such fiber can be challenging. Early possibilities and discussions with manufacturers sound promising but it may be difficult to simultaneously control the group velocity dispersion while minimizing all higher order dispersions.

In conclusion, here we investigate the possibility of mode-locking a fiber laser with a dispersion-decreasing fiber. While the theoretical results look very promising, several obstacles must be surpassed before this exciting new mode-locking technique can become a reality.

BIBLIOGRAPHY

[1] K. Kieu and F. W. Wise, Photonics Technology Letters, IEEE **21**, 128 (2009).

[2] F. Haxsen, D. Wandt, U. Morgner, J. Neumann, and D. Kracht, in *Lasers, Sources, and Related Photonic Devices* (Optical Society of America, ADDRESS, 2012), p. AM4A.24.

[3] R. Gumenyuk, I. Vartiainen, H. Tuovinen, and O. G. Okhotnikov, Opt. Lett. **36**, 609 (2011).

[4] L. Nugent-Glandorf, T. A. Johnson, Y. Kobayashi, and S. A. Diddams, Opt. Lett. **36**, 1578 (2011).

[5] K. Özgören and F. Ilday, Optics Letters **35**, 1296 (2010).

[6] K. Kieu and F. W. Wise, Optics Express **16**, 11453 (2008).

[7] T. Hirooka and M. Nakazawa, Opt. Lett. **29**, 498 (2004).

[8] C. Finot, B. Barviau, G. Millot, A. Guryanov, A. Sysoliatin, and S. Wabnitz, Opt. Express **15**, 15824 (2007).

APPENDIX A

CHAPTER 3 SIMULATION PARAMETERS

A.1 Dissipative soliton cavity

Simulations are solved with a standard symmetric split-step propagation algorithm. Passive single-mode fibers are modeled with the nonlinear Schrodinger equation with $\beta_2 = 230$ fs^2/cm and $\gamma = 0.0047$ (W m)$^{-1}$. The active fiber is modeled by a saturating gain, $g = g_o/(1 + E_{pulse}/E_{sat})$, where g_o corresponds to 30 dB of small-signal gain, $E_{pulse} = \int_{-T_R/2}^{T_R/2} |A|^2 dt$, where A is the electric field envelope, T_R is the cavity round trip time and E_{sat} is the gain saturation energy. The fiber is followed by a saturable absorber given by a monotonically increasing transfer function, $T = 1 - l_o/[1 + P(\tau)/P_{sat}]$ where l_o is the unsaturated loss, $P(\tau)$ is the instantaneous pulse power and P_{sat} is the saturation power. The absorber is followed by a variable output coupler. The cavity consists of a single 6-m segment of gain fiber with $E_{sat} = 7.2$ nJ. After the fiber is a saturable absorber with $l_o = 0.7$ and $P_{sat} = 3$ kW, a spectral filter with 12-nm bandwidth, and an 88% output coupler. The simulation is seeded with a picosecond Gaussian temporal profile and run until the pulse energy converges; the resultant output pulse energy is 12 nJ.

A.2 Dispersion-managed cavity

A 450-cm segment of SMF precedes 23 cm of highly Yb-doped gain fiber, and a 20-cm segment follows it. The gain fiber includes a 40-nm distributed Gaussian filter and no additional spectral filter is included. After the fiber section are the

diffraction gratings, modeled as an anomalous dispersive delay, the dispersion of which is varied to achieve a particular net GVD. The cavity has a net dispersion of 5000 fs^2, $l_o = 0.7$, 90% output coupling, 80% additional loss from the gratings and the collimator, P_{sat} =5 kW and $E_{sat} = 1.2$ nJ.

A.2.1 Passive self-similar mode-locking

The cavity consists of 25 cm of SMF with varying normal GVD, a section with saturating gain and a gain filter with 40-nm bandwidth, a saturable absorber with $l_o = 0.7$, a 70% output coupler and a section with variable anomalous GVD. If the anomalous GVD section is absent, the cavity represents a DS with 5000 fs^2 net dispersion. If the magnitude of anomalous dispersion is increased and an equal amount of normal dispersion is added to the fiber section, the net cavity dispersion will remain at 5000 fs^2 but the dispersion map will increase, modeling the cavity of a self-similar laser. The dispersion map was increased until the simulations no longer converged, with a dispersion of $-110,000$ fs^2 in the anomalous dispersion segment.

A.2.2 Stretched dissipative soliton mode-locking

Simulations are run with the net GVD= 5000 fs^2, $l_o = 0.7$, 90% output coupling, 50% additional loss from the gratings and the collimator, no nonlinearity in the first fiber, P_{sat} =1kW, 6kW, and 21kW and $E_{sat} = 0.2$nJ, 1.4 nJ and 5.0 nJ.